University of Alberta

Investigating the Effects of Liquid Droplets, Turbulence, and Flare Stack Dimensions on the Combustion Efficiency of the Modeled Flares in Crosswind

By

Muhammad Arshad

A thesis submitted to the Faculty of Graduate Studies and Research in partial fulfillment of the requirements for the degree of Master of Science.

Department of Mechanical Engineering

Edmonton, Alberta

Spring, 2004

Library and Archives Canada

Published Heritage Branch

395 Wellington Street
Ottawa ON K1A 0N4
Canada

Bibliothèque et Archives Canada

Direction du Patrimoine de l'édition

395, rue Wellington
Ottawa ON K1A 0N4
Canada

Your file Votre référence
ISBN: 0-612-96444-2
Our file Notre référence
ISBN: 0-612-96444-2

The author has granted a non-exclusive license allowing the Library and Archives Canada to reproduce, loan, distribute or sell copies of this thesis in microform, paper or electronic formats.

L'auteur a accordé une licence non exclusive permettant à la Bibliothèque et Archives Canada de reproduire, prêter, distribuer ou vendre des copies de cette thèse sous la forme de microfiche/film, de reproduction sur papier ou sur format électronique.

The author retains ownership of the copyright in this thesis. Neither the thesis nor substantial extracts from it may be printed or otherwise reproduced without the author's permission.

L'auteur conserve la propriété du droit d'auteur qui protège cette thèse. Ni la thèse ni des extraits substantiels de celle-ci ne doivent être imprimés ou aturement reproduits sans son autorisation.

In compliance with the Canadian Privacy Act some supporting forms may have been removed from this thesis.

Conformément à la loi canadienne sur la protection de la vie privée, quelques formulaires secondaires ont été enlevés de cette thèse.

While these forms may be included in the document page count, their removal does not represent any loss of content from the thesis.

Bien que ces formulaires aient inclus dans la pagination, il n'y aura aucun contenu manquant.

Canada

ABSTRACTS

A mixture of combustible gases, liquids, and water is collected with the extraction of oil. The gaseous mixture is known as "solution gas", which is either "conserved" or "flared". It is generally accepted that certain amount of liquid droplets eludes liquid knockout system and is carried to flare as liquid droplets entrained in flare stream. There are varying levels of turbulence in the atmosphere that have a potential impact on flare efficiency. This study reports results of an experimental study that adds droplets of three different liquids into gaseous flare stream, introduces varying levels of turbulence to crosswind, and changes flare stack wall thickness of scaled down modeled flares. Iso-octane and diesel droplets increased flare efficiency. Distilled water droplets decreased flare efficiency. Flare efficiency decreased with an increase in turbulence intensity, where scale of turbulence tested had little affect on flare efficiency. There is a general trend of decreasing efficiency with thicker walls.

ACKNOWLEGEMENTS

In the name of God, The Most Merciful, The Most Compassionate. I bare witness that there is only one God, worthy of worship and that Muhammad (peace and blessing be upon him) is His messenger. I am thankful to God, Who gave me the strength of completing this endeavor.

I wish to thank the following respected seniors, colleagues, and friends for their support and encouragement to make this thesis a success:

Dr. Larry Kostiuk for his kind support, trust, and helpful guidance throughout the dissertation.

Glen P. Thomas, Pascal Poudenx, Robert Prybysh, Mathew R. Johnson and Oleg Zastaviniuk for their help in keep me going on the track.

The whole machine shop members for their help in turning the idea into reality and making this dream come true.

Terry Nord for his electrifying and enlightening help.

The sponsors of the University of Alberta Flare Research Project, Environment Canada, The Government of Alberta, The NSERC, The Canadian association of Petroleum Producers (CAPP) for their financial support.

At last but not least, a special acknowledgement to my wife Saima Hanif, my father, my brothers and sisters, and my sincere friends for their prayers and moral support in achieving this goal.

TABLE OF CONTENTS

CHAPTER 1 INTRODUCTION		**1**
1.1	**Environmental Issue of Flaring**	**6**
1.2	**Approach of the Flare Research Project**	**9**
1.3	**Potential Source of Liquid Droplets**	**11**
1.4	**Objectives and Outline of This Thesis Research**	**13**
REFERENCES		**15**
CHAPTER 2 REVEW OF RELATIVE LTRATURE		**18**
2.1	**Diffusion Flame**	**19**
	2.1.1 Principles of Diffusion Flame Combustion	**20**
	2.1.2 Jet Diffusion Flame	**22**
2.2	**Jet in a Crosswind**	**24**
	2.2.1 Non-Reacting Jets in Crosswind	**25**
	2.2.2 Reacting Jets in Crosswind	**26**
2.3	**Field Studies on Flares**	**30**
2.4	**Combustion of Liquid Fuels**	**32**
	2.4.1 Combustion of Fuel Sprays	**34**
2.5	**Jet Diffusion Flame in Turbulent Crosswind**	**38**
REFERENCES		**44**

CHAPTER 3 EXPERIMENTAL SETUP AND METHODOLOGY 48

3.1 Generation and Addition of Liquid Droplets into Flare Gas 51

3.1.1 Mass Flow Rate of the Liquid Fuel Being Flared 52

3.1.2 Characteristic Size Distribution of the Droplets 54

3.2 Method of Measuring Combustion Efficiency of the Flares with Liquid Fuel Droplets 55

3.3 Effect of the Turbulent 60

3.4 Crosswinds Influence of Varying Flare Stack Dimensions 62

REFERENCES 74

CHAPTER 4 RESULTS OF THE FLARES WITH LIQUID DROPLETS IN THE FLARE STREAM 75

4.1 Effects of Iso-octane Droplets on the Flare Inefficiency of the Flares in Crosswind 77

4.1.1 Effects of the Flare Gas Exit Velocity on the Flare with Liquid Droplets in the Flare Stream 79

4.1.2 Effects of the Droplet size on the Flare inefficiency 81

4.1.3 Effects of the Mass Flow Rate of Iso-Octane on the Flare Inefficiency 83

4.2 Effects of Diesel Droplets on the Inefficiency of the Flares in Crosswind 86

4.2.1 Effects of the Droplet Size on the Flare Inefficiency 87

4.2.2 Effects of the Mass Flow Rate of Diesel on the Flare Inefficiency 88

4.3 Effects of Distilled Water Droplets on the Flare Inefficiency in Crosswind 90

4.3.1 Effects of the Water Droplet Size on the Flare Inefficiency in Crosswind 92

4.3.2 Effects of the Mass Flow Rate of Distilled Water on the Flare Inefficiency 93

4.4 Comparison Between the Effects of Iso-Octane, Diesel, and Distilled Water Droplets on the Flare Inefficiency of the Flares 95

Summary 97

REFERENCES 112

CHAPTER 5 RESULTS AND DISCUSSION ON THE EFFECTS OF TURBULENT CROSSWINDS AND STACK DIMENSION ON THE FLARES 113

5.1 Effects of Turbulent Crosswind on the Flare Inefficiency 113

5.2 Effects of the Flare Stack Wall Thickness on the Inefficiency of the Flares 118

Summary 122

CHAPTER 6 CONCLUSIONS 132

6.1 Effects of Liquid Droplets on the Flare Inefficiency 132

6.2 Effects of Turbulent Crosswinds on the Flare Inefficiency 134

6.3 Effects of Flare Stack Wall Thickness on the Inefficiency of the Flare 135

APPENDIX A: UNIVERSITY OF ALBERTA FLARE RESEARCH PROJECT 137

A.1 Combustion Wind Tunnel 137

A.1.1 Auxiliary Equipment in the Tunnel 138

REFERNCES 141

A.2 Flare Gas Supply System 142

A.3 Modeled Flare Stack 144

A.4 Gas Analyzers 142

A.4.1 Flame Ionization Detector (FID) 145

A.4.2 Non-Dispersive Infrared Analyzer (NDIR) 146

A.4.3 Paramagnetic Detector 147

REFERENCES 153

APPENDIX B: METHODOLOGY FOR MEASURING CARBON CONVERSION EFFICIENCY 154

REFERENCES 164

APPENDIX C: ULTRASONIC DROPLET GENERATOR 165

REFERENCES 170

APPENDIX D: DROPLET SIZE MEASUREMENT 171

REFERENCES 176

LIST OF TABLES

Table 1	**Solution Gas Conserved, and Flared and Vented (AEUB, 2002)**	**3**
Table 3.1	**Distances of grids upstream the flare stack for respective turbulence intensities and length scale**	**62**
Table 3.2	**Steel stacks with varying wall thickness**	**63**

LIST OF FIGURES

Figure 2.1	Diffusion Flame	40
Figure 2.2	Diffusion of fuel and oxidant to a flame	40
Figure 2.3	Combustion of gaseous fuel in diffusion flame	41
Figure 2.4	Combustion of liquid fuel in diffusion flame	41
Figure 2.5	Combustion of liquid fuel droplet	42
Figure 2.6	Combustion of a field of droplets	42
Figure 2.7	Shapes of diffusion flames surrounding a burning spherical fuel droplets (a) non-spherical (b) spherical	43
Figure 2.8	Parameter variation in double-film model	43
Figure3.1	Capsule for 18 kHz ultrasonic droplets generator	64
Figure 3.2	Capsule for 48 kHz ultrasonic droplets generator	65
Figure 3.3	Cap for holding the flare stack	66
Figure 3.4	Droplets generation and their introduction into the flare stream	67
Figure 3.5	Liquid supply system and mass flow rate of the liquid exiting the flare stack	68
Figure 3.6	Time trace of liquid mass flow rate	69
Figure 3.7	4 x 8 m and 1.6 mm thick grid with 25.4 mm square holes	70
Figure 3.8	4 x 8 m and 1.6 mm thick grid with 50.8 mm square holes	71
Figure 3.9	Hotwire anemometer calibration curve	72
Figure 3.10	Turbulence intensity decay behind the grid with 25.4 mm square holes	72
Figure 3.11	Turbulence intensity decay behind the gird with 50.8 mm square holes	73

Figure 4.1	Time trace of the concentrations of major carbon-containing species during a typical test in the wind tunnel	99
Figure 4.2	Effects of crosswinds and flare gas exit velocity on the inefficiency of the flares	100
Figure 4.3	Effects iso-octane droplets on the flare inefficiency in crosswinds	100
Figure 4.4	Effects of the flare gas exit velocities on the flare inefficiency having same sizes of droplets and mass flow rates of iso-octane	101
Figure 4.5	Inefficiency analysis of the flares with different flow rates of flare gas and same droplets size and flow rates of iso-octane	101
Figure 4.6	Effects of iso-octane droplet size on the inefficiency of the flares with low flare gas exit velocity in crosswind	102
Figure 4.7	Effects of iso-octane droplets size on the flare inefficiency with low jet exit velocity in crosswind	102
Figure 4.8	Effects of iso-octane droplets size on the inefficiency of the flares with higher jet exit velocity in crosswind	103
Figure 4.9	Effects of the mass flow rate of iso-octane on the flare inefficiency having same size of the droplets in the flare stream	103
Figure 4.10	Effects of the mass flow rates of natural gas and iso-octane on the flare inefficiency with the same size of droplets in the flare stream	104
Figure 4.11	Flare inefficiency as a function of mass flow rate of iso-octane using 18 kHz ultrasonic droplets generator	104
Figure 4.12	Flare inefficiency as a function of mass flow rate of iso-octane using 48 kHz ultrasonic droplets generator	105
Figure 4.13	Effects of diesel droplets on the inefficiency of the flares in crosswind	105
Figure 4.14	Effects of the diesel droplet size on the inefficiency of the flares With low flare gas exit velocity	106
Figure 4.15	Effects of the diesel droplet size on the inefficiency of the flares with higher flare gas exit velocity	106

Figure 4.16	Effects of mass flow rates of diesel on the inefficiency of the flares with low jet exit velocity in crosswinds	107
Figure 4.17	Effects of higher jet exit velocity and mass flow rates of diesel on the inefficiency of the flares in crosswinds	107
Figure 4.18	Effects of distilled water droplets on the inefficiency of the flare with low flare gas exit velocity in crosswind	108
Figure 4.19	Effects of distilled water droplets on the inefficiency of the flare with high flare gas exit velocity in crosswind	108
Figure 4.20	Effects of water droplet size on the flare inefficiency in crosswind	109
Figure 4.21	Inefficiency of the flares as a function of crosswind speed with two different sizes of water droplets in the flare stream	109
Figure 4.22	Inefficiency of the flares having low jet exit velocity with varying flow rates of distilled water using 18 kHz droplet generator	110
Figure 4.23	Inefficiency of the flares having high jet exit velocity with varying flow rates of distilled water using 48 kHz droplets generator	110
Figure 4.24	Effects of iso-octane, diesel, and distilled water droplets on the inefficiency of the flares of low jet exit velocities in crosswinds	111
Figure 4.25	Effects of iso-octane, diesel, and distilled water droplets on the inefficiency of the flares of high jet exit velocities in crosswinds	111
Figure 5.1	Inefficiency of the flares having low flare gas flow rate subjected to varying turbulence intensities generated by the gridwith 50.8 mm square holes	124
Figure 5.2	Eddies generated in turbulent flow	124
Figure 5.3	Inefficiency of the flares having high flare gas flow rate subjected to varying turbulence intensities generated by the grid with 50.8 mm square holes	125
Figure 5.4	Comparison of the inefficiencies of the flares with high and low flow rates of the flare gas under the same turbulent crosswind conditions	125

Figure 5.5	Inefficiency of the flares having low flare gas flow rate subjected to varying turbulence intensities generated by the grid with 25.4 mm square holes	126
Figure 5.6	Inefficiency of the flares having high flare gas flow rate subjected to varying turbulence intensities generated by the grid with 25.4 mm square holes	126
Figure 5.7	Inefficiency comparison of the flares with two different flare gas flow rates subjected to the same turbulent crosswind conditions	127
Figure 5.8	Effects of decreased wall thickness on the inefficiency of the flares having low flare gas flow rates and jet exit velocity in crosswind	127
Figure 5.9	Effects of decreased wall thickness on the inefficiency of the flares having high flare gas flow rates and jet exit velocity in crosswind	128
Figure 5.10	Effects of increased wall thickness on the inefficiency of the flares having low flare gas flow rates and jet exit velocity in crosswind	128
Figure 5.11	Effects of increased wall thickness on the inefficiency of the flares having high flare gas flow rates and jet exit velocity in crosswind	129
Figure 5.12	Effects of varying wall thickness on the inefficiency of low jet exit velocity flare at 4 m/s	129
Figure 5.13	Effects of varying wall thickness on the inefficiency of low jet exit velocity flare at 5 m/s	130
Figure 5.14	Effects of varying wall thickness on the inefficiency of high jet exit velocity flare at 5 m/s	130
Figure 5.15	Effects of varying wall thickness on the inefficiency of high jet exit velocity flare at 6 m/s	131
Figure A.1	Schematic of a closed-loop combustion wind tunnel	140
Figure A.2	Flare ignition system	140
Figure A.3	Schematic of natural gas supply system	143

Figure A.4	Schematic of gas sampling system	149
Figure A.5	The Flame Ionization Technology	150
Figure A.6	Non-dispersive Infrared Analyzer	151
Figure A.7	Paramagnetic Detector Technology	152
Figure B.1	A model for wind tunnel as constant pressure enclosure	161
Figure B.2	Time trace of concentrations of CO_2, HC and CO during an experiment in the closed-loop wind tunnel	162
Figure B.3	Ratio of concentrations of major carbon containing species divided by temperature during an experiment in tunnel	163
Figure C	Ultrasonic atomizing droplets generator	169
Figure D.1	Optical setup for the measurement of diffraction patterns	174
Figure D.2	Particle size analysis	176

NOMENCLATURE

a,b,d,e	Unknown stoichiometric coefficients
A, B, C	Arbitrary constants
AEUB	Alberta Energy and Utility Board
C1, C2, etc.	Hydrocarbons with 1 and 2 carbon atoms in each molecule
C7+	Hydrocarbons with 7 or more carbon atoms in each molecule
C_xH_y	General hydrocarbon fuel
C_mH_n	General hydrocarbon in the product of combustion
CO_2	Carbon dioxide
CO	Carbon monoxide
d	Flare stack diameter (mm)
	i Inside diameter
	o Outside diameter
ρ_j	Flare gas density (kg/m^3)
ρ_∞	Density of air (kg/m^3)
$\Delta\rho_o$	Density difference between the jet and surrounding air
ρ_m	Mean density of droplet
η	Carbon conversion efficiency
FID	Flame Ionization Detector
g	Gravitational constant ($9.81\ m/s^2$)
H_2	Hydrogen
He	Helium

H_2S	Hydrogen sulphide
HHV	High heating value (MJ/m^3)
HC	Hydrocarbon
L	A characteristics length scale (m)
LDV	Laser Doppler Velocimeter
$\dot{m}_L$	Mass flow rate of liquid (g/min)
$\dot{m}_G$	Mass flow rate of gas (g/min)
M	Molecular weight (kg/kmole)
α	Molar fraction between fully oxidized carbon (CO2) and partial oxidized carbon (CO)
N_2	Nitrogen
NDIR	Non-dispersive Infrared Analyzer
n	Number of atoms
ng	Natural Gas
O_2	Oxygen
Oct	Iso-octane
P	Pressure
PAH	Poly-nuclear aromatic hydrocarbons
Q_{in}	Volume flow rate of ambient air entering into wind tunnel
Q_{out}	Volume flow rate of tunnel gases flowing out of the tunnel
$Q_{combust}$	Volume flow rate of tunnel air involved in combustion
$Q_{i,emitted}$	Volume flow rate of the species *i* emitted in to the tunnel
$Q_{i,inert}$	Volume flow rate of the flare gases flowing into the wind tunnel unaffected by combustion

Q'_{fuel}	Volume flow rate of gaseous fuel
R	Momentum flux ratio
R_j	Radius of the stack (mm)
R_p	Radius of the plume (mm)
Re	Reynolds number
γ'	Ratio of gaseous moles of products to the gaseous moles of fuel
SO_2	Sulpher dioxide
T	Temperature
U_∞	Crosswind speed (m/s)
VOC	Volatile organic compound
V_j	Jet exit velocity (m/s)
V	Volume of wind tunnel
Y	Mole fraction

Chapter 1 INTRODUCTION

Both conventional and heavy oil exists in the form of underground pools known as "reservoirs". Under high pressure conditions, the light hydrocarbons trapped in these reservoirs exist either in the form of compressed liquid or as a gas dissolved in the liquid oil or water. When the oil and water are extracted from the high pressure reservoir to the surface, the light hydrocarbons become vapor at ambient conditions and are collected as a mixture of both combustible gas and liquid. The oil is then separated from any associated water and gaseous hydrocarbons at a facility that is called an "oil battery". The gas that is collected with the extraction of oil is commonly known as "solution gas" even though not all these gases were in solution. The water is usually re-injected into the reservoir of origin and the solution gas is either processed for commercial needs, flared or vented to the atmosphere.

The composition of the solution gas is highly variable from site-to-site. Johnson *et. al.* (2001), analyzed the data from 5614 well sites in Alberta, whose samples of solution gas were measured for concentrations of various gases at those sites. The results showed the presence of a wide variety of hydrocarbons (C1 to C7+) and other gases (N_2, CO_2, H_2, He, H_2S) in the solution gas. The concentration of methane varied essentially from 0 to 100%, however the average concentration of methane was 70% in the solution gas. Similarly, the average concentrations of heavier hydrocarbons (C2, C3, C4, C5, C6, C7+) and other gases also varied widely. Therefore, the composition of solution gas with

respect to various well sites cannot easily be characterized due to the wide variability in the concentrations of the gases contained in it.

Oil batteries are equipped to allow preliminary processing and storing the oil before transporting it to the oil refineries. These sites may also be capable of piping any solution gas produced to a gas plant. The solution gas is processed and modified at the gas plants, where most of its undesirable components (e.g. H_2S and excessive amounts of either CO_2 or N_2) are stripped off and the remaining gas is sold as a sales grade natural gas or propane. The treatment of the solution gas in this manner is referred to as "conservation" of the gas. In Alberta, 20.8×10^9 m^3 of solution gas was produced and 19.5×10^9 m^3 (94.1%) was conserved in the year 2001. The conservation rate of solution gas achieved in year 2001 was 1% more than that achieved in year 2000 and was equal to the volume conserved in the year 1999 (AEUB, 2002).

If the transportation cost of the solution gas to a gas plant is high due to the remote location of the oil battery, the solution gas becomes a waste product and requires disposal at the site. The most economical way to dispose of the solution gas is to vent it directly into the atmosphere. Most hydrocarbons are environmental pollutants and can be a strong source of emitting greenhouse gases into the atmosphere. The global warming potential of methane is approximately 21 times greater than CO_2 by mass (7.7 times greater by volume) (Houghton *et. al.*, 1996). Therefore, it is not recommended to release the solution gas untreated into the atmosphere. In Alberta, 1.2×10^9 m^3 (approx. 5.9%) of

solution gas was disposed of at battery sites in 2001 (AEUB, 2002). Table 1. shows yearly statistics of the solution gas conserved, flared and vented.

Table 1: Solution Gas Conserved, and Flared and Vented (AEUB, 2002)

Year	Conserved (10^9 m^3)	Conserved (%)	Flared and Vented (10^9 m^3)
1992	18.0	90.2	1.97
1993	18.5	90.2	2.02
1994	19.7	91.1	1.92
1995	20.1	91.3	1.92
1996	20.9	92	1.81
1997	21.1	92.7	1.66
1998	22.0	93.3	1.58
1999	22.3	94.1	1.40
2000	20.6	93.1	1.53
2001	19.5	94.1	1.22

A more appropriate way to dispose of these waste gases than venting is "flaring". Flaring is a process of burning waste combustible gases collected at the oil battery and releasing the products of combustion into the atmosphere. Flaring of solution gas is typically done with a long vertical pipe, known as flare stack that is usually made of Schedule-40 pipe, approximately 10 m high and 10 cm in diameter. Besides the size of the stack and composition of the gas being flared, other important parameters associated with flaring are the exit velocity (V_j) of the solution gas, and wind speed (U_∞). In Alberta, the yearly average wind speed can vary with location from 2 m/s to 5.5 m/s (Majeski, 2000). The estimated typical exit velocities for the solution gas flares would be less than 6 m/s (Johnson, 2000). The ratio U_∞/V_j may have a significant affect on flare performance and could easily vary from zero to 25 resulting in either upright or horizontally bent over

flames respectively (Johnson and Kostiuk, 2000). In flares, the air and fuel (solution gas) are not premixed, therefore combustion occurs as a diffusion flame in a crosswind.

The goal of flaring is to consume all the flammable gases directed to it in a reliable, efficient and safe way by oxidizing these gases. The solution gas can also contains hydrogen sulfide (H_2S) in varying amounts, which is also one of the distinguishing character of the gas collected at various oil batteries. If the gas has less than 10 ppm of H_2S, it is said to be "sweet" and the gas having more than 10 ppm of H_2S is referred to as "sour" (Johnson *et. al.*, 2001). Flaring is considered to be the most economical method of disposing waste gases by hopefully converting all the hydrocarbons and hydrogen sulphide to CO_2, SO_2 and water vapor (Prybysh, 2002).

In practice not all of the fuel gases are converted to CO_2, H_2O and SO_2. Some remains as fuels and some are converted to undesired products (*e.g.* carbon monoxide or smoke). This partial conversion of the fuel is often quantified by a conversion or combustion efficiency. A flare is said to be 100% efficient, when it fully oxidizes all combustible gases directed to it. Two types of combustion efficiencies are generally associated with flaring, the carbon conversion efficiency and the sulphur conversion efficiency. The ability of a flare to fully convert all the carbon in hydrocarbons into CO_2 is the carbon conversion efficiency. Similarly, if the flare stream contains H_2S, the portion of sulpher in this fuel that is converted into SO_2 is termed the sulphur conversion efficiency. For this study, the combustion efficiency is defined as the ratio of the mass flow rate of carbon in

the form of CO_2 produced by the flame to the mass flow rate of carbon contained in hydrocarbon fuel in the flare stream, as it deals with pure hydrocarbon fuel only.

Though this thesis focuses on flaring typical of solution gas flares, it may also be useful to see it within the context of flaring in general. Flaring is extensively used by energy and petrochemical industries worldwide. Flaring serves different purposes within various operations to meet the requirements of that industry. In the petroleum industry, it can be roughly categorized as either emergency or process and production flaring. At large facilities like refineries and gas plants, the main concern of flaring is the safety of both personnel and the plants in dealing with combustible gases. Therefore, a large volume of the gases may have to be disposed of in seconds in emergency situations. Flow rates of these gases can be very high with exit velocities that sometime approaches sonic speeds under these conditions. Process flaring also occurs at refineries, sour gas plants and petrochemical plants. At these facilities, gases that leak past relief valves are shunted to a process flare for disposal. Flow rates of the gases in process flares are relatively low and these flares burn almost continuously. Jones (1973), and Brzustowski (1976), provided an overview and discussed some of the technologies applied to emergency and process flaring. During the initial development of a gas well, gases are usually flared continuously at a very high flow rates for couple of days to determine the production capability of the well. This type of flaring is known as a well test flares. Based on these characteristic velocities, there is a similarity between solution gas flares and process flares but not emergency or well test flares (Johnson *et. al.*, 2001).

1.1 Environmental Issue of Flaring

In 1997, the estimated volume of the gas flared worldwide was 101.9 billion m^3 (EIA, 2000). In 2001, it was reported that 56.4 million m^3 of conventional oil and 20.7 billion m^3 of solution gas had been produced throughout Alberta. Although 19.5 billion m^3 of the solution gas was conserved, approximately 6% (1.22 billion m^3) of the solution gas was flared (AEUB, 2002). This huge volume of the gas being flared (or vented) raises the environmental concern in the public and regulatory industry (Johnson *et. al.*, 2001). Alberta Energy and Utility Board (AEUB) administers a framework in Alberta that gives a choice of conserving or flaring solution gas at any battery site. The reasons that compel flaring or venting instead of conserving the solution gas are flow rates of the gas, low energy density (low heating value) of the gas, presence of H_2S or other contamination in the gas, safety, proximity to the available infrastructure and economics. Emissions from the flaring may have a major affect on the environment. Johnson *et. al.* (2001), analyzed field data of the oil and bitumen battery sites scattered through out Alberta that flared or vented the solution gas. There were 4499 battery sites that reported flaring or venting of solution gas in year 1999. Information to distinguish the battery sites, where the solution gas was flared from those, where it was vented was not available in the data. While, AEUB (2002), reported 3742 oil and bitumen batteries that flared the solution gas in year 2001.

In case of inefficient flaring, the products of combustion could contain unburned hydrocarbon fuel (HC), carbon monoxide (CO), and soot along with other toxic

compounds (for the detail of these compounds see Strosher, 1996). The flare stream having methane and H_2S will emit these gases as products of incomplete combustion to the atmosphere causing an increase in greenhouse gases and toxic compounds in the environment. The emissions of CO_2 and unburned hydrocarbons are well known greenhouse gases having global warming potential. Therefore, on a global perspective, flare emissions contributes to global warming. At a local level, the emission of hydrocarbons and oxides of nitrogen contributes to smog and there is a strong evidence that flares produce and emit a variety of toxic compounds (Strosher, 1996).

AEUB (1999), Pohl and Soelberg (1986), Siegel (1980), and Pohl *et. al.* (1986), along with other researchers observed that as long as the flare remained stable, flare efficiencies were high (>95%). The United States Environmental Protection Agency (EPA) sponsored many of these studies and concluded that as long as the flame remained stable, the flare efficiencies were greater than 98% for the gas mixtures tested. This conclusion focused attention toward understanding the set of parameters that would ensure stable combustion in order to achieve this high combustion efficiency. The parameters they proposed for stable flares are the exit velocity (V_j) and the higher heating value (HHV) of the flare gas. Current United States Codes of Federal Regulations (CFR) on flaring are founded on the results from these EPA sponsored studies. But these regulations have a little impact on the guidelines recommended by the American Petroleum Institute (API) for flares and do not include any effects of the wind.

The Alberta Research Council (ARC) performed a multiyear study on flare efficiency in the field on one "sweet" and one "sour" solution gas oil battery. The tests were conducted at normal operating conditions and the wind conditions were also reported at the time of the tests. In 1996, ARC released a report with the results from these experiments performed in the field. According to this report, the combustion efficiencies of the flare at the chosen battery sites were as low as 62%. The main factor claimed to cause the decrease in combustion efficiency at both the sites, was the inclusion of liquid fuel and water in the flare gas. Both facilities were equipped to separate liquids from gases.

At the "sweet" battery site, two different liquid fuels were directed to the flare stream. First stream of liquid was directed from the separator, where it contained both liquid fuel and water. The second stream contained only liquid fuel as it was directed from the location downstream of the separator, where water had been separated. The mean wind speeds at the time of the tests were 3.5m/s to 7.2 m/s. The amount of liquid added to the flare gas at the time of the test could not be measured. The observed combustion efficiencies were 62.1% and 62.7% (Strosher, 1996).

The solution gas at chosen "sour" battery site contained 20% to 25% H_2S and the liquid hydrocarbons were collected at the top of the liquid knockout drum. The measured combustion efficiency at this site was 84.1%. ARC performed the study to look specifically for the toxic compounds in the flare emissions, which showed the existence of more than 150 volatile organic compounds (VOC) and poly-nuclear aromatic hydrocarbons (PAHs) in the products of combustion (Strosher, 1996).

The decrease in efficiency of the flares at both the sites were considered to be due to inclusion of the liquid droplets in the flare streams.

1.2 Approach of the Flare Research Project

The Alberta Energy and Utility Board (AEUB) sets regulations for the energy industry and has suggested guidelines to reduce the volume of solution gas flaring. According to AEUB, 1996 annual report, there should be a 15% and 25% decrease in the volume of solution gas flaring by the end of years 2000 and 2001, respectively (AEUB, 1999). The volume of the solution gas can be reduced if there is an alternative that could give a better outcome than flaring. The generation of electricity through a mini-gas turbine using the solution gas has been suggested to be good alternative to the flaring. A more detailed and complete presentation of alternatives is given in the report of the Alberta Clean Air Strategic Alliance (CASA) (Holford and Hettiaratchi, 1998). Unfortunately, these alternatives have not been broadly implemented because of technical and economic problems. For example, the solution gas may contain H_2S, which can be corrosive and can lead to sever corrosion of the metal parts. With the identification of alternatives to flaring, several barriers in implementing those alternatives were also identified. The strategy of reducing flaring or improving the performance of flares can only be successfully implemented, when accurate basic information is available (*e.g.* flow rates, composition etc.). The quality of available field data was not good enough to assess the economics barriers in the implementation of any strategy. Hence, flares currently in use must be dealt with for many years. Another task of AEUB is defining and then

implementing the requirements and conditions that would ensure the better performance of the flares. This means measuring the flare performance becomes an important issue that needs the attention of researchers. Since, there is currently no such technology available to measure flare performance accurately in the field, research is needed to work on this area. Also, contradiction between results from EPA and ARC requires further information and research on flares to resolve.

Requirements of AEUB, together with EPA and ARC results were initiating points for the University of Alberta Flare Research Project. The main goal of the project was to understand the main parameters that affect combustion efficiency and emissions from flares.

This research project has been built up with an approach to study scaled down flares under well-controlled conditions such as crosswind speed, exit velocity of the flare stream, complete collection and then analysis of the products of combustion using a closed-loop wind tunnel. This laboratory setting also allows blending together various gases to create a variety of flare streams. The advantage of having control on these conditions is that emission tests can be repeated. Furthermore, flares can be tested for results under a desired set of conditions. To obtain results as close to flaring of solution gases in the field, several flare gases can be tested in the wind tunnel along with the arrangement to blend them with inert compounds. Addition of inert compounds lowers the energy density of the gas, which has a significant affect on flare performance. These studies also showed that flare efficiency is a function of crosswind speed (U_∞), exit

velocity of jet (V_j), and stack diameter, d. For a given gas exit velocity, the overall efficiency of the flare decreases with the increase in crosswind speed and higher velocity jets are less susceptible to the crosswinds (Johnson and Kostiuk, 2000).

One issue that has not been dealt with at the University of Alberta Flare Research Project but brought up by ARC, is the inclusion of water or liquid hydrocarbons that escapes from the liquid knockout system and become part of the flare gas. These liquids could have a significant affect on the combustion efficiency of the flares. Results reported by ARC suggested that combustion efficiency decreased by the addition of liquid fuel droplets (Strosher, 1996). The study provided no information about the amount of the liquid fuel, droplet size, and mass fraction of the liquid fuel flared and corresponding influence on combustion efficiency. Therefore, one of the main focuses of this thesis is to conduct a detailed study in order to examine the effects of liquid droplets of various sizes on the flare efficiency at varying crosswind speed and exit velocity of the flare gas.

1.3 Potential Source of Liquid Droplets

As liquids and gases are separated at the oil battery, it is generally accepted that a considerable amount of liquid droplets elude the liquid knockout system, which are carried to the flare as liquid droplets entrained in the flare stream. Information regarding the composition, mass fraction and the size of these droplets does not exist. Given that solution gas is typically dissolved in an oil/water mixture in the underground formation, it is probable that the entrained liquids are a mixture of water and heavier hydrocarbons (C5

to C20). The other possible source of the liquid droplets is through condensation of saturated hydrocarbon or water vapors in the flare stream, which is associated with cooling of the flare stream from the process condition at the battery site to ambient conditions at the flare. These liquid droplets in the flare stream may have a significant affect on the flare efficiency and emissions from the flare depending upon the size, amount and composition of the droplets.

Thermal radiation emitted from the flame may cause droplets to evaporate. Small droplets will likely evaporate and mix within the flare stream before reaching the flame. While larger droplets only partially evaporate and reach the flame in the liquid phase. At the flame, some of the droplets evaporate but still a few large size droplets that survive evaporation remain in the combustion plume or fall out of the flow (Kostiuk, 2000). The droplets of heavier hydrocarbons increase the tendency of the flare to emit soot and toxic compound, when they evaporate before the flame (Glassman, 1977). Evaporation of droplets before reaching the flame also increases the energy density of the flare stream that is less susceptible to crosswinds. Therefore, it is hard to predict the effects of hydrocarbon droplets in the flare stream on the inefficiency of the flares.

If the flare stream contains water droplets, then the effects of these droplets on flare efficiency will be different than that of hydrocarbon fuels. Water droplets extract energy from the flame to evaporate, causing a decrease in the temperature of the products of combustion. However, water droplets that evaporate before the flame dilute the fuel gases and lower their energy density. If water contains any salt (*e.g.* Sodium Chloride), chlorine

could act as a chemical inhibitor to combustion, form a strong vapor-phase acid, or be emitted as a chlorinated hydrocarbon. It is also difficult to predict the overall effects of water droplets on the flare efficiency (Kostiuk, 2000). Strosher (1996), added two different liquid hydrocarbon streams to the flare to examine the emissions and effects of these droplets on flare efficiency. One stream was directed from the separator, where it contained hydrocarbon fuel and water. The other stream was directed from a location downstream of separator, where it only contained hydrocarbon fuel. Results showed that both streams have almost identical effects on the flare efficiency but emissions from the liquid stream without water produced more carbon particulate than the one with water droplets. This suggested that presence of liquid hydrocarbon droplets in the flare stream decreased the combustion efficiency of the flares.

1.4 Objectives and Outline of This Thesis Research

Previous research on investigating the efficiency of the flares has considered only gaseous flare streams. Information available on the effects of liquid droplets in the flare stream is not sufficient to predict the impact that these droplets on flare efficiency under varying atmospheric conditions. Hence, one of the main objectives of this thesis research is to measure effects of liquid droplets on the combustion efficiency of the flare in crosswinds. Sales grade natural gas is used as flare gas and three different liquids (*i.e.* iso-octane, diesel and distilled water) have been selected for this study. Important parameters that are manipulated as part of this study with liquid droplets are the mass fraction of the liquid droplets flared and mean droplet size.

The wind tunnel facility at University of Alberta is designed to produce low turbulence crosswinds (0.4% turbulence intensity), in the core flow (Johnson *et. al.*, 2001). Previous models have been developed to predict the efficiency of flares based on very low turbulence in the crosswind. Yet, flares in the field are exposed to turbulence of variable intensities in the crosswind. Hence, the second objective of this thesis research is to study the flare efficiency under turbulent crosswind conditions.

All the studies and research on the flares have been conducted with a fixed ratio of dimensions of the flare stack (*i.e.* inner and outer diameter). The inner diameter (d_i) and the outer diameter (d_o) of the full-scale flare are 102.3 mm and 114.3 mm, respectively (Kostiuk, 2000). University of Alberta Flare Research Project has been conducting the research on flares by keeping the ratio of d_i/d_o constant (*i.e.* 0.9) in order to maintain the geometric similarity for scale down flares. The third objective of this thesis research is to study the effects of varying outer diameter (d_o) of the flare stack on the efficiency of the flare while keeping the inner diameter (d_i) unchanged.

The structure of the thesis is that Chapter 2 provides a review of relevant literature on flares with and without liquid droplet in the flare stream. Chapter 3 discusses the experimental setup and methodology adopted for measuring effects of the liquid droplets, turbulence in the crosswind, and flare stack diameter ratios on flare efficiency. The results form all these experiments are presented in Chapters 4 and 5.

References:

1. Johnson, M. R., Spangelo, J. L, and Kostiuk, L. W. (2001), " *A characterization of Solution Gas Flaring in Alberta"*, Air & Waste Management Association, 51: 1167-1177.
2. Alberta Energy and Utility Board (2002), "*Upstream Petroleum Industry Flaring and Venting Report",* Alberta Energy and Utility Board Statistical Series 2002-60B, July 2002, 66 Pages.
3. Houghton, J. T., Meira Filho, L. G, Callader, B. A., Harris, N., Kattenberg, A., and Maskell, K. (1996), *"Climate Change 1995: The Science of Climate Change"*, IPCC (Intergovernmental Panel on Climate Change) Cambridge University Press, Cambridge, U. K., 572 pages.
4. Majeski, A. J. (2000), " *Size and Shape of Low Momentum Jet Diffusion Flames in Cross Flow"*, M.Sc. Dissertation, University of Alberta, Edmonton, Alberta, Canada
5. Johnson, M. R., Kostiuk, L. W. (2000), " *Efficiency of Low Momentum Jet Diffusion Flames in Crosswinds"*, Combustion and Flames 123, pp.189-200.
6. Prybysh, R. (2002), "*The Production of Toxic Emissions from Reacting Diffusion Jet Flame in a Crossflow"*, M.Sc. Dissertation, University of Alberta, Edmonton, Alberta, Canada
7. Jones, H. R. (1973), " *Pollution Control in the Petroleum Industry",* Noyes Data Corporation, Park Ridge, New Jersey, 322 pages.
8. Brzustowski, T. A. (1976), *"Flaring in the Energy Industry", Progress in Energy and Combustion Science,* 2, pp. 129-141.

9. Energy Information Administration (2000), " *International Energy Annual 1998"* DOE/EIA-0219(98), Office of Energy Markets and End Use, U.S. Department of Energy, 250 pages.

10. Strosher, M., (1996), *"Investigation of Flare Gas Emissions in Alberta",* Alberta Research Council Report to Environment Canada, Alberta Energy and Utility Board, and Canadian Association of Petroleum Producers, 145 pages.

11. Alberta Energy and Utility Board (1999), "*GUIDE 60: Upstream Petroleum Industry Flaring Requirements",* Alberta Energy and Utility Board Guide Series, 1st Ed., July, 75 Pages.

12. Pohl, J. H. and Soelberg, N. R. (1986), *" Evaluation of the efficiency of Industrial Flares: H2S Gas Mixtures and Pilot Assisted Flares"*, U.S. Environmental Protection Agency, Report Number:EPA/600/2-86/080, NTIS, September.

13. Siegel, K. D. (1980), *"Uber den Umsatzgard von Facelgas in Raffinerie-Hochfackeln" (Degree of Conversion of Flare Gas in Refinery Flare),* Ph.D Dissertation, University of Karlsruhe, Germany.

14. Pohl, J. H., Lee, J., Payne, R., and Tichenor, B.A. (1986), *"Combustion Efficiency of Flares",* Combustion Science and Technology, Vol. 50:217-231.

15. American Petroleum Institute (1997), *" Guide for Pressure-Relieving and Depressuring Systems",* API Recommended Practice 521, 4th Edition, 104 pages.

16. Holford, M. R. and Hettiaratchi, J. P. (1998), *"An Evaluation of Potential Technologies for Reducing Solution Gas Flaring in Alberta",* Report to Clean Air Strategic Alliance (CASA) Flaring Project Team, University of Calgary, Calgary, Alberta, 13 Pages.

17. Kostiuk, L. W. (2000), *"University of Alberta Flare Research Project, Interim Report November 1996-June 2000"*.

18. Glassman I. (1977), *"Combustion"*, Academic Press Inc., New York, U.S.A.

Chapter 2

REVIEW OF RELATIVE LITERATURE

Solution gas collected at the oil batteries is either conserved or disposed to the atmosphere by flaring. Since, fuel (solution gas) burns unmixed in an oxidizing environment, flares fall under the category of diffusion flames. Solution gas exits the flare stack with a certain velocity in the form of a jet in an environment, where the air has a certain cross-flowing velocity. Combustion occurs as a result of the reactions between the solution gas and the oxygen at the interface of mixing and defines the location of the flame. Therefore, a flare can be referred to as a jet diffusion flame in crosswinds. Jets in crosswinds can be classified as either reacting or non-reacting. For example, the dispersion of smoke from the chimneys is a non-reacting jet in crosswind. Similarly, an industrial flare is a good example of a reacting jet in crosswind. It is also generally accepted that some liquid fuel droplets escape from the liquid knockout system, combine and burn as part of the flare stream. Therefore, understanding of industrial flares requires knowledge of the combustion processes involved in diffusion flames and chemistry of diffusion flame. This chapter discusses the principles and processes involved in a diffusion flame. Reacting and non-reacting jets in crosswinds are also discussed in light of previous research conducted on laboratory as well as industrial flares. One of the major emphases of this thesis research is investigating effects of liquid fuel droplets on the flares. Therefore, processes involved in combustion of liquid fuel and liquid fuel in the form of a spray are also discussed in this chapter.

2.1 Diffusion Flames

There are many combustion processes and devices in which air and fuel are not premixed and remain separated until being brought into intimate contact with one another in the immediate vicinity of the flame. Diffusion flame is the name given to such a process in which air and fuel are not premixed but the fuel and oxidant diffuses into each other. A complex set of processes occurs in the flame that includes mixing, precombustion, combustion and post flame reactions and vaporization, when the fuel is liquid or volatilization, when it is a solid (Edwards, 1974). In this type of the flame, mixing is slow as compared to reaction rates, so mixing is controlled by burning rate. The most distinctive characteristic of a diffusion flame is that the burning rate is determined by the rate at which the fuel and oxidizer are brought together in proper proportions for the reaction (Glassman, 1977). In its simplest form, diffusion flames consists of an exothermic reaction zone separating relatively pure samples of oxidizer and fuel gases. As such it does not exhibit a characteristics propagation velocity. However, the characteristics of diffusion flames are markedly dependent on aerodynamics of the particular flow situation. Diffusion flames have been studied as an impinging-jet and the cylindrical diffusion flame that occurred above the circular port (Strehlow, 1968). It was observed that the increased flow rates of the fuel and oxidizer resulted in a thinner flame in the neighborhood of the axis of the flow, and at a particular flow rate the central portion of the flame could not support itself and the flame was blown out. The flame appeared to have a hole in its center completely surrounded by an ordinary diffusion flame. The limited behavior of the flame was related to gross aerodynamics of the flow.

Cylindrical diffusion flames of hydrogen have been studied in a large enclosure under laminar flow conditions. It was observed that the combustion rate at any level was controlled by diffusional processes and that all attached diffusion flames show a thin hot-reaction zone at the point of attachment. Diffusion flame is a slow burning process at the local level and its overall behavior is highly affected by buoyancy (Strehlow, 1968). Flaring by the energy and petrochemical industries also falls under the category of "diffusion flames", because the fuel (solution gas) burns in an open atmosphere, when it exits the flare stack.

2.1.1 Principles of Diffusion Flame Combustion

Since, a considerable quantity of air or oxidizer is needed for combustion to occur, the shape of a diffusion flame depends upon the quantity of air supplied. An excess of air results in a close and elongated flame. Similarly, supplying the air below the stoichiometric amount results in a fan-shaped, under-ventilated flame. The diffusion flame has a wide region over which composition of gases changes due to interdiffusion of reactants and products. The concentrations of fuel and oxidizer are minima at the flame front, where the product concentrations are maxima (Glassman, 1977). The processes that occur in a diffusion flame are arranged and shown in a sequence in Figure 2.1. As shown in this figure, the precombustion reactions occur before mixing of fuel and air. Therefore, it does not contain oxidizing species. The arrows represent the transfer of heat and radical species. The driving forces for these reactions are the transport of thermal energy by heat

transfer and active species by mass diffusion from the combustion zone to the precombustion zone.

Precombustion reactions of a diffusion flame are pyrolytic, reaction products contain unsaturated species such as olefins, acetylenes and small particles resulting from polymerization. There are some additional reactions as a result of interactions between unsaturated species. The existence of these particles enhances the transfer of thermal energy between precombustion and combustion zone of a diffusion flame. When these particles pass through the flame, they not only give the characteristic luminosity to the diffusion flame but also are responsible for the transfer of radiant energy to the particles forming in the precombustion zone. The particles forming in the precombustion zone absorb the energy radiated form the combustion zone. A portion of this energy is transferred by conduction to gaseous species in the precombustion zone resulting in the increase of temperature and promotes gas phase pyrolytic reaction. This exchange of radiant energy by the particles plays an important role in the luminous diffusion flame. In fact, it is this coupling of the zones that drive the pyrolytic precombustion reactions, which are generally endothermic (*i.e.* the reactions require energy to proceed). The detail of pyrolytic reactions can be seen elsewhere (Edwards, 1974).

In diffusion flames, the fuel and oxidant are initially separated, therefore, no combustion can occur no matter how high the temperature of the fuel rises before mixing. Certain physical processes such as turbulence influence mixing of both the fuel and oxidant, and control ignition of the flame. Since, the precombustion reactions continue until the

complete mixing of the fuel and oxidant, the extent of this mixing influence emission from the flame. Incomplete mixing may result in emission of soot or a large quantity of particulate material and other products of incomplete combustion.

The physical structure of a diffusion flame is shown in Figure 2.2. Air and fuel are not premixed and the flame only occurs in a region, where they properly mix. A considerable amount of thermal energy transforms from the flame, which is sufficient to raise the temperature of air near it. The width of the combustion zone depends upon the way fuel and oxidants are brought into contact.

2.1.2 Jet Diffusion Flames

Combustion of gaseous fuel is shown in Figure 2.3, where fuel and oxidant are shown as reacting in a thin reaction envelope (the flame). As the fuel passes through the neck of the jet to the reaction envelope, precombustion reactions take place in the region within this envelope. The hot products of combustion rise up due to buoyancy, allowing surrounding air to be drawn in around the base of the flame. Since, the fuel does not contain any oxidant or air, the flame cannot flash back in to the burner. Similarly, with an increase in velocity of the fuel, the length of the reaction zone changes to accommodate it without blowing off the flame (Edwards, 1974).

Flaring, which is mostly done by energy and petrochemical industries falls under the category of jet diffusion flames. Solution gas exits the flare stack with a certain velocity

into an environment, where the wind crosses it with a certain velocity, it may also be considered a jet diffusion flame in crosswind.

Jet diffusion flames have been investigated both as laminar and turbulent flames. The buoyancy of hot products of combustion and momentum of the fuel causes fresh air to be entrained in the flame, resulting in a continuous combustion process. Laminar diffusion flames have been studied by Hottel and Hawthorne (1949), who showed that the flames had a well-defined flame front. Similarly, the size and species concentrations of laminar jet diffusion flames under various conditions have also been studied by Roper (1977).

In turbulent diffusion flames, the flame appears wider due to increased air/fuel mixing caused by turbulence of the jet. The flame front is uneven and distorted due to eddies generated by the interactions of the jet and air. Turbulence may increase entrainment of air but still molecular diffusion dominates the transport of fuel and air near the flame. The surface of turbulent diffusion flame is wrinkled, molecular diffusion is enhanced due to the larger surface area of the flame. Hence, for the same mass flow rate, the length of a turbulent diffusion flame is much shorter than a laminar diffusion flame. Increasing mass flow rate of the fuel does not affect the length of turbulent flames, rather it enhances turbulence in the jet resulting in more surface area of the flame for molecular diffusion. A model was prepared by Pitts (1988), describing the length of turbulent diffusion flame, where it was shown that length of the flame remained consistent until the flame began to blow off.

Jet diffusion flames can also be classified as lifted and non-lifted flames. Lifted flames are ones with higher momentum flux and the base of the flame move away as the fuel exits the flare stack. Lifted jet diffusion flames in a crosswind have been studied by Muniz and Mungal (1997), Hasselbrink and Mungal (1998). Unfortunately, their work can not be interpreted relative to continuous flares, as lifted flames require higher jet exit velocities than the average exit velocity of solution gas.

2.2 Jet in a Crosswind

The dispersion of smoke from chimneys and industrial flares are good representations of jets in crosswinds. The jet of a fluid exiting from the chimney or flare stack is carried away by the wind and is subjected to buoyancy. The flows are described either by their momentum flux ratio or their ratio of momentum to buoyancy. Momentum flux ratio (R) is the ratio of the momentum flux of the jet to the momentum flux of the cross-flow and is given as:

$$R = \frac{\rho_j V_j^2}{\rho_\infty U_\infty^2} \tag{2.1}$$

where ρ_j and ρ_∞ represent densities of the jet and cross-flow, respectively.

The ratio of momentum of the cross-flow to the buoyancy of the jet is known as the Richardson number (R_i) and is given as (Poudenx, 2000):

$$R_i = g\frac{V_j}{U_\infty^3}\frac{\Delta\rho_o}{\rho_\infty}\left[\frac{R_j}{R_p}\right]^2 L \qquad (2.2)$$

where:

g = Gravitational constant

L = A characteristic length scale

$\Delta\rho_o$ = Density difference between the jet and surrounding air

R_j = Radius of the stack

R_p = Radius of the plume

U_∞ = Crosswind speed

ρ_∞ = Density of Cross-flow

V_j = Velocity of the jet

Due to the variations in the downstream direction of the plume, Richardson number is hard to predict. Therefore, it is difficult to use as compared to the momentum flux ratio.

2.2.1 Non-Reacting Jets in Crosswind

Before considering jet diffusion flames in crosswinds in detail, it is useful to review the non-reacting case first. Dispersion of smoke from chimneys is one of the good examples of non-reacting jet in crosswind. Jets and plumes in a crosswind can also be distinguished as buoyant and non-buoyant. If the density of the jet or plume is less than the surrounding air and the initial jet momentum is low, then the dominant factor in plume rise in

downstream direction will be buoyancy. A "2/3 power law" predicts the rise of such plumes. The plume rises as the distance from the stack with the power of 2/3.

When, the densities of the jet or plume and the surrounding air are same then momentum is the dominant factor in predicting the plume rise in the downstream direction. A "1/3 power law" is used for the rise of such plumes (*i.e.* the plume rises as the distance from the flare stack with the power of 1/3).

In case of the plumes with momentum flux ratios less than 2.5 (R<2.5), part of the plume is drawn downward on the leeward face of the stack. Such plumes are known as "downwash", which is also an important phenomenon in both reacting and non-reacting jets (Majeski, 2000).

The structure and trajectory of the jet in crosswind was studied in detail by Smith and Mungal (1998). They also investigated the concentration profile and mixing of the jet in a crosswind. They observed that the interaction between the jet and the crosswind generated vorticity that appeared in various forms and shapes.

2.2.2 Reacting Jets in Crosswind

When, the flows are allowed to react with each other, several new phenomena are introduced. Since, the fuel jet is introduced to an oxidizing environment in industrial flares. Combustion occurs, when the fuel mixes eventually by molecular diffusion with a

stoichiometric amount of oxygen. Gollahalli *et. al.* (1975), conducted research on the length and shape of hydrogen flames in a cross-flow. The objective of the study was to compare their results with emergency release of hydrogen from industrial processes. Flames with jet Reynolds number (*Re*) from 16,000 to 68,300 and momentum flux ratio (*R*) from 63 to 1873 were studied to determine the size and trajectory of these flames. The conclusion from their research was that both the cold flowing (non-reacting) and reacting jets had almost similar trajectories but the width of cold flowing plume was less than the width of the reacting jet.

Kalghatgi (1981 and 1983), conducted a study on jet diffusion flames in still air and a crosswind in order to find out their blow-off limits. He did not attempt to measure the combustion efficiency of these flames. He also studied the shape and size of jet diffusion flames in a crosswind using the flare stacks of various sizes (6mm to 22mm). He observed similar patterns in the sizes and shapes of these flames and concluded that these small-scale flames could be used to predict the shape and size of larger diffusion flames in a crosswind.

Huang and Chang (1994), studied lifted flames. They observed that the base of the flame lifted from the stack, when it was ignited below a critical crosswind speed (U_∞) irrespective of the change in the jet exit velocity (V_j). Whereas, above that particular crosswind speed, the flame did not lift. These flames were termed as never-lift or non-lifted flames, respectively. They also studied jet diffusion flames with low momentum flux ratios. They described such flames as "wake-stabilized", where a portion of the

flame was trapped in recirculation zone in the wake of the flare stack. The structure and stability of small diameter (about 6mm) cross-flowing jet flames were examined during their study. Laser Doppler Velocimeter (LDV) was used to measure the mean velocity field for different locations and the flame temperature with the concentrations of CO_2, CO, and O_2 were measured by a linear transverse having numerous probes. They also classified the flame in six modes. Based on photographs and visual examination, at a given crosswind speed (U_∞), they identified the flame as developing, down-washed, flickering, flashing, dual, and pre-blowoff. The detail description of these modes can be found elsewhere (Majeski, 2000).

Jet diffusion flames were further investigated by Huang and Wang (1999). Based on momentum of the jet and the crosswind, they classified the flame in five different modes as: down-washed ($R<0.1$), cross-flow dominated ($0.1<R<1.6$), transitional ($1.6<R<3.0$), jet dominated ($3.0<R<10$) and strong jet ($R>10$). Besides the clear limits between the flame modes, it was still observed that there was no significant difference between jet dominated flame at low momentum ratio (R) and transitional flame at high momentum ratio (R) (Majeski, 2000).

Measuring the combustion efficiency of a jet diffusion flame in an open environment is a difficult task and research published on industrial flares in either crosswind or in quiescent environment is limited. Siegel (1980), subjected 0.7 m flare to crosswind using multi-point sampling technique, observed that the combustion efficiency was 99%. The draw back in his apparatus was that the crosswind could only affect the portion of the

flame above the stack, which means that the vortex shedding from the stack or a low pressure region in the wake of the flare stack would have not been created.

Johnson *et. al.* (2001), performed the most recent study on the efficiency of low momentum jet diffusion flames in crosswind. Using a different diameter quartz stacks with turbulence plugs, sales grade natural gas and commercial grade propane as fuel, he showed that the fuel type, exit velocity of fuel (V_j), crosswind speed (U_∞), and flare stack diameter had a notable effect on combustion efficiency. It was observed that some of the fuel stripped off from the jet before passing through the flame, resulting in an inefficient flame. With the increase in crosswind speed, the amount of fuel stripping was also increased. The results from both natural gas and propane were almost identical except that the natural gas flames were more susceptible to the effects of crosswind than propane flame. The fuel was also blended with inert compounds to decrease its energy density. It was observed that blending the flare gas with inert gases also had a significant affect on combustion efficiency. The efficiencies of the flame were higher at low crosswinds and decreased with the increase in the crosswind speed. Similarly, high velocity jets were less affected by the crosswind.

Poudenx (2000), conducted research on jet diffusion flames in crosswind. A technique was developed to analyze composition of the plume near the flame and then measure overall efficiency. The thermal cross-section of a plume near the flame was mapped using a linear array of 20 sample probs. The study described the structure of the plume to understand the causes of inefficient flame.

Majeski (2000), studied low momentum jet diffusion flames and measured the shape and trajectory of these flames in crosswind. He also modeled the length of jet diffusion flames in crosswind.

Prybysh (2002), conducted detailed research on particulate material in the emissions from flares. The observed affect of particulate material on the efficiency was negligible (0% for methane and 0.5% for propane). Therefore, research on measurement of particulate material production could be considered separate from measuring the efficiency of flares.

2.3 Field Studies on Flares

Research on combustion efficiency of flares in the field has been conducted by McDaniel (1983), and Keller and Noble (1983). They burned a mixture of nitrogen and propylene in various compositions, with the heating value of the fuel varied between 3 MJ/m^3 and 81 MJ/m^3. They observed that efficiency of the flare could be as low as 55% and 66%.

A field study was conducted on flares by Leahly and Davies (1984). The main focus of the study was on plume rise from these flares. It was observed that the plume behaved similar to a non-reacting jet, following "2/3 power law" over a distance of 450 m downstream of the flare stack.

Pohl *et. al.* (1986), conducted research on measuring the combustion efficiency of gaseous hydrocarbon fuels. They studied stable diffusion flames on a large scale. Vertical

pipes with diameters from 0.076 to 0.305 m were used to burn the fuel in near quiescent conditions and the entire plume was collected for calculating the efficiency. They concluded that as long as the flame remained stable, the combustion efficiencies were in excess of 98%. Where, flame stability was considered to be function of fuel exit velocity and higher heating value of the flare gas. They also blended the flare gas with inert compounds to lower the energy density of the fuel and observed that it lowered the combustion efficiency of the flare.

Kuiper *et. al.* (1996), measured the efficiency of a methane flare in an open but calm atmosphere using passive Fourier Transform Infrared and Differential Light Detection technique. The efficiency of the flare was observed to be 99%. The efficiencies of such low momentum jets may decrease, if exposed to the crosswind.

A field study was conducted by Strosher (1996), on the solution gas flares. He collected the products of combustion form the flares using a single-aspirating probe. The solution gas was observed to be a mixture of various hydrocarbons (C1-C6) and the combustion efficiency of the flare was as low as 67%.

2.4 Combustion of Liquid Fuels

When, most of the liquids or solid fuels are exposed to an atmosphere, where they can form a combustible mixture. A flame surrounds the liquid or solid phase as soon as this mixture is ignited. The flame is said to be a diffusion flame, when the condensed phase is considered to be liquid fuel and air as gaseous oxidizer. The fuel evaporates from the liquid surface and diffuses into the flame front, whereas oxygen diffuses from the surrounding to the flame front. An example of burning of a condensed phase in such a manner is considered to be the combustion of a liquid droplet. One of the factors that generally determines the rate of evaporation and burning of the liquid droplet is the rate at which the heat is transferred from the flame front to the droplet surface (Glassman, 1977).

The theory and experimental work on combustion of a liquid fuel droplet that leaves no solid residue on evaporation and has no solid products of combustion showed that there are three phases in the life of a fuel droplet, when it is exposed to hot gaseous oxidizer (Strehlow, 1968). First, ignition-delay time in which the concentration of the fuel vapors rises due to evaporation from the surface of the droplet to an extent, where ignition could occur. The diameter of the droplet changes very slightly during this period. Second, after ignition the burning of fuel occurs and the size of the droplet decreases until the whole liquid fuel is evaporated. Due to the small size of the droplet, large relative velocities do not occur and it may be assumed that the burning droplet is completely surrounded by

diffusion flame. The third period is the postdroplet period during which the residual fuel is consumed (Strehlow, 1968).

The processes involved in the combustion of the liquid fuel are shown in Figure 2.4. The rate of vaporization of liquid fuel is influenced by a number of factors (*e.g.* dispersion of liquid, energetics of the vaporization process, pressure etc.) that are explained elsewhere (Edwards, 1974). When, the fuel is vaporized it must be mixed with an oxidant (air) for combustion to occur. In case of diffusion flame, the way this mixing occurs is very important. The combustion of a droplet that is vaporized prior to combustion is different than a droplet that is engulfed or surrounded by the flame.

The physical structure of combustion of liquid fuel droplets is shown in Figure 2.5, where the fuel is completely vaporized before entering the combustion zone. However, it is not mixed with air and the diffusion flame occurs in a region, where this vaporized fuel mixes with air.

The flame that surrounds a drop provides energy that is sufficient for vaporization of the drop. The resulting fuel vapors leave the droplet surface and move towards the inner boundary of a diffusion flame. In this case, the combustion occurs in a thin zone, where air and fuel exist in a proportion that is sufficient for sustaining the flame. The fuel vapor already undergoes through pyrolytic precombustion reactions before entering the combustion zone. The final products of combustion diffuse away. Incomplete oxidation

of these vapors before passing through the reaction envelope may result in the generation of particulate material as they mix with the cool surrounding air.

2.4.1 Combustion of Fuel Sprays

As in case of a single isolated liquid fuel droplet, the combustion process is controlled by diffusive heat transfer at the droplet surface. However, it has been found experimentally that the flame propagates through a highly concentrated cloud of fine combustible particles. Exposure of a sufficiently small liquid fuel droplet to an oxidizing atmosphere results in a laminar flame that has quite similar characteristics to that of an ordinary premixed flame. To determine the structure and the burning mechanism of spray flames, particle size and relative volatility is important. For small droplets of high volatility, complete evaporation occurs in the preheat zone of the flame. Therefore, the flame appears to burn as a premixed flame. On the other hand, large droplets with low volatility do not evaporate completely before entering the reaction zone. The reaction zone consists of number of droplets in various stages of diffusive burning in this case, resulting in a thick laminar flame and the flame propagation mechanism becomes dependent on the heat transfer and diffusion processes occurring at the individual droplet (Strehlow, 1968).

Combustion of liquid fuel is often carried out by dispersing the fuel as a spray of droplets. There may exist interactions between the droplets that may affect combustion process. Figure 2.6, is the representation of six such droplets in a spray for simplicity. The concentric dotted circles around each droplet represent the amount of air that is

required for complete combustion of the droplet. If these droplets are considered to be so apart that there is no overlap of regions then the combustion of the fuel droplet will be complete. On a mass average basis, the combustion is fuel lean, but this does not actually happen. The distance between the droplets vary and some times they come so closer that the regions of air overlap each other. In other words, the amount of air would not be sufficient for complete oxidation of the droplets. Combustion in this case is fuel rich on a local basis. The products of combustion may contain large amount of partially oxidized products like CO.

As vapors from the droplet surface diffuse to the flame front surrounding the droplet, while oxygen diffuses from the surrounding atmosphere to the flame front, the resulting flame may or may not be round. The relative motion between droplets and surrounding gases and convection effects cause the flame to be non-spherical. But if the droplet is very small, then the relative motion between droplets and surrounding gases becomes small too, which results in a spherical diffusion flame. Both types of flame shapes are shown in Figure 2.7.

The rate of vaporization of a droplet depends upon the rate at which heat transfers from the flame front to the fuel droplet. A double-film model is used theoretically to represent the combustion of a single fuel droplet, one film separates the droplet surface from the flame front and the other separates the flame front from the surrounding atmosphere as shown in Figure 2.8 (Kuo, 1986).

The liquid surface of the droplet surrounded by the diffusion flame is assumed to be at the normal boiling temperature of the liquid fuel. Kuo (1986), showed that actually it is few degrees below the boiling temperature. The droplet temperature is assumed to be uniform and slightly below the boiling temperature for the analysis (Kuo, 1986). Godsave (1952), found that the fuel vaporizes from the heat that conducts from the flame front, indicated as *film I*, in Figure 2.8. The fuel does not react chemically until it is heated to the flame temperature and reaches to the flame front. *Film II*, represents the diffusion of oxygen to the flame front. The products of combustion and the heat that releases as a result of this combustion process is transferred to the surrounding atmosphere.

Since, the main objective of this dissertation is to determine the effects of liquid fuel droplets on the combustion efficiency of scaled down modeled flare in crosswinds. The droplet in this case, does not burn directly in an oxidizing environment and it may not have a spherical shape under the action gravity force. Therefore, the scope of this thesis research is more complicated than the above discussion.

The published research on the effects of liquid fuel droplets on combustion efficiency of industrial flares is very limited. Strosher (1996), conducted research on emissions from flaring in Alberta. The study was carried out in three stages (*i.e.* laboratory, pilot scale and field scale studies). Pure fuels were burned in the laboratory to identify unburned hydrocarbons in the products of combustion. Complex fuel mixtures in crosswind were burned under pilot scale study. The field study was carried out on one "sweet" and one "sour" battery sites, where the samples from the flare were collected and analyzed for

emission products. Strosher (1996), observed that combustion efficiency of pure gases (methane, propane and commercial grade natural gas) were in excess of 98% both in laboratory and pilot scale tests. However, the addition of liquid fuel droplets to pure gaseous streams affected the combustion efficiency. The extent of the effects depended upon the type and amount of liquid fuel added to the gaseous stream in a crosswind.

Strosher (1996) selected a sweet gas and a sour gas battery site for the field study. The flare gas at the sweet battery site had an unknown amount of liquid fuel in the flare stream escaping from the liquid knockout drum. While, the flare stream at sour battery site was considerably drier than the sweet battery site. The observed combustion efficiencies of sweet solution gas flares were between 62% to 71%, depending upon the amount of liquid flared with gaseous fuel stream and levels of the liquid in the liquid knockout drum. The sour solution gas had a more efficient flame, being considerably drier gas. The observed efficiency was 84% based on carbon mass balance and 82% based on sulfur mass balance.

Emissions from flares at both sites were also examined and it was noticed that unburned gases contained both hydrocarbons that were already present in the flare stream and those produced as a result of pyrolytic reactions. Depending upon the composition of the flare stream, flare design and atmospheric conditions at the time of flaring, the amount and the composition of those unburned hydrocarbons in the emissions might be different at different sites.

2.5 Jet Diffusion Flame in Turbulent Crosswind

Most of the research on the scaled down flares in the laboratory setup has been conducted in laminar crosswind conditions. Since, the industrial flares are subjected to the turbulent crosswinds, it is also necessary to study the flares under turbulent crosswind conditions and to measure its effects on the combustion efficiency of the flares.

Johnson *et. al.* (2000), studied the flares in turbulent crosswind conditions. For generating turbulence in crosswind, he placed a rectangular grid with 24.1 x 23.5 cm square holes, in the closed-loop wind tunnel facility at University of Alberta (the detail of wind tunnel facility is given in Appendix A.1). The measured average turbulent intensity produced by the grid at the flare stack was approximately 5% and characteristic length scale of the turbulence was 20 cm. With 3 m/s exit velocity of the flare gas and 2-14 m/s turbulent crosswinds, the efficiency of a natural gas flare was measured. It was observed that the ambient turbulence in crosswind had only a modest effect on the combustion efficiency of the flares.

Research has also been conducted on flare efficiency at Natural Resources Canada under the turbulent crosswind conditions. Two grids with 7.62 cm and 2.54 cm square holes were used to produce the turbulence of 1-8% intensity in the crosswind. The crosswind speed ranged from 0-40 km/h. The observed combustion efficiency of the flare decreased with the increase in turbulence intensity of the cross-flowing air (Gogolek, 2002).

On-going research on industrial flares does not provide any information regarding the effects for flare stack dimensions on the combustion efficiency of the flares. In this thesis research, scaled down flares have been studied under the influence of varying wall thickness of a modeled flare stack.

Figure 2.1: Diffusion Flame

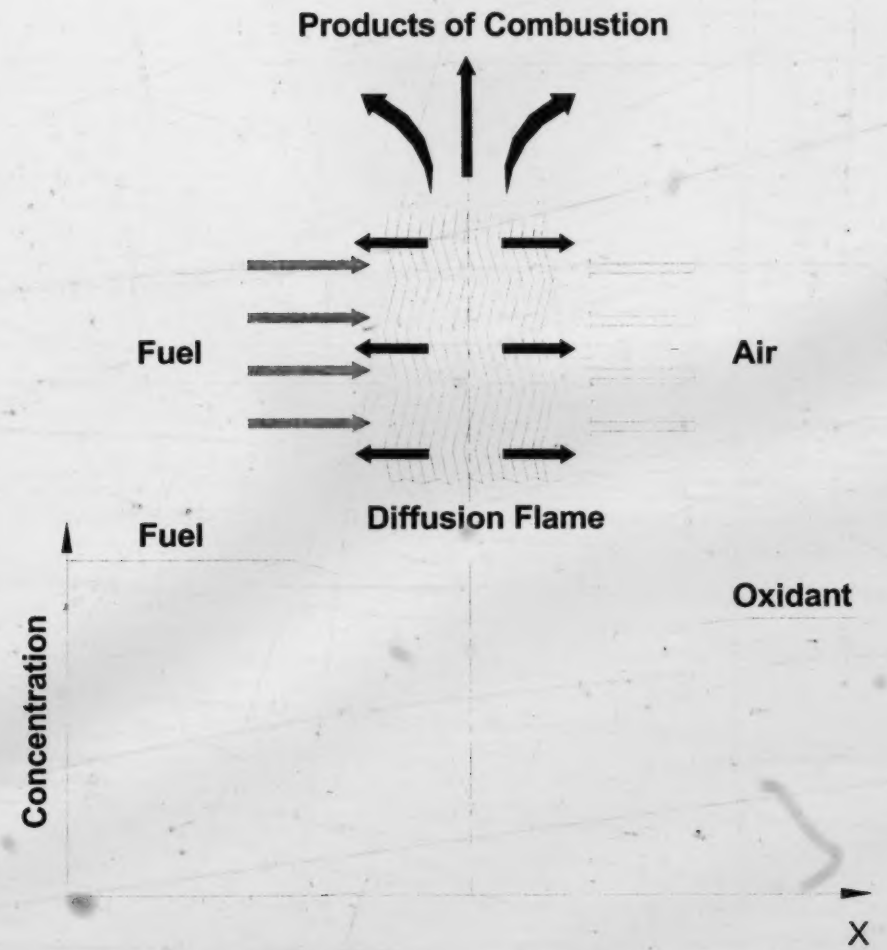

Figure 2.2: Diffusion of fuel and oxidant to a flame

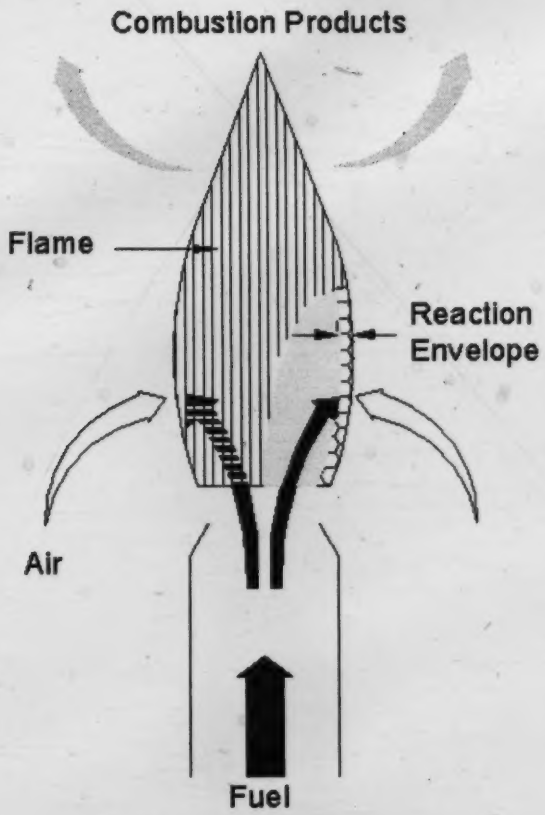

Figure 2.3: Combustion of gaseous fuel in diffusion flame (Edwards, 1974)

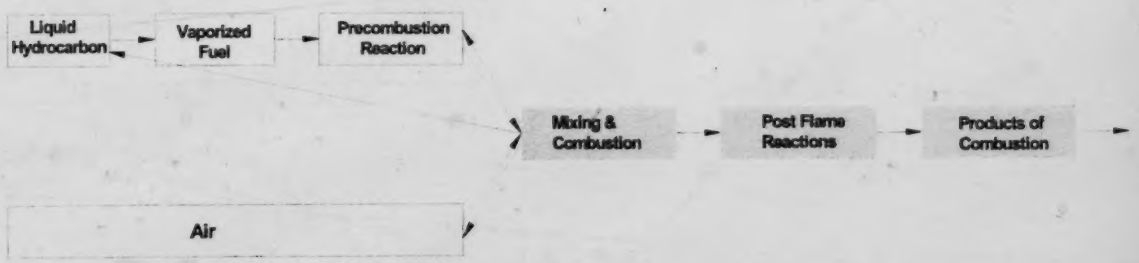

Figure 2.4: Combustion of liquid fuel in diffusion flame

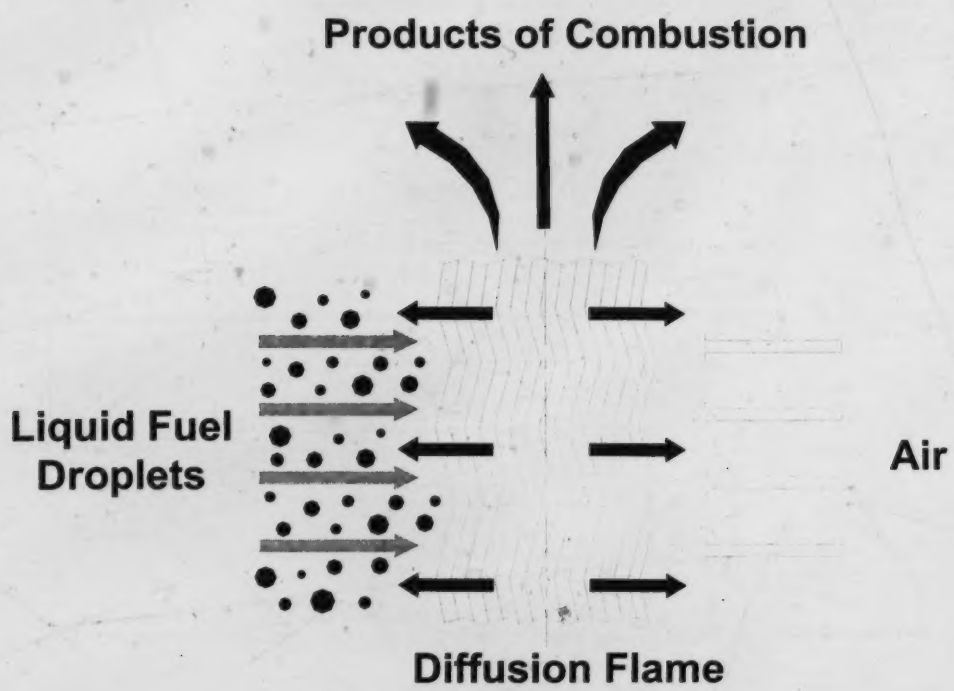

Figure 2.5: Combustion of liquid fuel droplet

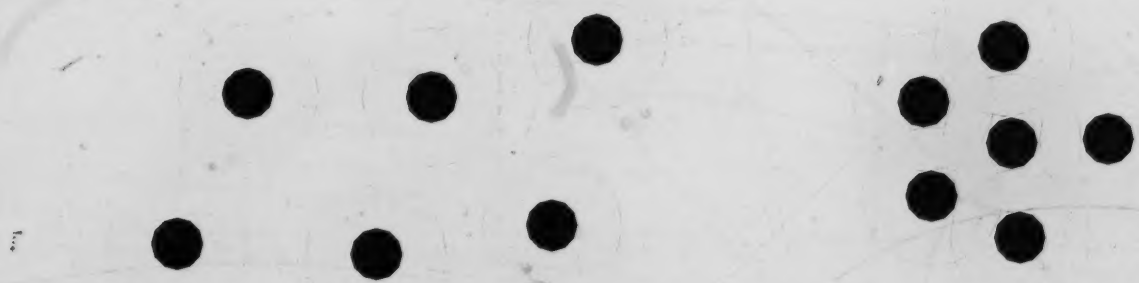

Figure 2.6: Combustion of a field of droplets

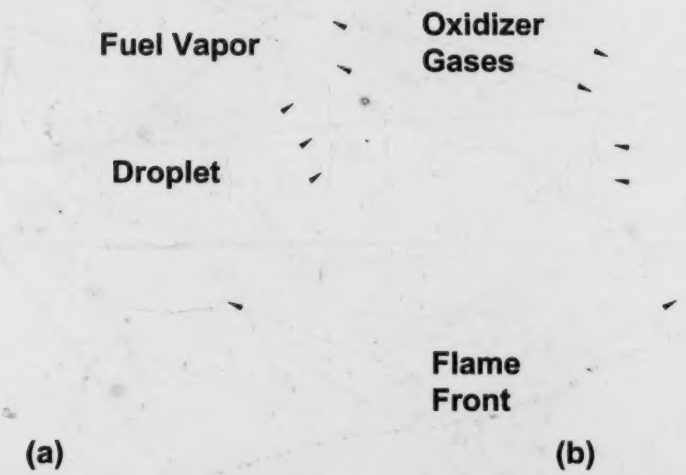

Figure 2.7: Shapes of diffusion flames surrounding a burning spherical fuel droplet (a) non-spherical (b) spherical (Kuo, 1986)

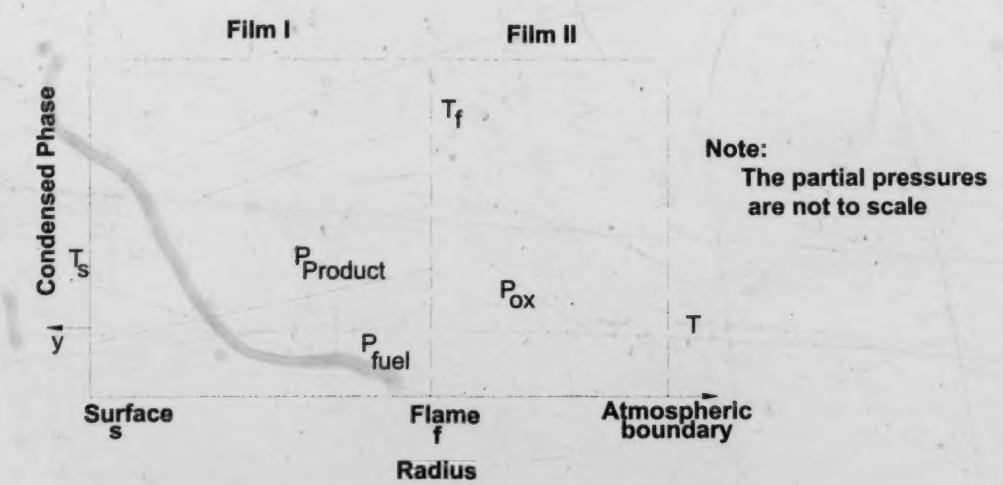

Figure 2.8: Parameter variation in double-film model (Kuo, 1986)

References:

1. Edward, J. B. (1974), *"Combustion Formation and Emission of Trace Species"*, Ann Arbor Science Publishers, Inc. U.S.A.
2. Johnson, M. R., Spangelo J. L., and Kostiuk, L. W. (2001), *"A characterization of Solution Gas Flaring in Alberta"*, Air & Waste Management Association, 50: 1167-1177.
3. Kuo, K. (1984), *"Principles of Combustion"*, John Wiley & Sons, Inc. U.S.A.
4. Siegel, K. D. (1980), *"Uber den Umsatzgard von Facelgas in Raffinerie-Hochfackeln" (Degree of Conversion of Flare Gas in Refinery Flare),* Ph.D Dissertation, University of Karlsruhe, Germany.
5. Godsave, G. A. E. (1952),*" Studies of The Combustion of Drops In a Fuel Spray-The Burning of Single Drops of Fuel"*, Fourth Symposium (International) on Combustion, pp.818-829, The combustion Institute, Pittsburg.
6. Johnson, M. R., Kostiuk, L. W. (2000),*" Efficiency of Low Momentum Jet Diffusion Flames in Crosswind"* Combustion and Flames 123, pp.189-200.
7. Pohl, J. H., Lee, J., Payne, R., and Tichenor, B.A. (1986), *"Combustion Efficiency of Flares"*, Combustion Science and Technology, 50, pp. 217-231.
8. Kuipers, E. W., Jarvis, B., Bullman, S. J., Cook, D. K. and Mchugh, D. R. (1996), *" Combustion Efficiency of Natural Gas Flare, Effects of Wind Speed, Flow Rate and Pilot"*, Internal Report, Shell Research and Technology Thorton and British Gas Research Center, 13 Pages.

9. Strosher, M. (1996), *"Investigation of Flare Gas Emission in Alberta"*, Alberta Research Council Report to Environment Canada, Alberta Energy and Utilities Board, and Canadian Association of Petroleum Products, 145 pages.

10. Kalghatgi, G. T. (1981), *"Blow-out Stability of Gaseous Jet Diffusion Flames. Part 2: Effect of Crosswind"*, Combustion Science and Technology, 26, pp. 241-244.

11. Kalghatgi, G. T. (1983), *"The Visible Shape and Size of a Turbulent Hydrogen Jet Diffusion Flame in a Cross-wind"*, Combustion and Flame, 52:91-106.

12. Smith, S. H., and Mungal, M. G. (1998),*" Mixing, Structure, and Scaling of the jet in Cross Flow"*, Journal of Fluid Mechanics, 357:83-122.

13. Hottel, H. C., and Hawthorne, W. R. (1949),*" Diffusion in Laminar Flame jets"*, Third Symposium on Combustion and Flame and Explosion Phenomena, pp.254-266.

14. Pitts, W. M. (1988),*" Assessment of Theories for the Behavior of Lifted Turbulent Jet Diffusion Flames"*, Twenty-Second Symposium (International) on Combustion, pp.809-816, The combustion Institute, Pittsburg.

15. Muniz, L., and Mungal, M. G. (1997),*"Instantaneous Flame-Stabilization Velocities in Lifted-Jet Diffusion Flames"*, Combustion and Flame, 111:16-31.

16. Hasselbrink, E. F., and Mungal, M. G. (1998),*" Observation on the Stabilization Region of Lifted Non-Premixed Methane Transverse Jet Flames"*, Twenty-Seventh Symposium (International) on Combustion, The Combustion Institute, Pittsburg.

17. Huang, R. F., and Chang, J. M. (1994),*" The Stability and Visualized Flame and Flow Structures of a Combustion Jet in Cross Flow"*, Combustion and Flame, 98, pp.267-278.

18. Huang, R. F., and Wang, S. M. (1999),*" Characteristic Flow Modes of Wake-Stabilized Jet Flames in Transverse Air stream"*, Combustion and Flame, 117:59-77.

19. Gollahalli, S. R., Brzustowski, T. A., and Sullivan, H. F. (1975),*" Characteristics of a Turbulent Propane Diffusion Flame in a cross-Wind"*, Transaction of the CSME, Vol. 3, No. 4:205-214.

20. Majeski, A. M. (2000),*" Size and Shape of Low Momentum Jet Diffusion Flames in Crosswind"*, M.Sc. Dissertation, University of Alberta, Edmonton, Canada.

21. Pascal, P. (2000),*" Plume Sampling of a Flare in Crosswind: Structure and Combustion Efficiency"*, M.Sc. Dissertation, University of Alberta, Edmonton, Alberta, Canada

22. Prybysh, R. (2002),*" The Production of toxic Emissions from Reacting Diffusion Jet Flames in a Crossflow"*, M.Sc. Dissertation, University of Alberta, Edmonton, , Alberta, Canada.

23. Keller, N. and Nobel, R. (1983),*"RACT for VOC Burning Issue"*, Pollution Engineering, July.

24. McDaniel, M. (1983),*" Flare Efficiency Study"*, EPA Report No. 600/2-83-052,July.

25. Leahly, D. M. and Davies, M. J. E. (1984),*" Observation of Plume Rise From Sour Gas Flares"*, Atmospheric Environment, Vol. 18, No. 5, pp917-922.

26. Roper, F. G. (1977),*"The prediction of Laminar Jet diffusion Flame Sizes: Part I, Theoretical Model "*, Combustion and Flame, 29:219-226, Pittsburgh.

27. Gogolek, P. (2002),*"Flare Tip Design"*, 2002 Air Issues Forum and Technical Review, November 27th-28th, 2002.

28. Strehlow, R. A. (1968), *"Fundamentals of Combustion"*, International Textbook Company, Scranton, Pennsylvania, U.S.A.

29. Glassman, I. (1996), "*Combustion"*, Academic Press Inc., New York, U.S.A.

Chapter 3

EXPERIMENTAL SETUP AND METHODOLOGY

The limited research regarding the combustion of liquid hydrocarbon or water droplets, size of droplets, and mass flow rates of the liquid in a gaseous fuel stream makes it difficult to predict their effects on the flare efficiency without knowing these factors. Therefore, an approach was needed that could examine parameters of the liquid fuel droplets as part of their addition to the flare stream. This thesis research is an attempt to study the effects of liquid droplets on the flare efficiency by conducting tests on modeled flares under various crosswind conditions in a close-loop wind tunnel facility at University of Alberta. Before the addition of droplets to the flare stream, the size distribution of the droplets and mass flow rates of the liquid fuel that exit the flare stack in the form of spray at various exit velocities of the flare gas were calculated separately. Keeping in mind that information about composition, size distribution and amount of the liquid droplets in the stream of an industrial flare is very limited, three different liquids were selected (*i.e.* iso-octane, diesel, and distilled water). These liquids do not cover the full range of liquids that an industrial flare may have in its flare stream, still the results and observations from these liquids are significant to help understand the effects of liquid droplets on efficiency of industrial flares.

Sales grade natural gas was used as a flare gas. Since, carbon conversion efficiency of flares requires accurate carbon mass balance measurement. This needed the investigation of major carbon-containing species (*i.e.* CO_2, CO, HCs) along with the presence of any

soot or particulate materials in the products of combustion. Therefore, flares were examined for production of particulate emissions from reacting jet diffusion flames in crosswinds. Details of the technique adopted for investigating soot or particulate material in the combustion products is given elsewhere (Prybych, 2002). This technique has been used to examine products of combustion from flares with and without liquid hydrocarbon droplets for any soot or particulate materials. Since, flares with and without droplets did not emit any soot or particulate materials, the overall carbon conversion efficiency of the flares were calculated with the same method used by Johnson *et. al.* (2001). These researchers also used the closed-lop wind tunnel facility for conducting their research.

The close-looped wind tunnel facility has been used to study the scale down flares with only gaseous fuel in their flare streams under well-controlled conditions. A separate system was built-up for the generation of liquid droplets and their addition to the flare stream. The detail description of this system will be discussed later in this chapter. The wind tunnel was designed to generate laminar crosswinds in the test section. To study the flares under turbulent crosswinds, turbulence-generating grids were placed at various positions upstream of the flare stack in the wind tunnel to generate turbulence of various intensities at the tip of the flare stack. Similarly, modeled flare stacks with various wall thicknesses were made to study their effects on the flare efficiency. The inner stack diameters of all those stacks were all the same.

Two different ultrasonic droplet generators (*i.e.* 18 kHz and 48 kHz) were used to produce a spray of small and large droplets, respectively. Since, the droplet generators are

capable of handling a wide range of liquid flows, liquids were supplied at various flow rates to generate droplets of various sizes. Details of the ultrasonic droplets generators are given in Appendix C. These droplet generators can produce spray in any orientation, but for this dissertation, they were needed to be in upright position. Two custom capsules were made to keep the ultrasonic droplet generators in upright position, which are shown schematically in Figures 3.1 and 3.2. These capsules were designed to allow flow of flare gas so as to carry maximum amount of the droplets along with it to the top of the flare stack. To accommodate the modeled flare stack upon the capsules, a cap was made that is shown in Figure 3.3.

Most of the experimental work on flares in this laboratory setup is done under low turbulence crosswind conditions (<0.5% turbulence intensity), as the closed-loop wind tunnel facility is designed to study scaled down flares under laminar crosswinds. Since, solution gas burns in turbulent crosswinds in the open atmosphere, one of the goals of this thesis research was to study scaled down flares in turbulent crosswinds. To generate turbulent crosswind, two types of grids were made and introduced into the wind tunnel. The grids had 25.4 mm and 50.8 mm square hole, respectively, and were placed at specified locations upstream of the flare stack so as to create turbulence of various intensities at the tip of the flare stack. The length scales of the turbulence induced by these grids were also calculated at the specified locations. Using a 24.7 mm modeled stack, natural gas flares with two different exit velocities of the flare gas were subjected to 4 m/s turbulent crosswinds. The method used by Johnson *et. al.* (2001), was used for measuring efficiencies of the scaled down flares in the closed-loop wind tunnel.

Another important parameter that has not been investigated previously is wall thickness of the flare stack and its effects on combustion efficiency of flares. Therefore, natural gas flares were also studied using modeled flare stacks of various wall thicknesses. Tests were conducted in the same laboratory setup (close-loop wind tunnel), and flares with two different gas exit velocities were subjected to various crosswind conditions. Efficiencies of the flares were calculated using the same method as used before for flares with and without droplets.

3.1 Generation and Addition of Liquid Droplet into Flare Gas

This section explains the procedure of how droplets of various liquid fuels were generated and added into the flare stream. The mass flow rates of liquid fuels and characteristic size distribution of droplets before their inclusion into the flare stream is also discussed. The schematic in Figure 3.4, shows the method of how the droplets were generated and then introduced into the flare stream (Kostiuk, 2000).

3.1.1 Mass Flow Rate of the Liquid Fuel Being Flared

One important parameter that is needed to be known as part of measuring efficiency of flares containing liquid droplets is the mass flow rate of liquid fuel that exits the flare stack in the form of droplets and actually participates in the combustion process. The technique that was adopted for measuring mass flow rate of the liquid fuel is shown schematically in Figure 3.5. The system shown in the figure can be divided in two separate sections, one that controls the flare gas and the other controls liquid fuel. In order to measure the flow rate of the liquid, the flow of the flare gas (sales grad natural gas) was turned on first. The power to the generator was then turned "On", which allowed the liquid to flow through the generator for producing a spray at a fix flow rate of the liquid. The ultrasonic droplet generator produces a spray of conical pattern due to the shape of its tip. As a result, a considerable amount of the droplets ends up on the walls of the flare stack, which makes a thin film of liquid after few seconds that flows to the base of the stack. To avoid this phenomenon, the flare gas was introduced as an annular jet surrounding the tip of ultrasonic droplet generator to carry maximum amount of droplets by redirecting the droplets away from the stack wall. The gap size that produced the annular jet was approximately 2.5 mm and the flare gas was directed at an angle of approximately 15 degrees inward from the vertical (Kostiuk, 2000).

The flare gas carried maximum amount of droplets generated to the top of the flare stack. Still a considerable amount of large size droplets impacted on the inside wall of flare stack. After a few seconds, these droplets converted into a thin film of liquid that fell

down through the passages provided in the capsule and collected in a return vessel as shown in Figure 3.5. Besides the droplets generated by the ultrasonic droplet generator, some of the liquid mass on the wall evaporates to form saturated vapors and becomes part of the flare stream. The liquid supply tank and liquid return vessel both were placed on scale so as to measure the total rate of change in the mass of the liquid. The difference in mass on the scale during a particular interval of time for a specific experiment gave the total flow rate of the liquid fuel that exited the flare stack in the form of droplets and saturated vapors.

Masses on the scale were recorded every second during each test. The mass flow rate of the liquid during a particular test is shown in Figure 3.6. In this figure, the slope of the line represents the average mass flow rate of the liquid fuel during that test (exit velocity of the flare gas was 2 m/s and crosswind speed was 4 m/s). The transient period represents the interval, when the liquid spray starts and moistening of the inside wall of the flare stack occurs due to accumulation of these liquid droplets. The liquid film develops due to accumulation of droplets in a few seconds and then the liquid fuel starts to flow down to the return vessel. Once this flow starts to the liquid return vessel, the scale shows a steady decrease in the mass of the liquid. Since, the difference of mass on the scale was recorded every second, mass flow rate of the liquid was calculated from the slope of the line during the steady state period. The steady state period of the graph represents the time, when there was a gradual and steady decrease in mass of the fuel in the tank due to the loss of the liquid fuel in the form of droplets and saturated vapors that were carried by the flare gas.

For various test conditions, mass flow rate of the liquid fuel changed either by increasing or decreasing the flow of the liquid to the ultrasonic droplet generator. It was also observed that the exit velocity of the flare gas affected the efficiency to carry liquid droplets. Therefore, tests were conducted with two different exit velocities of the flare gas (*i.e.* 1 m/s and 2 m/s, with flow rates of 20 l/min and 40 l/min).

3.1.2 Characteristic Size Distribution of the Droplets

The ultrasonic droplet generator produces droplets of various sizes depending on a control setting. Another important parameter that characterized the test conditions was size distribution of the droplets that made its way up to the top of the flare stack along the gaseous flare stream. The equipment used to characterize the probability size distribution of the droplets that exited the flare stack was a Helos BSF, manufactured by Sympatec Corporation, Clausthal-Zellerfeld, Germany. This equipment is capable of measuring droplets with sizes ranging from 0.5 μm to 875 μm. A description of the equipment and the droplet size distribution is given in Appendix D. The quoted characterized size for any droplet flow was the mass mean diameter.

3.2 Method of Measuring Combustion Efficiency of the Flares with Liquid Fuel Droplets

An appropriate means to test the performance of a flare is its ability to fully oxidize the fuel directed to it. In this thesis research, the most relevant and useful term that defines the efficiency of the flare, is the "carbon conversion efficiency", which is its effectiveness to convert carbon present in the fuel stream into carbon dioxide (CO_2). The mass-based mathematical expression of the combustion efficiency (η) in terms of rate may be written as follows (Kostiuk, 2000):

$$\eta \equiv \frac{\text{Mass Flow Rate of Carbon in The Form of } CO_2 \text{ Produced by The Flare}}{\text{Mass Flow Rate of Carbon in The Form Hydrocarbon Fuel Supplied to The Flare}}$$

$$\eta = \frac{\dot{m}_{C,CO_2}}{\dot{m}_{C,Fuel}} \qquad \text{Eq. 3.1}$$

For this dissertation, sales grade natural gas was used as fuel and it has been observed that natural gas flares do not emit soot with or without droplets of the kind used here. Since, measuring the internal volume of the wind tunnel accurately is difficult due to complex structure of the tunnel, the methodology adopted for measuring flare combustion efficiency was to perform the test in two parts. To fully close the wind tunnel and accurately measuring the mass balance of different species during the tests, two valves (one way) were placed between the capsule and liquid return vessel as shown in the Figure 3.5. The purpose of these valves was to prevent the vapors from escaping out of

the droplet generation system into the wind tunnel, when liquid was not wanted. In first part of the test, only gaseous fuel was flared and the tunnel was completely purged after measuring the combustion efficiency. Details for measuring and calculating combustion efficiency of the flares burning gaseous fuel only is given in Appendix B. Liquid droplets were then added to the flare stream in the second part of the test. Since, the flare stream contained liquid fuel, mass flow rates of carbon can now be calculated as follows (Kostiuk, 2000):

$$\dot{m}_{C,Fuel} = \dot{m}_{C,ng} + \dot{m}_{C,Liquid} \qquad \text{Eq. 3.2}$$

where

$\dot{m}_{C,ng}$ = mass flow rate of carbon in natural gas

$\dot{m}_{C,Liquid}$ = mass flow rate of carbon in liquid fuel

Amount of liquid fuel that flares with gaseous fuel is calculated from decrease in the mass of liquid fuel on scale during a test, as shown in Figure 3.6. Mathematical expression for calculating mass flow rate of carbon in liquid fuel is given as:

$$\dot{m}_{C,Liquid} = \dot{m}_{Liquid} \times \frac{n_c M_c}{M_{Liquid}} \qquad \text{Eq. 3.3}$$

Mass flow rate of liquid fuel ($\dot{m}_{Liquid}$) was calculated from the slope of curve obtained from the time trace of scale reading during the test and it varies for each individual test. The flare gas used in this thesis research was not pure methane (CH_4) but a mixture of gases. The sales grade natural gas contains 95.2% CH_4, 2.1% C_2H_6, 1.7% N_2, 0.8% CO_2, 0.2% others (Johnson *et. al.*, 2001). Therefore, mass flow rate of carbon in natural gas was calculated according to the above composition considering carbon-containing species only.

Mass flow rate of CO_2 present in the products of combustion produced by the flare was calculated from the rate of accumulation of CO_2 within the wind tunnel. It is accepted that the tunnel leaks and ambient air infiltrate while air exfiltrates the tunnel during the test. The process is also not isothermal so the rate of accumulation of CO_2 within the tunnel is not the total measure of the mass flow rate of carbon in the form of CO_2 present in the products of combustion. A reference test was needed to calibrate the mass flow rate of CO_2 by burning fuel of known input for onward calculation of the efficiency. Therefore, only natural gas was burned in the first part of the test and efficiency based on the products of combustion was calculated as follow

$$\eta_{HC} = \frac{\frac{d}{dt}\left\{\frac{CO_2}{T}\right\}}{\left[\frac{d}{dt}\left\{\frac{CO_2}{T}\right\} + \frac{d}{dt}\left\{\frac{CO}{T}\right\} + \frac{d}{dt}\left\{\frac{HC}{T}\right\}\right]} \qquad \text{Eq. 3.4}$$

where

HC = Natural Gas, (ng)

As each compound in the above equation contains carbon, therefore, leakage from the tunnel during the test can be omitted. With the known efficiency for this part of the test, the slope of CO_2 can be related to the source strength of CO_2 (*i.e.* $\dot{m}_{CO_2}$) for the test. Therefore, Eq. 3.4, can be written as:

$$\eta_{ng} = \frac{\dot{m}_C \text{ as } CO_2}{\dot{m}_C \text{ present in flare gas}} \qquad \text{Eq. 3.5}$$

Since, η_{ng} and the denominator on the right hand side of Eq. 3.5 were known, the numerator ($\dot{m}_C \, as CO_2$) can be calculated. The mass flow rate of carbon that became CO_2 or mass flow rate of carbon formed ($\dot{m}_{C\,formed}$) was then converted into mass flow rate of CO_2 that was emitted into the wind tunnel during the test as follows:

$$\dot{m}_{CO_2} \text{ that was emitted into tunnel} = \dot{m}_C \text{ that became } CO_2 \text{ x } \frac{M_{CO_2}}{M_C} \qquad \text{Eq. 3.6}$$

Relating mass flow rate of carbon that became CO_2 to the accumulation rate of CO_2 or slope of the graph of $\frac{(CO_2)}{T}$ during the test can then be established. Assuming that for

any $\dot{m}_{C\ formed}$, there is a unique slope on the graph, the mass flow rate of carbon during the second part of the test with both gaseous and liquid fuels in the flare stream was then calculated as:

$$\left.\frac{\dot{m}_{C,Co_2}}{\frac{d}{dt}\left[\frac{CO_2}{T}\right]}\right|_{ng+Liquid} = \left.\frac{\dot{m}_{C,CO_2}}{\frac{d}{dt}\left[\frac{CO_2}{T}\right]}\right|_{ng} \qquad \text{Eq. 3.7}$$

Combining Eq. 3.6, and Eq. 3.7, the final expression for the efficiency of the flare with gaseous and liquid fuels in the flare stream was obtained. Therefore, Eq. 3.1, can now be written as follows:

$$\eta = \eta_{ng} \times \frac{\dot{m}_{C,ng}}{\dot{m}_{C,ng+Liquid}} \left[\frac{\frac{d}{dt}\left\{\frac{CO_2}{T}\right\}_{ng+Liquid}}{\frac{d}{dt}\left\{\frac{CO_2}{T}\right\}_{ng}} \right] \qquad \text{Eq. 3.8}$$

where

η_{ng} = efficiency of the flare having natural gas in the flare stream

$\dot{m}_{C,ng}$ = mass flow rate of carbon in the flare stream with natural gas only

$\dot{m}_{C,ng+Liquid}$ = mass flow rate of carbon in the flare stream with natural gas and liquid fuel

Eq. 3.8, is the mathematical expression for calculating the efficiency of the flares that have soot or particulate materials in the products of combustion. Since, the flares studied for this dissertation did not emit soot with or without liquid droplets in the flare stream. Eq. 3.1, was used to calculate the combustion efficiency of the flares with or without liquid droplets. The procedure adopted for calculating the efficiencies of these flares was the same as was used by Johnson *et. al.* (2001).

Since, compositions of the flare stream in both parts of the tests were known, the uncertainties in calculating the efficiencies in both parts of a test were found to be very small. These small uncertainties provided the confidence that the combustion efficiency could be measured accurately with this methodology. The sensitivity analysis on the measured and calculated efficiencies showed that the error in the calculated efficiency was less than 0.1% (Johnson and Kostiuk, 2000).

3.3 EFFECT OF THE TURBULENT CROSSWINDS

Solution gas flares operate under turbulent crosswind conditions in an open atmosphere. Whereas, the closed-loop wind tunnel is designed to generate low turbulence crosswinds. Measured turbulent intensity in the core flow of the test section was less than 0.5% (Johnson *et. al.*, 2001). Therefore, to study scaled down modeled flares in turbulent crosswinds, two different types of turbulence generating grids were used to generate turbulence of various intensities by placing them at various positions upstream the flare stack in the wind tunnel. These grids were made of 1.6 mm steel sheets with 25.4 mm and 50.8 mm square hole, respectively and are shown in Figures 3.7 and 3.8.

A hot-wire anemometer was used to measure the turbulence intensities generated by these grids with 4 m/s crosswind speed. It was first calibrated with no grid in the tunnel by placing its probe at the same position and height as the flare stack. The wind speed was increased gradually from 1.5 m/s to 6.5 m/s. Figure 3.9, shows the calibration curve of the hotwire anemometer with wind speed as a function of bridge voltage. Once the hotwire was calibrated, both grids were placed at a fix position upstream the flare stack in the wind tunnel. To find the exact locations of the grids for the generation of required turbulence intensities at the tip of the flare stack, moving the grids was difficult. Therefore, the grids were fixed at a position far enough from the flare stack and hotwire anemometer was moved to find the locations for the grids to generate turbulence of various intensities at the tip of the flare stack. The height of the hotwire anemometer was equal to the height of the flare stack from the tunnel floor. It was also observed that turbulence was homogenous along the width and height of the tunnel.

Four different locations (*i.e.* 30 cm, 51 cm, 105.41 cm, 256.54 cm) were found upstream of the flare stack for the grid with 50.8 mm square holes to generate turbulence intensities of 20%, 10%, 5%, and 2.5% at the tip of the flare stack. The data during each test were recorded and a standard software was used to calculate the turbulence length scale. Characteristics length scales of turbulence produce by the grid at those four locations were 3.77 cm, 2.71 cm, 2 cm, and 1.66 cm, respectively.

Similarly, the grid with 25.4 mm square hole was placed at three locations (*i.e.* 30 cm, 47 cm, and 118 cm) upstream the flare stack to generate 8.61%, 5%, and 2.5% turbulence

intensities at the tip of the flare stack. Similarly, the turbulence length scales generated by this grid were 2.03 cm, 1.36 cm, and 1.08 cm, respectively. Table 3.1, shows the locations of the grids to generate the respective turbulence intensities at the tip of the flare stack. The turbulence decay behind both the grids are shown in Figures 3.10 and 3.11.

Table 3.1: Distances of grids upstream the flare stack for respective turbulence intensities and length scale

5.08 cm Square Hole Grid		
Distance Upstream The Flare Stack (cm)	**Turbulence Intensity (%)**	**Turbulence Length Scale (cm)**
256.54	2.5	1.66
105.41	5	2.0
51	10	2.71
30	20	3.77
2.54 cm Square Hole Grid		
Distance Upstream The Flare Stack (cm)	**Turbulence Intensity (%)**	**Turbulence Length Scale (cm)**
118	2.5	1.08
47	5	1.36
30	8.61	2.03

3.4 INFLUENCE OF VARYING FLARE STACK DIMENSION

At the battery sites solution gas is flared through a long vertical pipe (Schedule-40 pipe) approximately 10 m in length and 10 cm in diameter. The ratio of its inner diameter to outer diameter (d_i/d_o) is 0.9 (Kostiuk, 2000). The present wind tunnel facility at

University of Alberta is not capable of accommodating the actual size of the flare stack. Therefore, the flare stack used for this dissertation is a 24.7 mm scale down modeled quartz stack with a wall thickness of 1.3 mm. In order to maintain the geometric similarity for the scaled down flares, ratio of its inner to the outer diameter is kept the same (*i.e.* 0.9). Flares have not been studied to understand the effects of changing flare stack dimensions (*i.e.* wall thickness) on the combustion efficiency of the flares. In this thesis research, the scaled down modeled flares are studied and their efficiencies are measured under the influence of varying wall thickness of the flare stack while keeping their inner diameters constant (*i.e.* 22.1 mm). Eight modeled steel stacks have been selected with the wall thickness ranging from 0.65 mm to 13 mm. The dimensions of these flare stacks are given in Table 3.2. Tests have been conducted under crosswind speeds ranging from 2 m/s to 7 m/s with the flare gas exit velocities of 1 m/s and 2 m/s, respectively.

Table 3.2: Steel stacks with varying wall thickness

S/N	Description	ID (mm)	OD (mm)	Wall Thickness (mm)
1	Steel Stack	22.10	23.67	0.65
2	Steel Stack	22.10	24.70	1.30
3	Steel Stack	22.10	28.65	3.30
4	Steel Stack	22.10	31.80	4.85
5	Steel Stack	22.10	35.00	6.45
6	Steel Stack	22.10	38.10	8.00
7	Steel Stack	22.10	41.35	9.62
8	Steel Stack	22.10	48.16	13.00

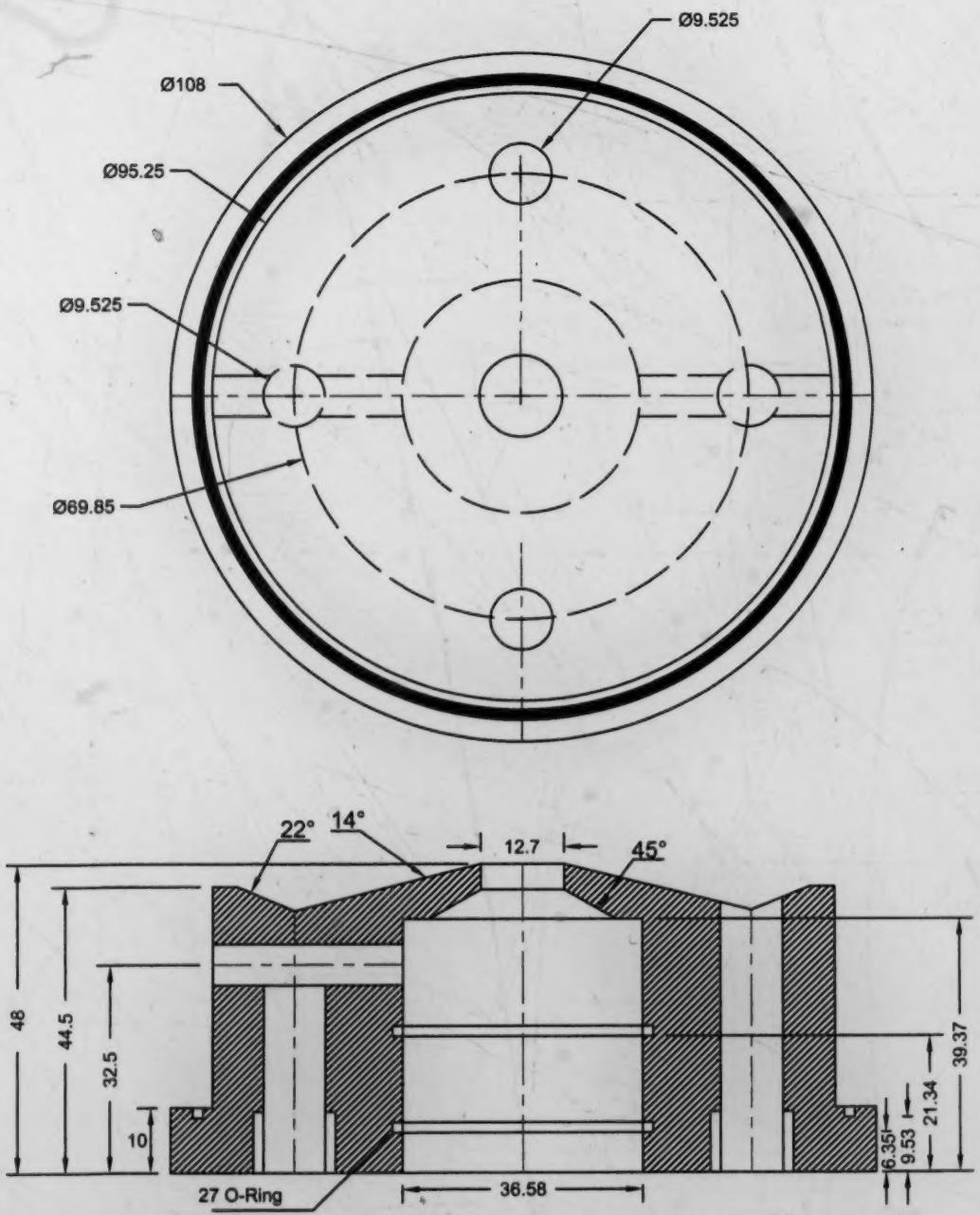

Figure3.1: Capsule for 18 kHz ultrasonic droplets generator (All dimensions are in mm)

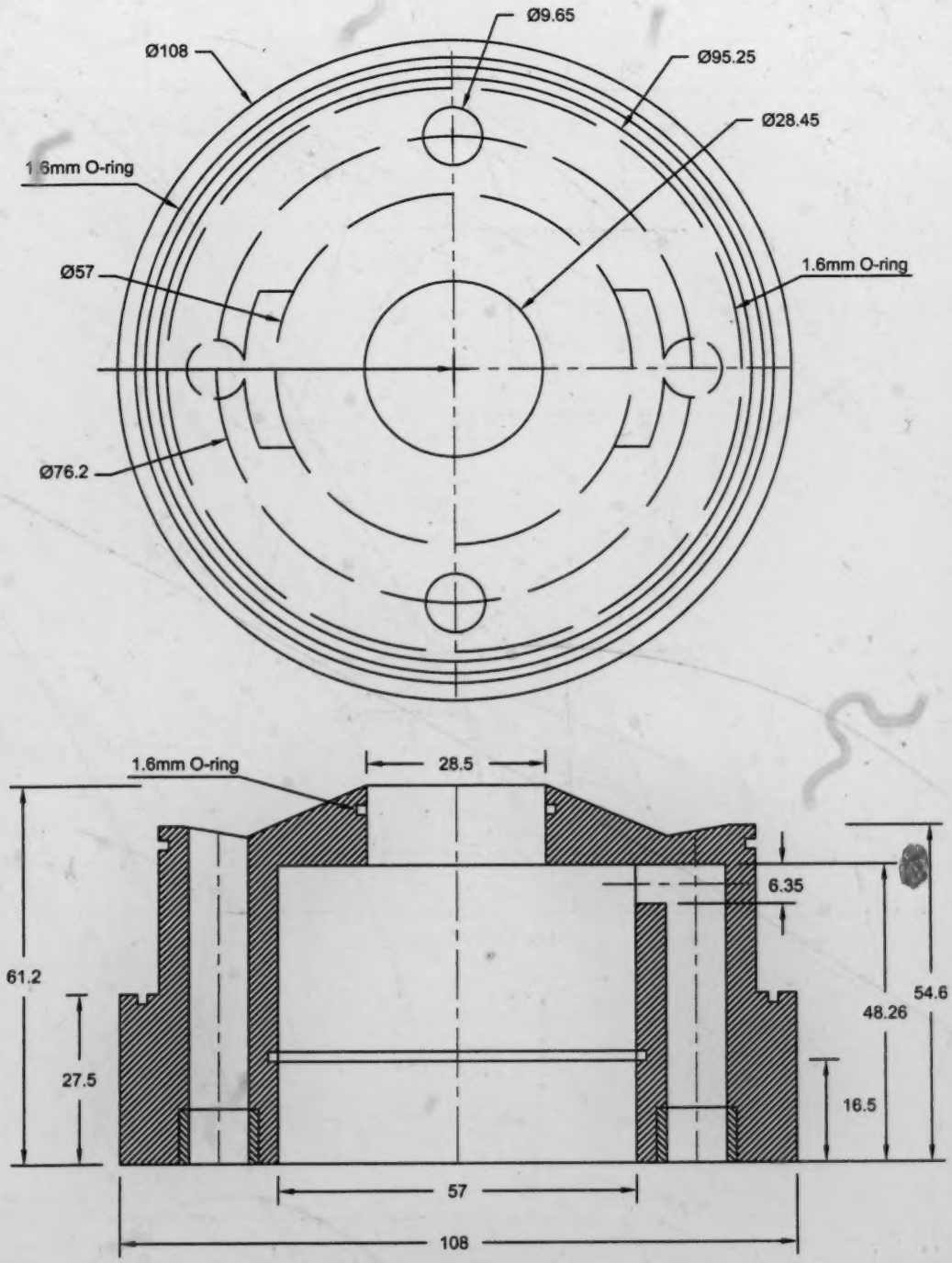

Figure 3.2: Capsule for 48 kHz ultrasonic droplets generator (All dimensions are in mm)

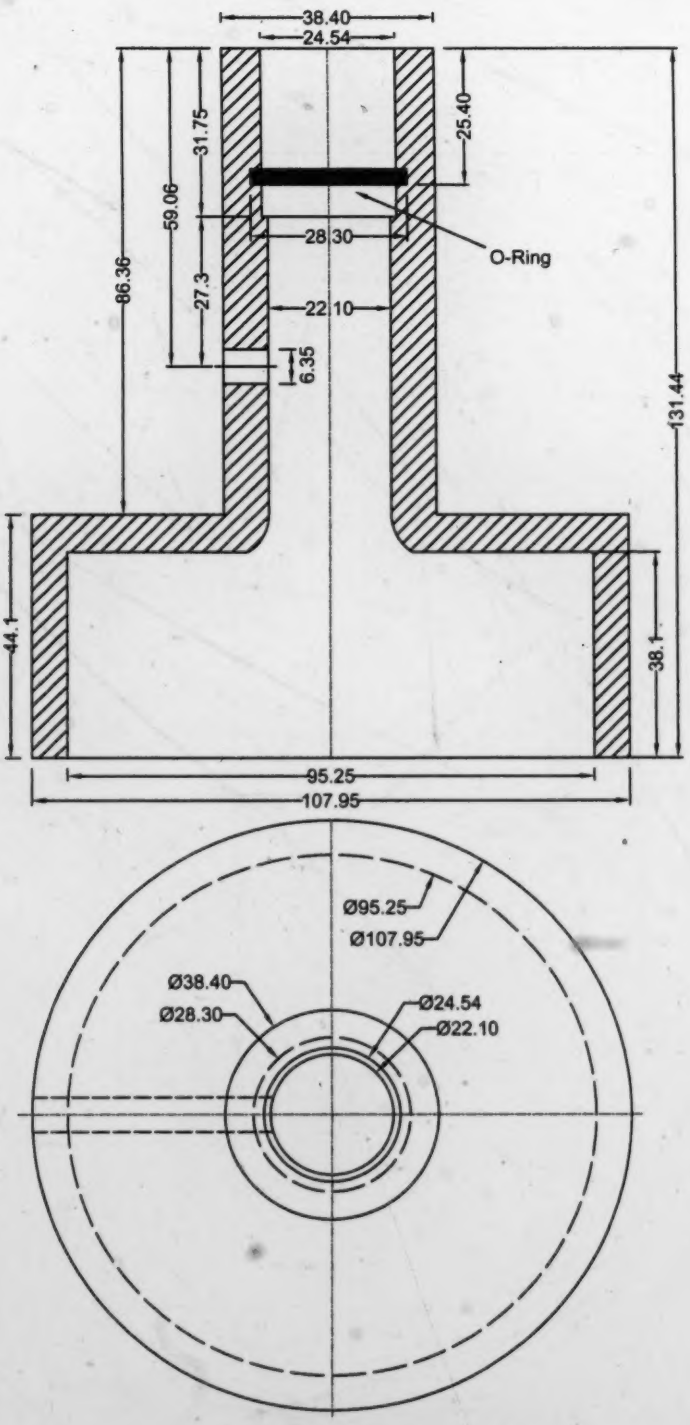

Figure 3.3: Cap for holding the flare stack
(All dimensions are in mm)

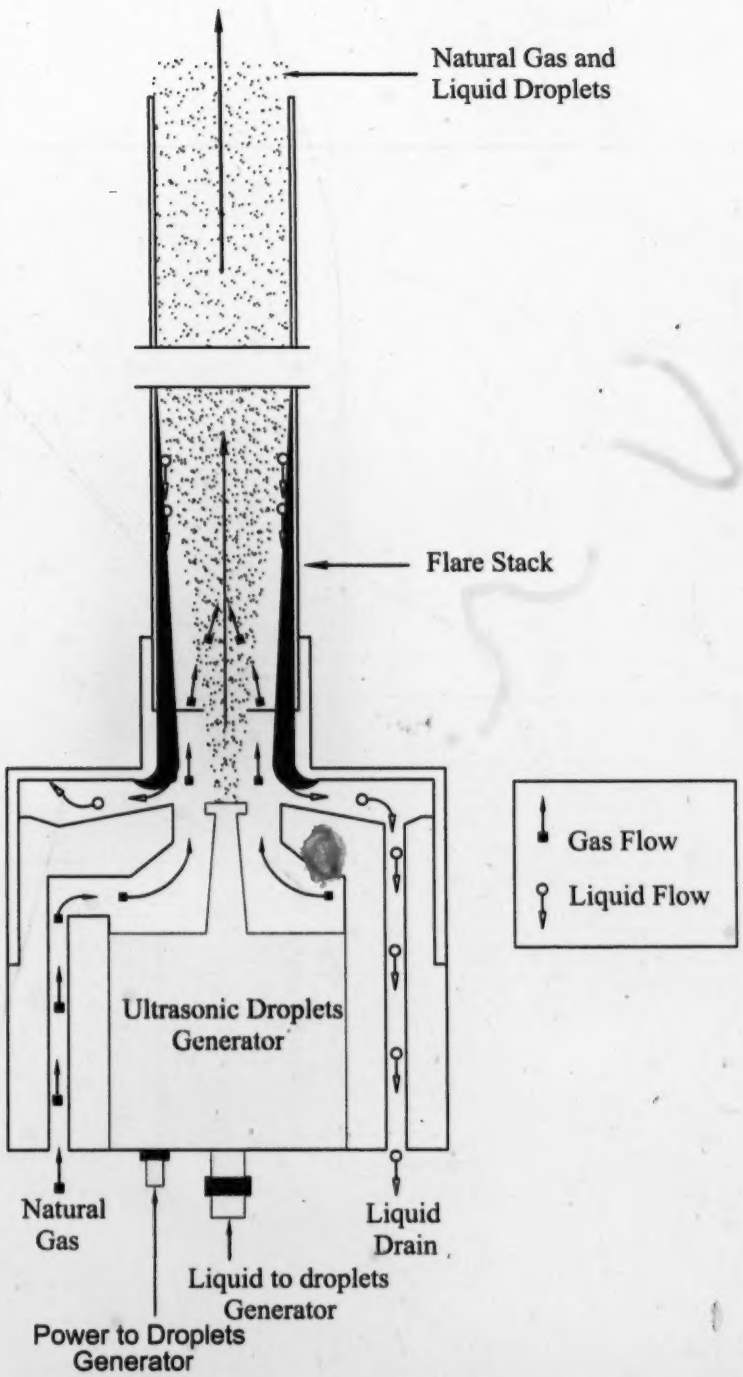

Figure 3.4: Droplets generation and their introduction into the flare stream (Kostuik, 2000)

Figure 3.5: Liquid supply system and mass flow rate of the liquid exiting the flare stack (Kosiuk, 2000)

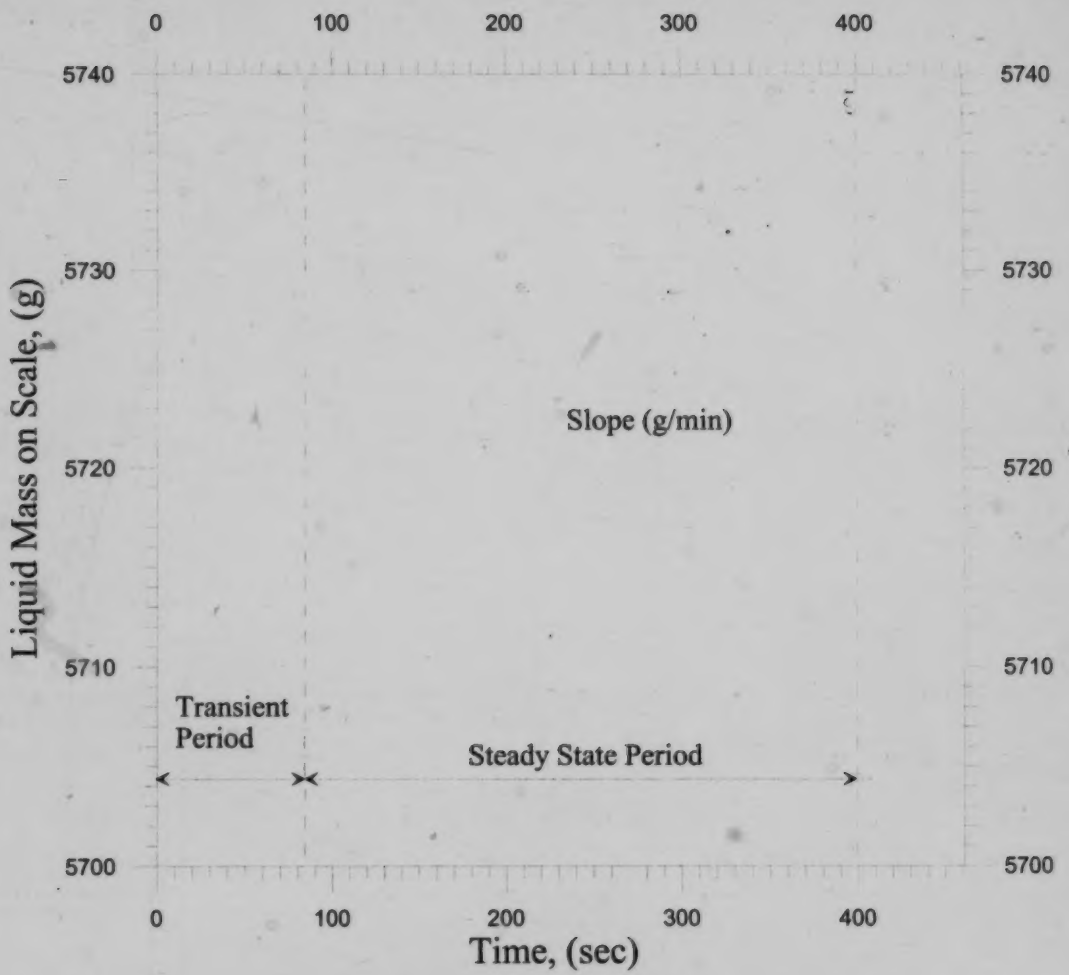

Figure 3.6: Time trace of liquid mass flow rate

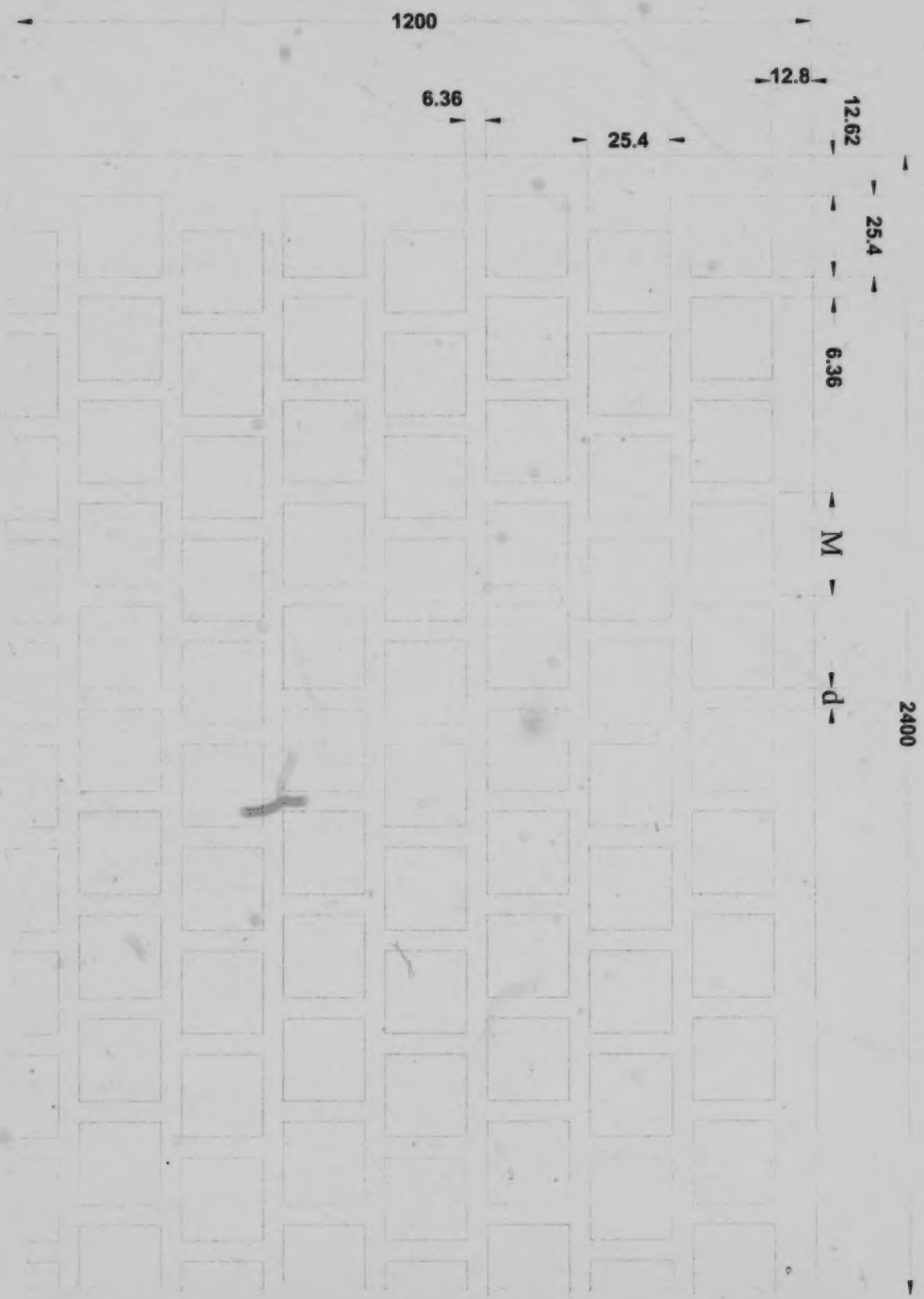

Figure 3.7: 4 x 8 m and 1.6 mm thick grid with 25.4 mm square holes (All dimensions are in mm)

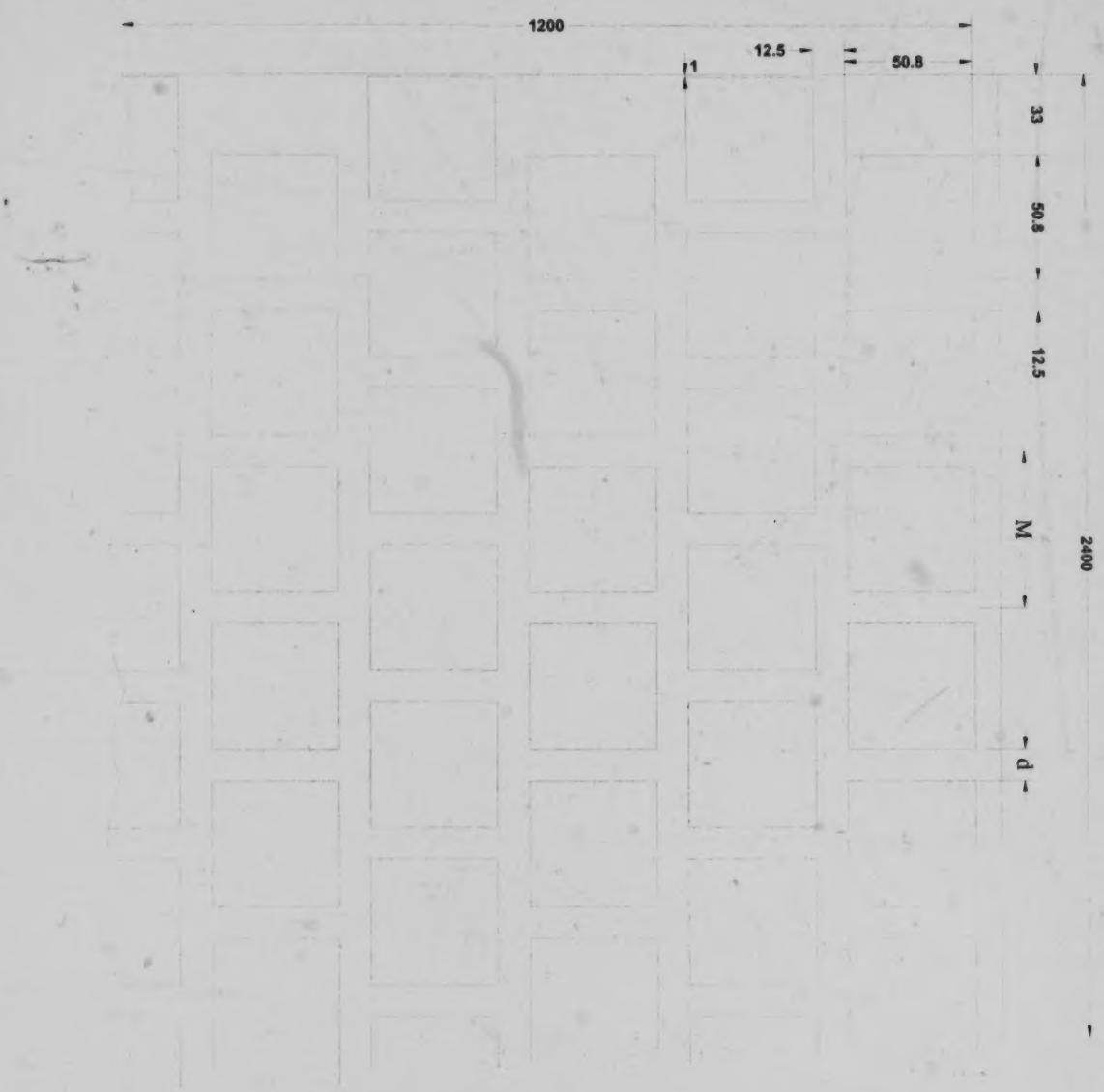

Figure 3.8: 4 x 8 m and 1.6 mm thick grid with 50.8 mm square holes (All dimensions are in mm)

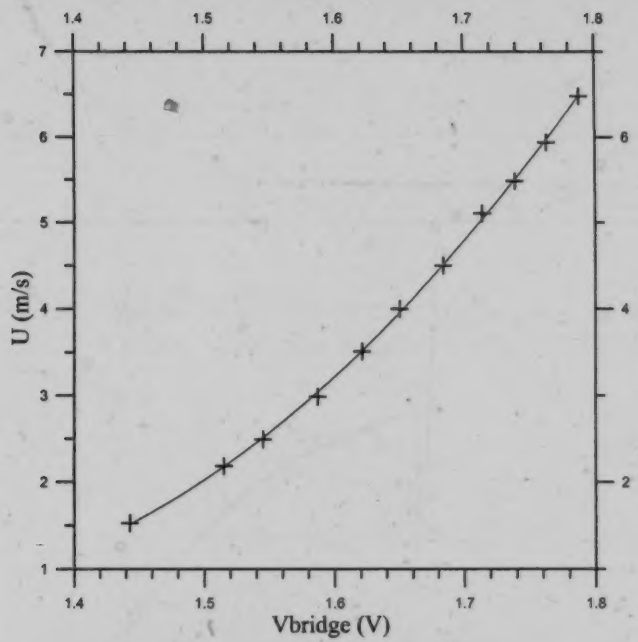

Figure 3.9: Hotwire anemometer calibration curve

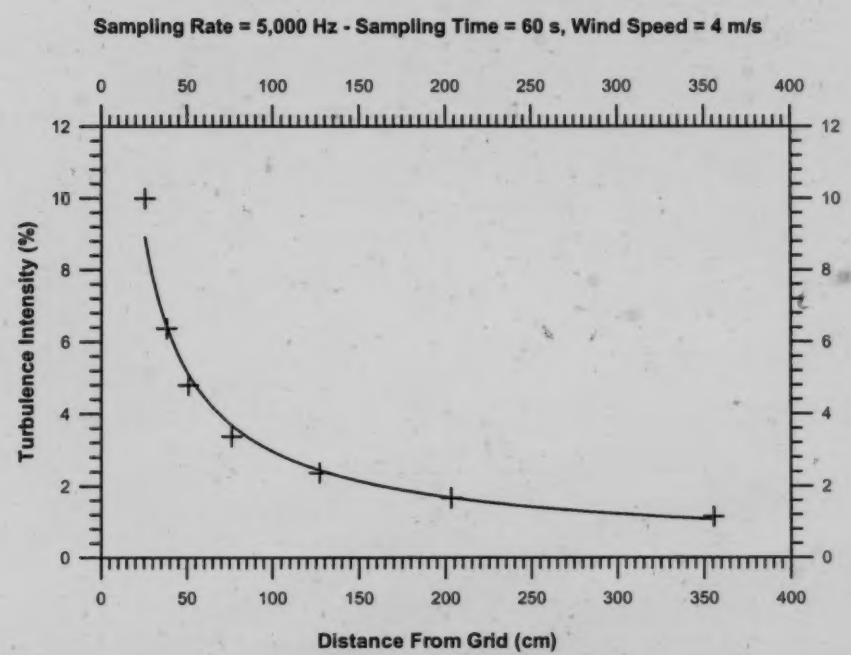

Figure 3.10: Turbulence intensity decay behind the grid with 25.4 mm square holes

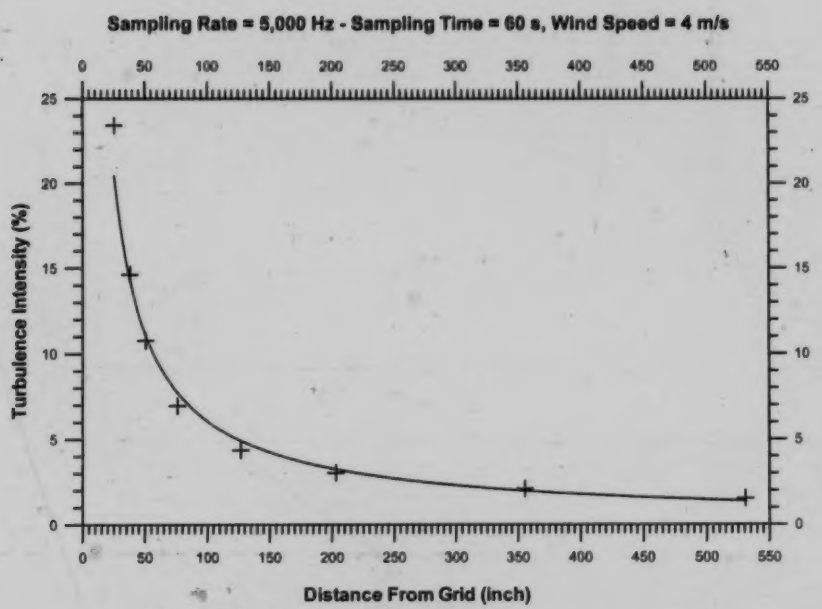

Figure 3.11: Turbulence intensity decay behind the gird with 50.8 mm square holes

References:

1. Prybysh, R. (2002),"*The Production of Toxic Emissions from Reacting Diffusion Jet Flame in a Crossflow*", M.Sc. Dissertation, University of Alberta, Edmonton, Alberta, Canada
2. Johnson, M. R., Spangelo, J. L, and Kostiuk, L. W. (2001)" *A characterization of Solution Gas Flaring in Alberta*", Air & Waste Management Association, 51: 1167-1177.
3. Johnson, M. R., and Kostiuk, L. W. (2000)," *Efficiency of Low Momentum Jet Diffusion Flames in Crosswind*", Combustion and Flare, 123: 189-200.
4. Kostiuk, L. W. (2000)*"Interim Report November 1996-June 2000"*, University of Alberta Flare Research Project.
5. Glassman I. (1977) *"Combustion"*, Academic Press Inc., New York, U.S.A.

Chapter 4

RESULTS OF THE FLARES WITH LIQUID DROPLETS IN THE FLARE STREAM

This chapter discusses the results obtained from experimental work on measuring the effects of that liquid droplets have on combustion efficiency of the scaled down modeled flares. Tests have been conducted on a 24.7 mm outside diameter flares and data were collected by adding droplets of iso-octane, diesel, or distilled water into the flare stream. Similarly, these liquids were added to the flare stream with various mass flow rates in order to obtain various mass ratios (*i.e.* $\dot{m}_L/\dot{m}_G$). It was hard to control the droplet size therefore, droplet sizes were divided into two broad categories, *i.e.* "small" and "large", depending upon the type of liquid. For iso-octane, "small" means droplets whose mass mean diameter ranged from 4 μm to 15 μm. Whereas, "large" means droplets with mass mean diameters between 80 μm and 90 μm. In case of diesel, "small" is meant for droplets having the mass mean diameters between 69 μm and 89 μm. "Large" means droplets with mass mean diameters between 127 μm and 197 μm. Similarly, "small" distilled water droplets are droplets with mass mean diameters between 48 μm and 70 μm. "Large" droplets mean droplets that have a mass mean diameter between 103 μm and 111 μm.

The notion behind selection of these three different types of liquids was to understand the effects of lighter and heavier liquid hydrocarbons. Distilled water was selected, as water is also collected with liquids that are extracted out with conventional oil at a battery site and to study the effects of a non-combustible liquid on flare efficiency. Sales grade natu-

ral gas was used as flare gas with two different mass flow rates ($\dot{m}_G$) and jet exit velocities, (V_j). In order to focus on the portion of fuel that remains unburned and exists in the products of combustion from the flare, the results are presented in terms of percentage inefficient, which is simply (1-η)*100%. Scaled down modeled flares were tested under the crosswind speeds of 2 m/s to 9 m/s. The major portion of the results is shown in terms of inefficiency as a function of crosswind speed.

Since efficiency of scaled down flares is calculated based on concentrations of carbon-containing species (*i.e.* CO_2, HC, and CO) present in the products of combustion, the background concentrations of these major carbon-containing species were noted in ambient air inside the tunnel before starting an individual test. Online gas analyzers continuously monitored these concentrations during each test. Similarly, the products of combustion were thoroughly mixed with the help of mixing fans before sampling. It has been shown that the unburned hydrocarbons have the same volume fraction distribution as the flare stream, which means that hydrocarbons emitted are stripped off from the flow and are not a result of incomplete combustion (Kostiuk, 2000). Figure 4.1, shows the time trace of the concentrations of CO_2, CO, and HC during a particular test. With the background concentration of CO_2~361ppm, CO~0.3ppm, and HC~3ppm, the flare was ignited having 20 l/min (14.93 g/min) flow rate of the flare gas. The crosswind speed during the test was 4 m/s. Burning continued for 470 seconds and then the tunnel was purged with fresh air. Figure 4.2, shows the measured inefficiencies of two different gas phase flares that were tested under the crosswind speeds of 2m/s to 9 m/s. The results indicate that both crosswind speed and jet exit velocity have a notable effect on flare inefficiency.

With a flare gas exit velocity of 1 m/s, the exponential rise in inefficiency of the flare at 5 m/s to 7 m/s shows the strong effect of the crosswinds, while the flare remains less inefficient (<1%) at moderate crosswinds (*i.e.* 2m/s to 4 m/s). On the other hand, the crosswind does not show much effect on inefficiency of the flare with 2 m/s jet exit velocity. The inefficiency is less than 1% until 7 m/s crosswind speed and rises gradually with further increase in the wind speed. It was observed that the flares with higher jet exit velocities were less sensitive to the effects of crosswinds.

4.1 Effects of Iso-Octane Droplets on the Inefficiency of the Flares in Crosswind

Tests were conducted on scaled down flares having droplets of iso-octane in their flare stream in various sizes and proportions. Figure 4.3, shows the results obtained from one set of tests. Since, flares were tested under the crosswind speed varying from 2 m/s to 7 m/s, each individual test comprised of six experiments on flares with gaseous fuel only and six experiments on the flares with both liquid and gaseous fuel in the flare stream. Mass flow rate of natural gas was 14.93 g/min during each experiment with 1 m/s jet exit velocity. Iso-octane was added to the flare stream at a flow rate of 2.25 g/min and the mass ratio of liquid to gaseous fuel was 0.15. The mass mean diameter of the droplets was ~10 μm. Figure 4.3 demonstrates combustion inefficiency versus crosswind speed with and without iso-octane droplets in the flare stream. Focusing on the flares with natural gas only, the crosswinds showed a strong effect on the combustion inefficiency. The inefficiency of flares increased with an increase in crosswind velocity.

Addition of iso-octane droplet into the flare stream showed a good affect on the combustion inefficiency. Iso-octane droplets lowered the inefficiency of the flares, when tested under the same crosswind conditions. At moderate crosswinds (2 m/s to 4 m/s) the inefficiencies of both types of flares remained under 1% inefficiency. At higher crosswinds (5 m/s to 7 m/s), the inefficiency of natural gas flares only raised up to 6%, where the inefficiency of the flares with iso-octane droplets raised only up to 3%. It was also observed that at moderate crosswinds, addition of iso-octane droplets did not show a profound effect on the inefficiency but it lowered the inefficiency at higher crosswind speeds.

Johnson and Kostiuk (2000) studied low momentum jet diffusion flames and discussed the visual observations on these flames in detail. The flares under that study were the ones with gaseous fuels only in their flare stream. The structure of the flares with iso-octane droplets was almost the same as they described but in this case, the flares were more luminescent at lower crosswind speeds. This luminosity was likely due to burning of the droplets that exited the flare stack with gaseous stream and actually took part in combustion. At higher crosswinds, an increasing portion of the fuel is striped off from the flame by a recirculation zone behind the stack and results in higher inefficiency. Burning of some larger droplets could be observed in the flame by small streaks of light appearing at the flare surface.

Even though the fuel droplets require energy to vaporize before burning, their chemical energy extensively increases the energy density of the flare compared to the natural gas only. Being a volatile combustible liquid, iso-octane droplets mostly vaporize before en-

tering the flame. The addition of a combustible liquid to the flare stream results in raising the carbon content in the fuel. Accumulation rates of major carbon-containing species (*i.e.* CO_2, HC, and CO) during each experiment showed that the concentrations of CO_2 and CO were higher in the products of combustion, when the droplets were added to the flare stream. Similarly, concentrations of unburned hydrocarbons in the products of combustion from the flares having gaseous fuel only were higher than flares with both gaseous and liquid fuels in the flare stream. The presence of higher concentrations of CO_2 and lower concentrations of HC showed that the oxidation rate of the liquid fuel was higher that resulted in lower inefficiency of the flares.

4.1.1 Effects of the Flare Gas Exit Velocity on the Flares with Liquid Droplets in the Flare Stream

Figure 4.4, shows the inefficiencies of the flares with iso-octane droplets, as a function of crosswind speed and mass flow rate of the flare gas. The flares have same size of the droplets (~15 μm) and the same flow rates of iso-octane (2.5 g/min) but different jet exit velocities. The flare with 14.93 g/min (20 l/min) of flare gas had 1 m/s as a jet exit velocity and the flares with 29.86 g/min (40 l/min) of the flare gas had 2 m/s as a jet exit velocity. The effect of jet exit velocity on the flares with both gaseous and liquid fuel was observable. The flares with higher jet exit velocities (2 m/s) were less inefficient than the ones with lower jet exit velocities (1 m/s) having the same flow rate and droplet size of iso-octane. The inefficiency of the flares with 29.86 g/min of flare gas remained under 1%. Where, the inefficiency the flares with 14.93 g/min of the flare gas remained under

1% only up to 5 m/s crosswind speed but increased drastically at 6m/s and 7 m/s). The effects of momentum ratio on flare inefficiency were also observed. Both types of the flares had low momentum ratios (0.19 to 0.012 and 0.72 to 0.033). The concentrations HC and CO increased and concentration of CO_2 decreased in the products of combustion with decrease in momentum ratios of flares having lower and higher jet exit velocities, respectively. The increase in HC and CO concentrations and decrease in CO2 concentration were observed to be quicker in combustion products from flare with low jet exit velocity. Inefficiency raised at 3 m/s and dropped down at 4 m/s in flares of both low and high jet exit velocities. The reasons of this variation in flare inefficiency at these crosswinds were not investigated.

A second set of experiments was conducted on the flares with liquid droplets in the flare stream in crosswinds. The flares had the same jet exit velocities as that of the previous test (*i.e.* 1 m/s and 2 m/s). Same size droplets (*i.e.* ~15 μm) were added to the flare stream but the mass flow rate of iso-octane was increased to 5 g/min in order to see the effects on flare inefficiency. Figure 4.5, is the representation of inefficiency of the flares with two different jet exit velocities having same sizes of the droplets and flow rate of iso-octane in their flare stream. The measured inefficiencies showed that an increase in the jet exit velocity and mass flow rate of flare gas decreased the inefficiency of flares with same size droplets and flow rate of iso-octane. The results from these two tests agree to the fact that the inefficiency of the flares with iso-octane droplets in their flare stream decreases with an increase in flow rate and exit velocity of flare gas for the same flow rate

of iso-octane. The effects of increasing flow rates of iso-octane on the flare inefficiency were not under consideration here and it will be discussed later.

4.1.2 Effects of the Droplet Size on the Flare Inefficiency

The effects of droplet size on flare inefficiency are shown in Figure 4.6. The inefficiency of two flares having the same mass ratio (0.27) but different sizes of droplets are demonstrated as a function of crosswind speed. The mass flow rate of natural gas was 14.93 g/min with 1 m/s jet exit velocity. Iso-octane was added to the flare stream with a mass flow rate of 4 g/min. Small droplets (~5 μm) were added to one flare and large droplets (~66 μm) were added to the other flare. It was observed that droplet size had no significant affect on the flare inefficiency. The inefficiencies of the flares with large size droplets were slightly higher than the flares with small size droplets at moderate crosswind speeds (*i.e.* 2 m/s to 4 m/s). Differences in the inefficiency were observed to be due to different concentrations of the major carbon-containing species in the products of combustion from these flares. Accumulated concentrations of HC were higher, where concentrations of CO_2 and CO were lower from the flares with large size droplets compared to flares with small size droplets, when examined at 2m/s to 5 m/s. At higher crosswinds (*i.e.* 6m/s to 7 m/s) inefficiencies of flares with large size droplet were lower than the flares with small size droplets. It was observed that at these crosswind speeds, concentrations of CO_2 and CO were higher, where the concentration of HC was lower in the products of combustion from the flare that contained large droplets compared to one that contained small droplets. The difference in the inefficiencies of the flares with small and

large droplets at each individual crosswind speeds from 2 m/s to 7 m/s were less than 1%. Droplet size has no profound influence on flare inefficiency, though iso-octane droplets lowers flare inefficiency.

Another set of tests was selected to confirm whether the size of the iso-octane droplets changes inefficiencies of the flares significantly at various crosswind speeds. Figure 4.7, shows inefficiency analysis of such flares with small and large droplets in crosswinds. The mass flow rate of the gas was 14.93 g/min. Iso-octane was added to the flare with a mass flow rate of 4.5 g/min. Droplets sizes of ~ 4 μm and ~ 85μm. Since the difference in combustion inefficiencies of flares containing small and large size droplets in their flare streams at each individual crosswind speed were less than 1%. It leads to a conclusion that there is no noticeable difference in the effects of both small and large size droplets on inefficiency of flares in crosswinds.

The effects of small and large size iso-octane droplets on the measured flare inefficiencies with higher flow rate of the flare gas are shown in Figure 4.8. Two different sizes of the droplet (~14 μm and ~80 μm) were added to the flare stream with 29.86 g/min flow rate of the flare gas. Iso-octane was added at flow rate of 4.5 g/min and the mass ratio was 0.15. The observed inefficiencies of the flares with small size droplets were lower at moderate crosswind speeds (*i.e.* 2 m/s to 4 m/s) compared to flares with large size droplets. Concentrations of unburned hydrocarbons and CO_2 were lower in products of combustion from flares with small size droplets at these crosswind speeds. At crosswind speeds of 5 m/s to 9 m/s, measured inefficiencies of flares with small size droplets were

higher compared to flares with large size droplets. This increase in inefficiency was due to higher concentrations of unburned hydrocarbons and CO and lower concentrations of CO_2 in the products of combustion. Since differences in flare inefficiencies at the crosswind speeds of 2 m/s to 9 m/s were observed to be very small, the overall effects of iso-octane small and large size droplets on inefficiency of flares with the same mass flow rate of flare gas were considered the same.

4.1.3 Effects of the Mass Flow Rate of Iso-Octane on the Flare Inefficiency

To understand the effects of mass flow rate of iso-octane on the flare inefficiency, experiments were conducted on natural gas flares with a mass flow rate of 14.93 g/min. Iso-octane was added at the flow rates of 3.0 g/min and 6.5 g/min to the flare stream. The droplets size in both cases was approximately 35 μm and the mass ratios were 0.18 and 0.44, respectively. Figure 4.9, is the representation of the inefficiency of the flares as a function of crosswind speed having same size of the droplets and different flow rate of liquid in their flare stream. The data presented in Figure 4.9, are collected from the result of two different ultrasonic droplet generators (*i.e.* 48 kHz and 18 kHz respectively). The measured inefficiencies of flares with higher flow rate of iso-octane were lower than inefficiencies of flares with lower flow rate of iso-octane. It was observed that the inefficiency of flares decreased almost by half a percent, when the flow rate of iso-octane was approximately doubled at each individual crosswind speed from 2 m/s to 7 m/s. The inefficiency of flares with the higher flow rate of iso-octane at 2 m/s is not shown in the Figure 4.9 because as soon as the flow of iso-octane was started to the flare stream, the flame

blew off. Accumulated concentrations of CO_2 within the tunnel during the experiments showed that increased mass flow rate of iso-octane resulted in the increased concentration of CO_2 in the products of combustion. Similarly, the concentrations of unburned hydrocarbons were lower in combustion products from flares having higher flow rate of iso-octane than flares with lower flow rate of iso-octane. Difference in the concentrations of CO in the products of combustion from both types of flares was small. Therefore, measured inefficiencies of flares with higher flow rate iso-octane were lower based on the concentrations of major carbon-containing species in the products of combustion.

Figure 4.10, shows the inefficiency of the flares as a function of mass flow rate of iso-octane at 5 m/s and 6 m/s crosswind speeds. Tests were conducted by adding iso-octane with increasing flow rate from 3.5 g/min to 7 g/min into the flare. Flare gas flow rate was 14.93 g/min with 1 m/s jet exit velocity. The results showed that the flare inefficiencies decrease with the increase in the flow rate of iso-octane at both crosswind speeds.

A series of tests were conducted to study the effects of iso-octane flow rates on the inefficiency of the flares with the higher flow rate of the flare gas. Figure 4.11, shows the results of the two sets of tests, when iso-octane was added to the flare stream in two different proportions. Natural gas flow rate was 29.86 g/min with a jet exit velocity of 2 m/s. Iso-octane was added to the flare stream with flow rates of 2.5 g/min and 5 g/min. Mass ratios were 0.08 and 0.17 and the droplets size was ~15 μm. At crosswind speeds of 2 m/s to 8 m/s, iso-octane flow rate did not show an observable effect as the measured flare inefficiencies were almost the same. At higher crosswind speed (*i.e.* 9 m/s), a slight change

in the inefficiency was observed. The inefficiencies of both types of flares were below 1% from the crosswind speeds of 2 m/s to 7 m/s and raised up to 2.5% with the further increase in crosswinds. The results showed that inefficiencies of the flares having higher flare gas flow rate were unaffected by increasing the flow rate of iso-octane.

Figure 4.12, shows test results of flares with 2 m/s flare gas exit velocities, when iso-octane was added to the flare stream with the flow rate ranging from 2.5 g/min to 9 g/min. Since inefficiencies of the flares were less than 1% up to crosswind speeds of 7 m/s, higher crosswind speeds (*i.e.* 8 m/s and 9 m/s) were selected to study any observable effects of increasing flow rate of iso-octane on the flare inefficiency. It was observed that increasing flow rate of iso-octane did not show a profound effect on the flare inefficiency at both speeds. Since, the inefficiency fluctuated within a percent, the inefficiency of the flares having higher flow rates of the flare gas were considered to be unaffected by increasing flow rate of iso-octane.

4.2 Effects of Diesel Droplets on the Inefficiency of the Flares in Crosswind

A series of tests were conducted on the natural gas flares by adding various sizes of diesel droplets to the flare stream using two different ultrasonic droplet generators. To study the effects on flare inefficiency, diesel was added to the flare gas with various flow rates. Figure 4.13, shows results from one such set of tests and illustrates flare inefficiency as a function of crosswinds with and without diesel droplets in the flare stream. Natural gas flow rate was 14.93 g/min and diesel was added at flow rate of 2.5 g/min. Using 18 kHz ultrasonic droplet generator, droplets size was ~97 μm and the mass ratio was 0.17. The flares were subjected to crosswind speeds of 2 m/s to 7 m/s. The raise in inefficiency of both types of flares showed a strong affect of the crosswinds. Addition of diesel droplets to the flare stream did not show a substantial effect on flare inefficiency at low crosswind speeds (*i.e.* 2 m/s to 4 m/s). At higher crosswind speeds (*i.e.* 5 m/s to 7 m/s), flare inefficiency decreased, when diesel droplets were added to the flare stream. With an increase in crosswind speed, the difference in inefficiencies of flares with and without diesel droplets increased (*i.e.* ~1% at 5 m/s, ~1.5 % at 6 m/s, and ~ 2.5% at 7 m/s).

Addition of droplets of a heavy liquid hydrocarbon (diesel) to the natural gas flare changes the energy density of the flare. The droplets that vaporized within the flame and took part in the combustion process raised the carbon content of the fuel, which was observed from accumulation rates of major carbon-containing species (*i.e.* CO_2, CO, and HC) during a test. Concentrations of CO_2, and CO were higher, when diesel droplets were added to the flare stream. Whereas, concentrations of unburned hydrocarbons were

lower. An increase in CO_2 concentration and decrease in concentration of unburned hydrocarbon in the products of combustion from the flares with diesel droplets in the flare stream shows the higher oxidation rate of the diesel fuel that results lower inefficiency of the flares. Comparison between the effects of diesel and iso-octane droplets on the flare inefficiency will be discussed later in this chapter.

4.2.1 Effects of the Droplet Size on the Flare Inefficiency

Tests were conducted by adding two different sizes of diesel droplets to the natural gas flares to examine the effects of droplet size on flare inefficiency. Natural gas flow rate was 14.93 g/min with exit velocity of 1 m/s and diesel droplets were added to the flare stream at the flow rate of 2.5 g/min. Figure 4.14, shows the inefficiency of the flares as a function of crosswind speed, when two different sizes of diesel droplets were added to the flare stream. The mass ratio was 0.17 and the droplet sizes were ~69 μm and ~127 μm, respectively. It was observed that inefficiency of the flares decreased with an increase in size of the diesel droplets. At moderate crosswind speeds (*i.e.* 2 m/s to 4 m/s) the droplet size has little effect on the flare inefficiency, as the inefficiencies of the flares having both sizes of diesel droplets were less than 1%. At higher crosswind speed (*i.e.* 5 m/s to 7 m/s) the inefficiency rose up to 6% and the effects of the droplet size on the flare inefficiency were noticeable. At each of the three crosswind speeds, differences in flare inefficiencies with both sizes of droplets were approximately 1/2%.

The decrease in inefficiency of the flares with small size diesel droplets shows higher oxidation rate of the diesel fuel, as the accumulated concentrations of CO_2 at the end of each test were higher in combustion products. Similarly, concentrations of CO and HC were lower, when small size droplets were added to flare than flares with large size droplets. It was observed that some of the large droplets dropped out of the flame before their complete combustion. The incomplete combustion of the diesel fuel caused a decrease in CO_2 concentrations, which resulted in higher inefficiency of the flares.

Another set of tests was conducted on the flares with higher flow rate of the flare gas having two different sizes of diesel droplets in their flare streams. Figure 4.15, shows the effects droplet size on the flare inefficiency of the flares with higher flare gas exit velocity under varying crosswind conditions. Diesel was added to the flare stream at the flow rate of 3.5 g/min and the flare gas flow rate was 29.86 g/min. Droplets sizes were ~87 μm and ~197 μm, respectively, and the mass ratio was 0.12. The observed flare inefficiencies of the flares with small droplets were lower than the flares with large droplets. These results agree with the results shown in previous figure and shows that the effects of droplet size are not influenced by the flow rate of flare gas.

4.2.2 Effects of the Mass Flow Rate of Diesel on the Flare Inefficiency

Figure 4.16, shows the inefficiency of flares as a function of crosswind speed, when diesel was added to the flare stream in varying proportions. Natural gas flow rate was 14.93 g/min with 1 m/s flare gas exit velocity. Diesel was added to the flare stream in varying

flow rates ranging from 2.5 g/min 5 g/min. The results showed that flare inefficiencies were unaffected by the increasing flow rates of diesel at the crosswind speeds of 2 m/s to 5 m/s. At the crosswind speed of 6 m/s and 7 m/s, a slight variation was observed in the inefficiency of the flares with an increase in the flow rate of diesel. From data shown in Figure 4.16, it was observed that an increase in the flow rate of diesel into the flare stream had very little effect on inefficiency of the flares as flare inefficiency did not show noticeable change, when the flow rate of diesel was increased.

A series of tests were conducted to observe the effects of varying flow rates of diesel on inefficiency of the flares that have high flare gas flow rates. Natural gas flow rate was 29.86 g/min having 2 m/s jet exit velocity during the tests and diesel was added to the flare stream at varying flow rates ranging from 2.5 g/min to 5.5 g/min. Figure 4.17, shows results of the tests conducted on these flares and flare inefficiencies are presented as a function of crosswind speed. The crosswind had a strong effect on flare inefficiency as an increase in the crosswind speed resulted in the increase in the flare inefficiency. The results showed that inefficiency did not change very much, when diesel was added to the flare stream at various flow rates. At crosswind speeds of 2 m/s to 8 m/s, the inefficiencies were less than 1.5%. A slight scatter in the flare inefficiencies was observed at 9 m/s crosswind speed. Since inefficiencies fluctuate within 0.5% at this crosswind speed, it was considered that any increase or decrease in flow rate of diesel has a similar effect on flare inefficiency at higher crosswind speed. A conclusion that could be drawn in light of results obtained from tests conducted on the flare at higher and lower flare gas flow rates is that varying the flow rates of diesel into the flare stream has similar effects on the inef-

ficiency of these flare. Though, adding diesel droplet to the flare stream lowered the flare inefficiency.

4.3 Effects of Distilled Water Droplets on the Flare Inefficiency in Crosswind

Droplets of distilled water in various sizes and proportions were added to the natural gas flares to understand their effects on the inefficiency. The droplets were generated using 18 kHz and 48 kHz ultrasonic generators and distilled water was added to the gaseous flare stream with various flow rates. Tests were conducted in different sets on natural gas flares having two different flow rates and flare gas exit velocities. Figure 4.18, represents results of one such set of tests. Where inefficiencies of two types of flares (*i.e.* with & without water droplets) are shown as a function of crosswind speed. Natural gas flow rate was 14.93 g/min with 1 m/s jet exit velocity in all the tests. Distilled water droplets were added to the flare stream at the flow rate of 2.5 g/min. Mass ratio was 0.17 and the droplets size was ~96 μm. It was observed that addition of distilled water droplets to the flare stream increased inefficiency of the flares under the crosswind speeds of 2 m/s to 7 m/s. The effects of water droplets on flare inefficiency was not visible at 2 m/s and 3 m/s crosswinds speed as the inefficiencies were lower than 1%. At crosswind speeds of 4 m/s to 7 m/s, the droplets had a strong effect on flare inefficiency (~1% to ~8%). The crosswind has also shown its notable effect on the inefficiencies of both types of flares.

The adding of droplets of a non-combustible liquid (distilled water) to the gaseous fuel stream decreases the energy density as the droplets extract energy from the flame for their

vaporization. The flame temperature decreases as a result of energy loss as the droplets do not take part in the combustion process and affect the concentrations of carbon-containing species in the products of combustion. It was observed that the concentrations of unburned hydrocarbons HC and CO were lower in the combustion products of flares with gaseous fuel only compared flares with distilled water droplets in the flare stream. Similarly, addition of distilled water droplets to the flare stream lowered the concentration of CO_2 in the products of combustion. Since, an increase in crosswind speed causes the incomplete combustion of gaseous phase flares with or without liquid droplets and results in more inefficient flares. The addition of a non-combustible liquid to the gaseous fuel stream slowed down the combustion of fuel and resulted in an increase in the flare inefficiency.

A set of tests was also conducted to examine the effect of jet exit velocity on the inefficiency of natural gas flares with and without distilled water droplets in the flare stream. The flow rate of natural gas was 29.86 g/min during the tests. Distilled water was added to the flare stream at a flow rate of 2.5 g/min with the droplet size of ~57 μm and the mass ratio was 0.08. Figure 4.19, demonstrates the inefficiencies of the flares with and without distilled water droplets as a function of crosswind speed. It was observed that inefficiencies of the flares with water droplets were higher than flares with gaseous fuel only. The increase in inefficiency by adding distilled water droplets to the flare stream was less than 1% at each particular crosswind speed. Water droplets did not show a profound effect on the inefficiency of flares having higher flow rate of flare gas and jet exit velocity, though it raised the inefficiency by a fraction of a percent.

4.3.1 Effect of the Water Droplet Size on the Flare Inefficiency in Crosswind

Figure 4.20, shows the inefficiency of natural gas flares as a function of crosswind speed with two different sizes of water droplets in the flare stream. Natural gas flow rate was 14.93 g/min and distilled water was added to the flare stream at the flow rate of 4 g/min. The droplet sizes were ~70 μm and ~111 μm and the mass ratio was 0.27. The inefficiencies of flares having both sizes of droplets were observed to be almost the same except at higher crosswind speed (*i.e.* at 7 m/s). The difference in the inefficiency was approximately 3%, where the inefficiency of the flare with 70 μm droplets was higher than the flare with 111 μm droplets. The reason for this difference was unknown, though the concentrations of major carbon-containing species (*i.e.* CO_2, CO, and HC) in the products of combustion from the flares were different. The droplets of two different sizes did not show an observable effect on the inefficiency of flare having low flare gas flow rate.

The effects of droplet size on flares with a higher gas flow rate were studied by conducting tests on natural gas flares. The flares were tested in the varying crosswind speeds from 2 m/s to 9 m/s. Figure 4.21, shows results of one such set of tests, where two different sizes of distilled water droplets were added to the gaseous flare stream. Inefficiency is shown as a function of crosswind speed in Figure 4.21. The flow rate of natural gas was 29.86 g/min and the flow rate of distilled water was 3.5 g/min. The mass ratio was 0.12 and droplet sizes were ~ 48 μm and ~ 103 μm, respectively. The results showed that comparatively small and large droplets had the almost the same effect on flare inefficiency under the crosswind speeds of 2 m/s to 7 m/s. At 8 m/s and 9 m/s crosswind

speeds, a change in flare inefficiency was observed, as inefficiencies of flares with small droplets were higher than flares with large droplets. When, the products of combustion from the flare at these crosswind speeds were examined, it was observed that accumulated concentrations of HC and CO in the products of combustion from flares with small droplets were higher than flares with large droplets. The addition of two different sizes of water droplets simultaneously to the gaseous fuel with higher flow rate has the same affect on flare inefficiency at low and moderate crosswind speeds. At higher crosswind speeds, inefficiency of the flares with small water droplet is higher than flares with large water droplets in their gaseous fuel stream.

4.3.2 Effects of the Mass Flow Rate of Distilled Water on the Flare Inefficiency

Droplets of distilled water were added to the natural gas flares at various flow rates that ranged from 2 g/min to 5 g/min and tested under the crosswind speeds of 2 m/s to 7 m/s. A series of tests were conducted on a natural gas flare having low jet exit velocity, when droplets of various sizes were added to the gaseous fuel stream. Natural gas was flowing at the rate of 14.93 g/min. The droplets were generated by two ultrasonic droplet generators (*i.e.* 18 kHz and 48 kHz). Figure 4.22, demonstrates the effects of varying flow rates of distilled water on the flare inefficiency in varying crosswind conditions. The flare inefficiencies fluctuated within 0.5%, when distilled water was added to the flare stream with varying flow rates under the crosswind speed of 2 m/s to 5 m/s. However, at 6 m/s and 7 m/s crosswind speeds, the flare inefficiencies increased with the increase in the flow rate of distilled water. It was observed that inefficiencies fluctuated within a 1% inefficiency

at these crosswind speeds. Therefore, the effects of increasing flow rate of distilled water were considered to be the same on inefficiency of the flares having low flare gas flow rate and jet exit velocity under the investigated crosswind speeds.

To understand the effects of varying flow rates of distilled water on inefficiency of flares having high flare gas flow rate and jet exit velocity, a series of tests were conducted on natural gas flares in crosswind. The flow rate of natural gas was constant during the tests (*i.e.* 29.86 g/min) and distilled water was added to the gaseous fuel at varying flow rates ranging from 2 g/min to 4 g/min. Figure 4.23, shows the inefficiency of flares as a function of crosswind, when distilled water was added to the flare stream. It was observed that variation in the inefficiency of the flares were very small under the crosswind speed of 2 m/s to 7 m/s. However, at higher crosswinds (*i.e.* 8 m/s and 9 m/s), flare inefficiency changed significantly. The inefficiencies of flares with higher flow rate of distilled water (4 g/min) were comparatively higher. After comparing inefficiencies of flares at these higher crosswind speeds, it was observed that differences in flare inefficiencies with increasing flow rates of water were less than 1%. The overall affect of varying flow rate of distilled water was considered to be the same on the inefficiency of the flares having low and high flare gas flow rates, respectively.

4.4 Comparison Between Effects of Iso-Octane, Diesel, and Distilled Water Droplets on the Inefficiency of the Flares

The effects of droplets of two liquid hydrocarbons and a non-combustible liquid on the inefficiency of scaled down natural gas flares have been discussed separately in the previous sections of this chapter. Comparison between the effects of these liquids are discussed in this section. Figure 4.24, shows the inefficiencies of natural gas flares as a function of crosswind speed having droplets of iso-octane, diesel, and distilled water in the flare stream. Natural gas flow rate was 14.93 g/min having 1 m/s jet exit velocity. The liquids were added at the flow rate of 2.5 g/min, though the droplet sizes of each liquid were different. In previous sections, it was observed that droplet size did not have a profound effect on flare inefficiency. At low crosswind speeds (*i.e.* 2 m/s to 3 m/s) the effects of the droplets of all the three liquids on the flare inefficiencies were observed to be the same as the inefficiencies were very low. The distinguishing effects of these different kinds of droplets were visible from the crosswind speed of 4 m/s to 7 m/s. Iso-octane droplets made the flares less inefficient, being a volatile combustible liquid, most of its droplets vaporized before entering the flame and resulted in the improved combustion of the fuel in the flare stream. Diesel droplets also reduced the inefficiency, when added to the gaseous fuel stream. As it is a combustible liquid with less volatility, its droplets extracted energy from the flame for their vaporization so as to take part in the combustion process. The resulting inefficiencies of the flares having diesel droplets were higher than the flares with iso-octane droplets. Though, liquid hydrocarbon droplets reduced the flare inefficiency, the distinguishing effects of both light and heavy liquid hydrocarbon drop-

lets were also visible. The inefficiencies of flares having droplets of iso-octane were lower than inefficiencies of flares with diesel droplets in the flare stream under the investigated crosswind speeds. The droplets of a non-combustible liquid (distilled water), raised the inefficiency of natural gas flares, when added to the flare stream. The energy density of flares with distilled water droplets reduced due to loss of the energy in vaporizing the droplets. Since, water vapors do not take part in the combustion process, it resulted in the more inefficient flares. The results showed that inefficiencies of the flares with distilled water droplets were higher than the flares with liquid hydrocarbon droplets.

Figure 4.25, shows the effects of iso-octane, diesel, and distilled water droplets on the inefficiency of the flares in crosswinds having higher flow rate of the flare gas. Liquid droplets were added at the rate of 2.5 g/min. Natural gas flow rate was 29.86 g/min with jet exit velocity of 2 m/s. Flares were tested under the crosswind speeds of 2 m/s to 9 m/s and the mass ratio was 0.08. Since, the flares having high flow rate of the gaseous fuel are less inefficient at moderate crosswind speeds, the droplets of the three different liquids showed the same kind of effects on flare inefficiency under crosswind speeds of 2 m/s to 6 m/s. A distinguishable affect was observed at higher crosswind speed (*i.e.* 7 m/s to 9 m/s), where inefficiencies of the flares with liquid hydrocarbon droplets were lower than flares having water droplets in the flare stream. The observed difference in inefficiency was approximately 0.4% at 7 m/s, when droplets of light and heavy liquid droplets were added to the flare stream. Similarly, flares with distilled water droplets were more inefficient than flares with diesel droplets and the observed difference in inefficiencies were less than 0.5% at a crosswind speed of 7 m/s. However, at higher crosswind speeds

(*i.e.* 8 m/s and 9 m/s), inefficiency of the flares with water droplets increased up to 4.5%, while inefficiencies of the flares with liquid hydrocarbon droplets were less than 2.5%. The flares were less inefficient, when iso-octane droplets were added to the gaseous fuel than the flares with diesel droplets in the flare stream under the investigated crosswind speeds. Similarly, adding water droplets to the gaseous fuel resulted in higher inefficient flares than the flares with liquid hydrocarbon droplets when tested under the crosswind speeds of 2 m/s to 9 m/s.

Summary:

To understand the effects of liquid droplets on inefficiency of scaled down modeled flares, droplets of iso-octane, diesel, and distilled water were added to natural gas. The addition of iso-octane and diesel decreased flare inefficiency, while distilled water increased the flare inefficiency. The study on flares with liquid droplets in their flare stream conducted by Strosher (1996), showed that the droplets of both combustible and non-combustible liquids increased flare inefficiency. The results of this thesis do not support the results of the study conducted by Strosher.

It was observed that droplet size and mass fraction of liquid could have a modest effect on inefficiency of lower flow rate flares but almost none on the inefficiency of high flow rate flares. It was also observed that the flares were sensitive to higher crosswind speeds as inefficiency of flares increased drastically with increase in crosswind speed.

Addition of the droplets of a combustible liquid (*e.g.* liquid hydrocarbon) to flare stream results in a decrease in flare inefficiency. These droplets do extract energy from flares for their vaporization but the chemical energy they contain is far greater. Therefore, the droplets that vaporize prior to flame cause an increase in the energy density of flare stream. Participation of liquid hydrocarbon droplets in combustion process enhances the combustion of flare stream and lowers the flare inefficiency.

Droplets of a non-combustible liquid (*e.g.* water) only extract energy from the flare to vaporize and lowers the energy density of the flare stream. The combustion rate of the flare stream slows down due to the presence of droplets that become inert vapors and results in an increase in flare inefficiency.

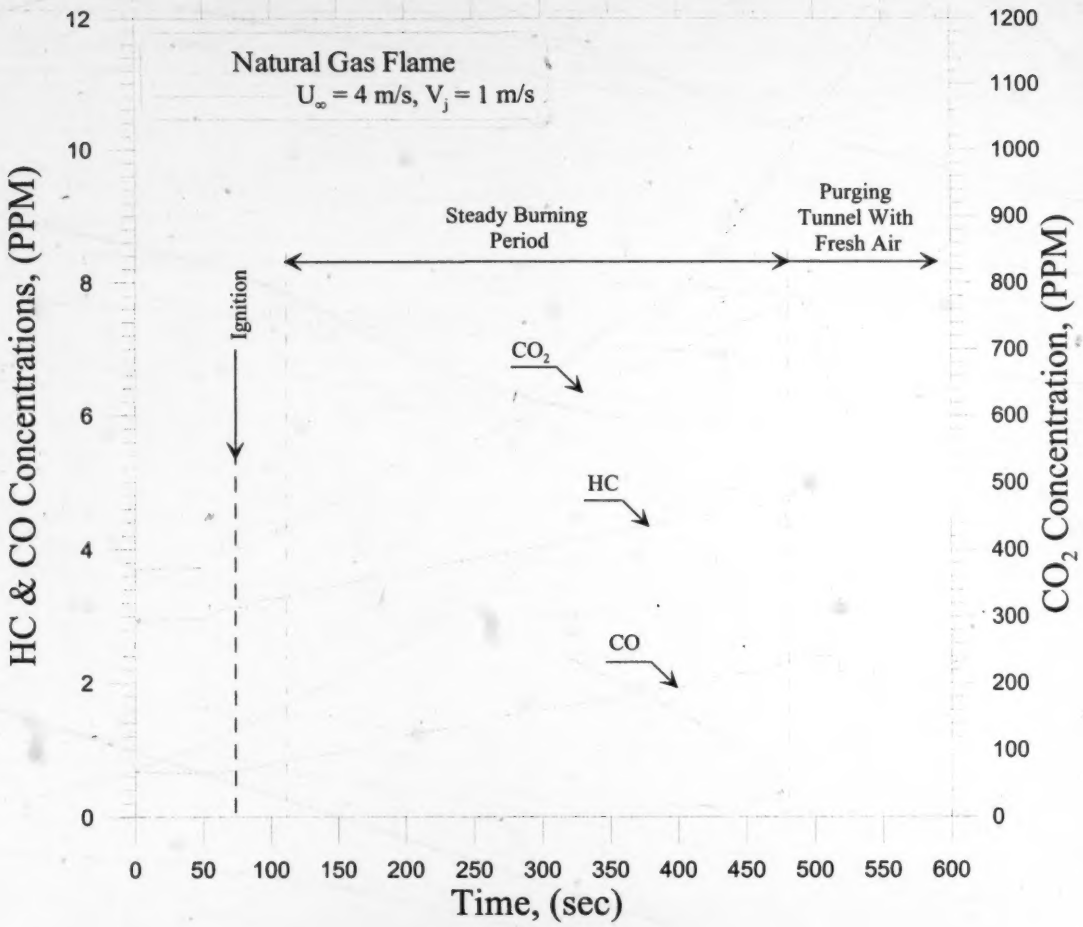

Figure 4.1: Time trace of the concentrations of major carbon-containing species during a typical test in the wind tunnel

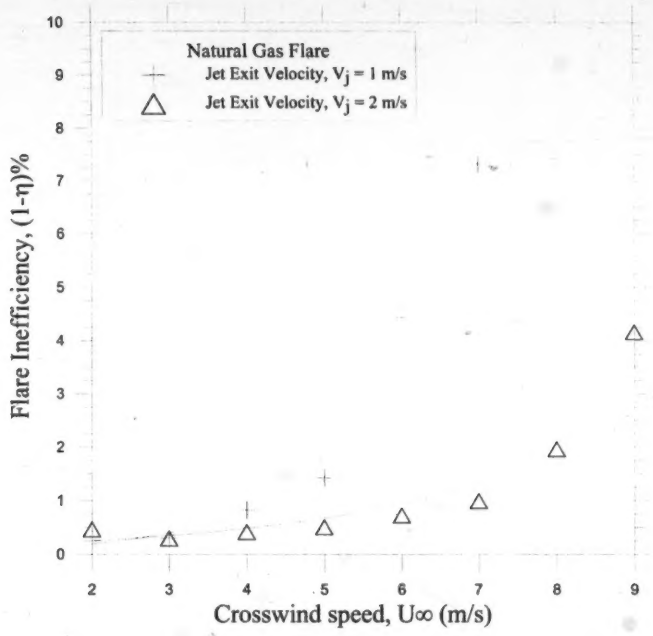

Figure 4.2: Effects of crosswinds and flare gas exit velocity on the inefficiency of the flares

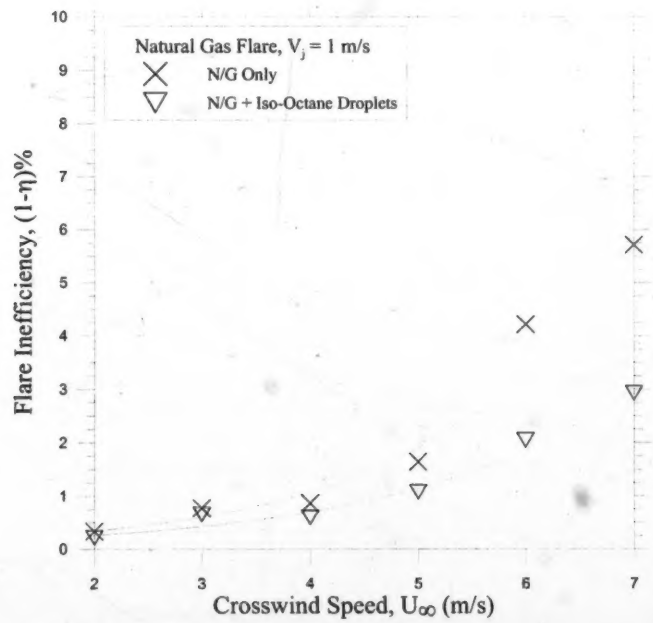

Figure 4.3: Effects iso-octane droplets on the flare inefficiency in crosswinds

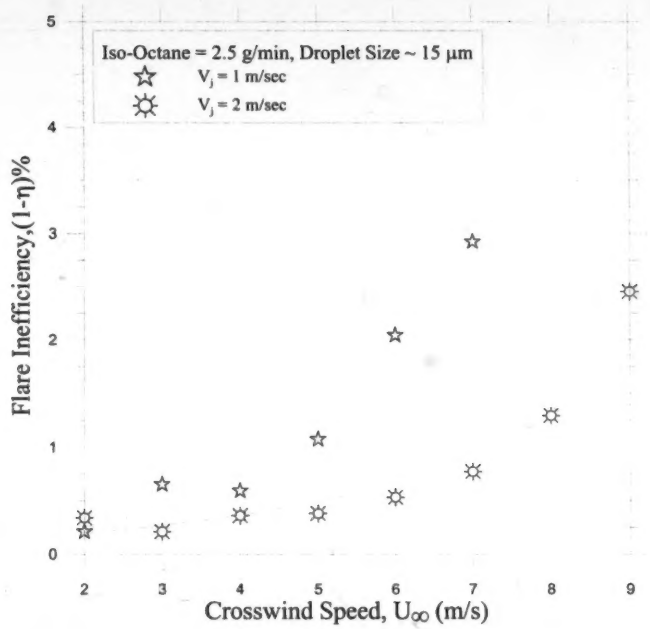

Figure 4.4: Effects of the flare gas exit velocities on the flare inefficiency having same sizes of droplets and mass flow rates of iso-octane

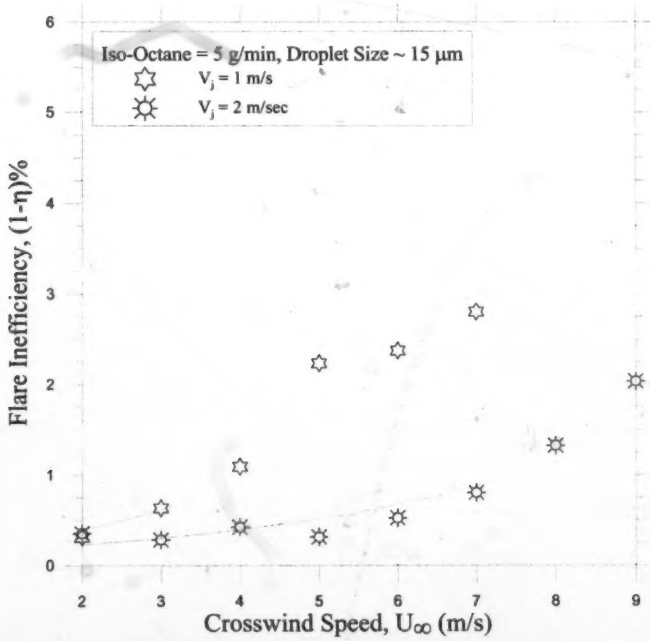

Figure 4.5: Inefficiency analysis of the flares with different flow rates of flare gas and same droplets size and flow rates of iso-octane

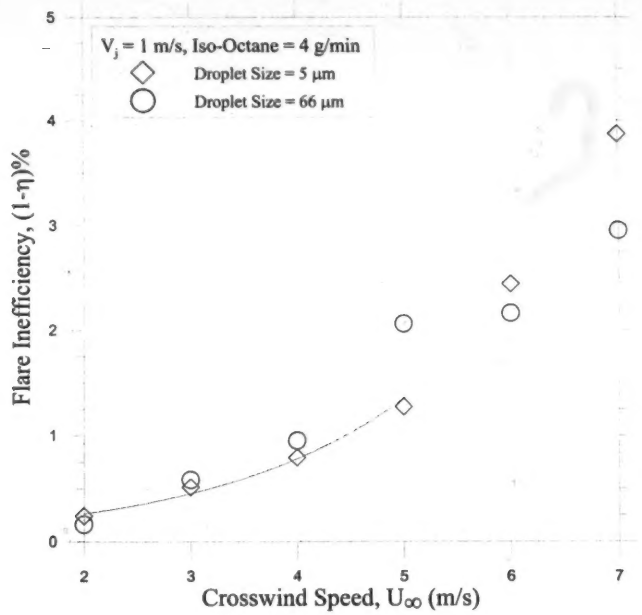

Figure 4.6: Effects of iso-octane droplet size on the inefficiency of the flares with low flare gas exit velocity in crosswind

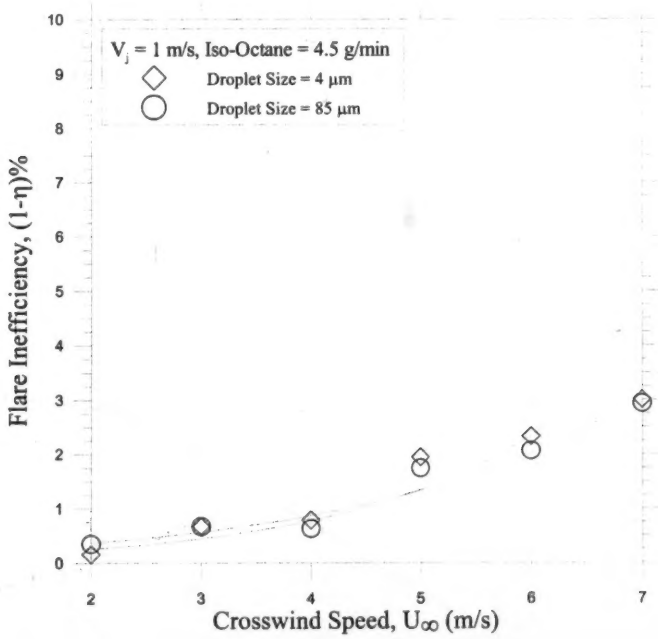

Figure 4.7: Effects of iso-octane droplets size on the flare inefficiency with low jet exit velocity in crosswind

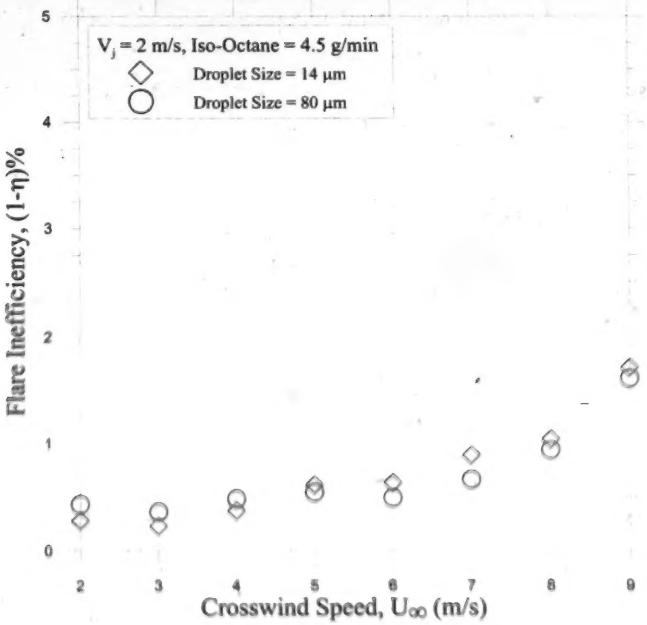

Figure 4.8: Effects of iso-octane droplets size on the inefficiency of the flares with higher jet exit velocity in crosswind

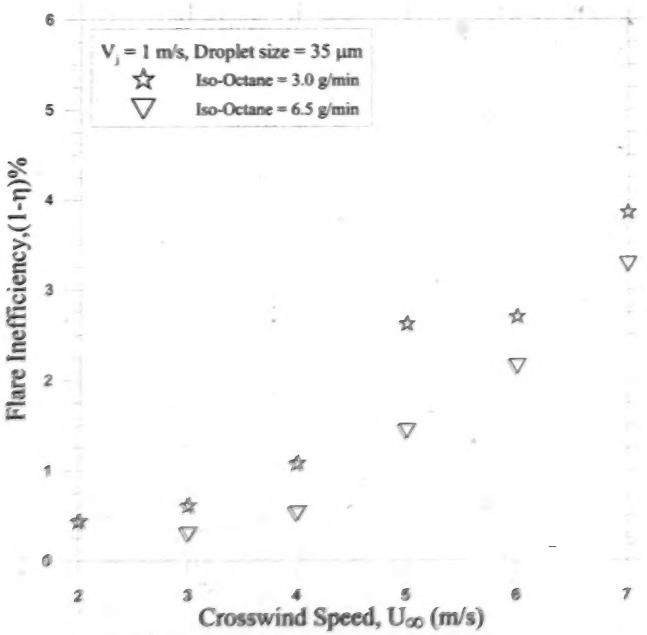

Figure 4.9: Effects of the mass flow rate of iso-octane on the flare inefficiency having same size of the droplets in the flare stream

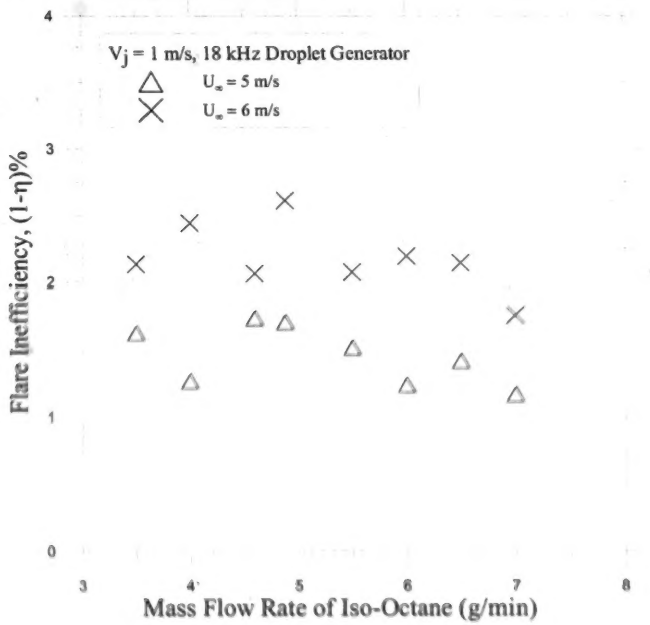

Figure 4.10: Flare inefficiency as a function of mass flow rate of iso-octane using 18 kHz ultrasonic droplets generator

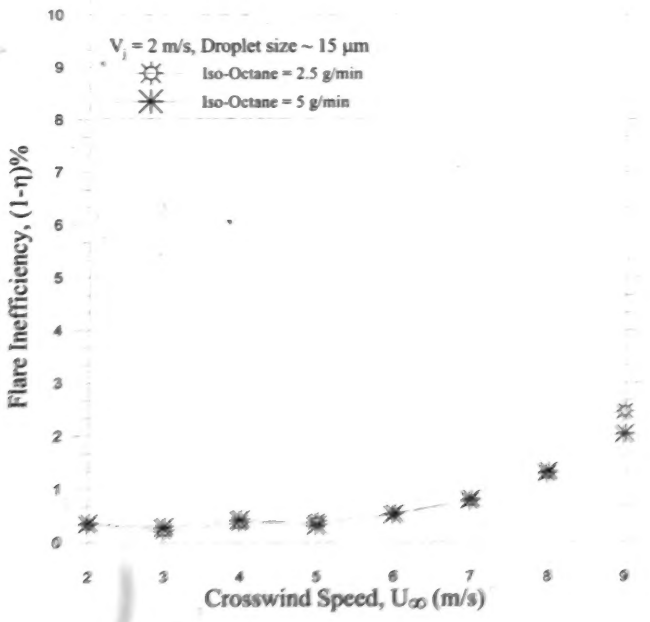

Figure 4.11: Effects of the mass flow rates of natural gas and iso-octane on the flare inefficiency with the same size of droplets in the flare stream

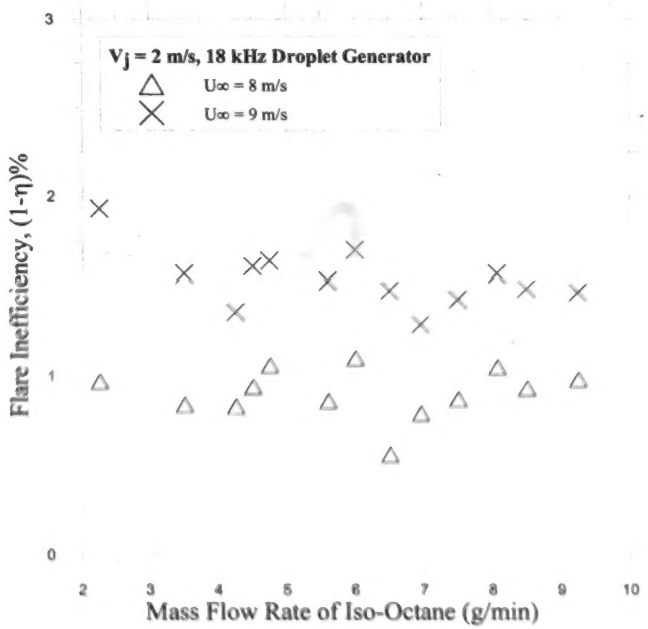

Figure 4.12: Flare inefficiency as a function of mass flow rate of iso-octane with higher jet exit velocity using 18 kHz droplets generator

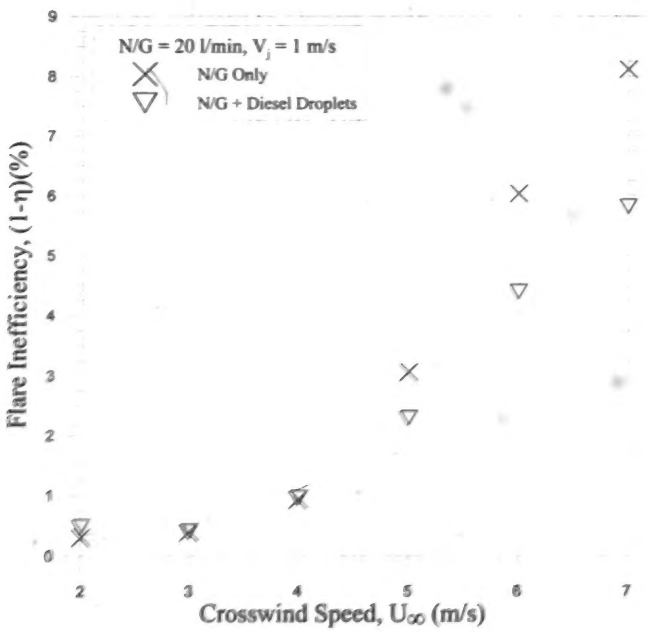

Figure 4.13: Effects of diesel droplets on the inefficiency of the flares in crosswind

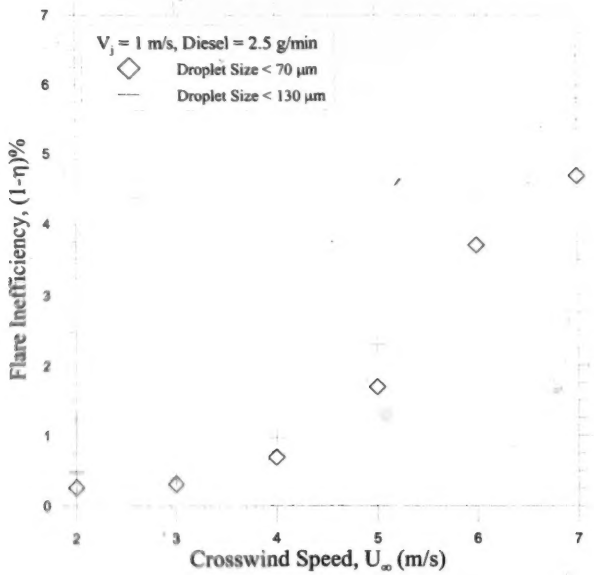

Figure 4.14: Effects of the diesel droplet size on the inefficiency of the flares with low flare gas exit velocity

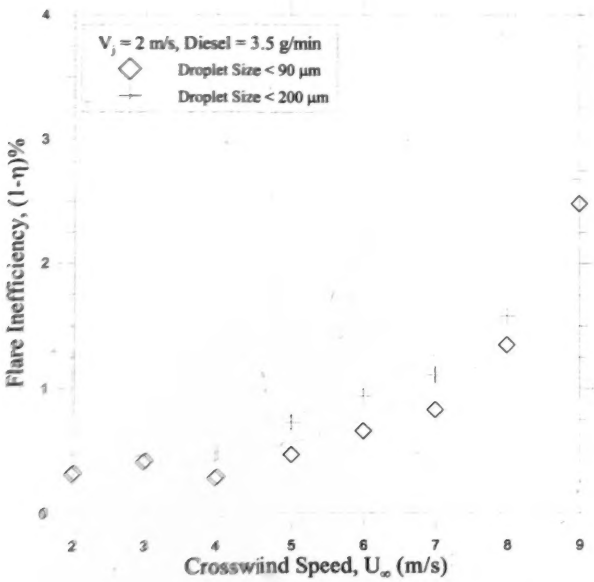

Figure 4.15: Effects of the diesel droplet size on the inefficiency of the flares with higher flare gas exit velocity

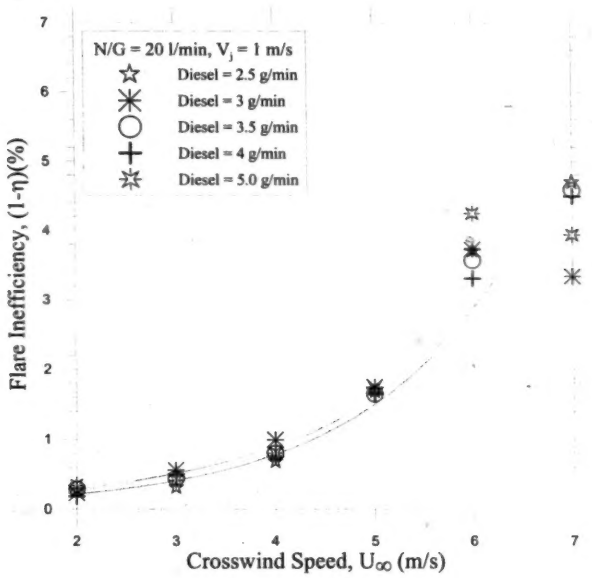
N/G = 20 l/min, V$_j$ = 1 m/s
Diesel = 2.5 g/min
Diesel = 3 g/min
Diesel = 3.5 g/min
Diesel = 4 g/min
Diesel = 5.0 g/min
Flare Inefficiency, (1-η)(%)
Crosswind Speed, U∞ (m/s)

Figure 4.16: Effects of mass flow rates of diesel on the inefficiency of the flares with low jet exit velocity in crosswinds

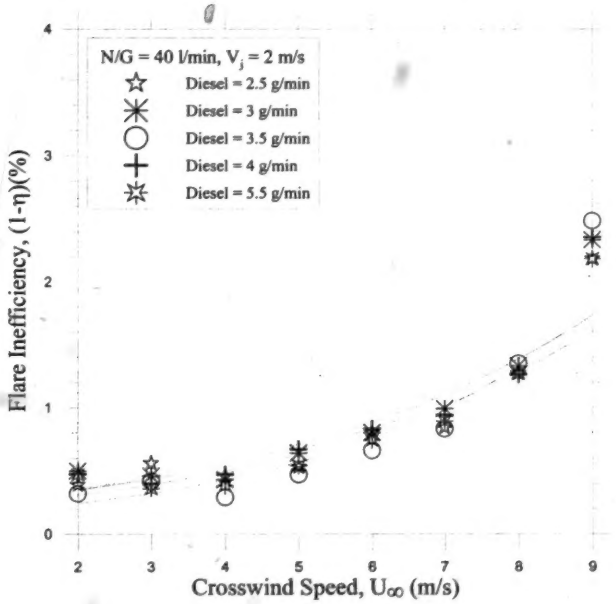
N/G = 40 l/min, V$_j$ = 2 m/s
Diesel = 2.5 g/min
Diesel = 3 g/min
Diesel = 3.5 g/min
Diesel = 4 g/min
Diesel = 5.5 g/min
Flare Inefficiency, (1-η)(%)
Crosswind Speed, U∞ (m/s)

Figure 4.17: Effects of higher jet exit velocity and mass flow rates of diesel on the inefficiency of the flares in crosswinds

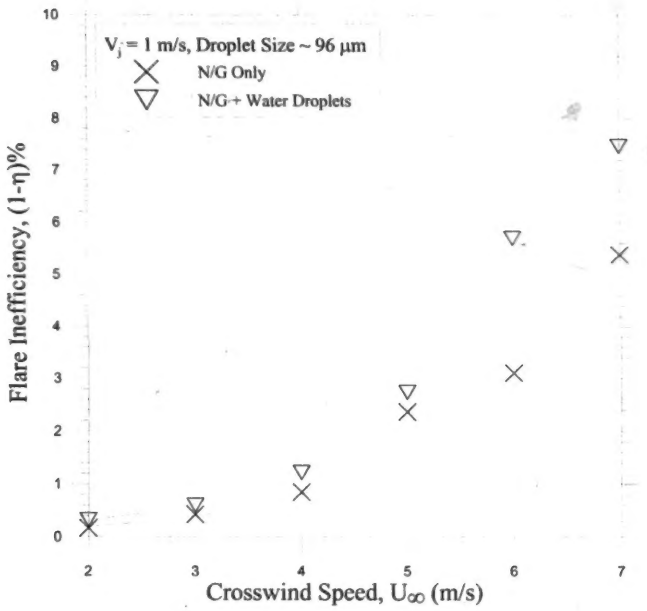

Figure 4.18: Effects of distilled water droplets on the inefficiency of the flare with low flare gas exit velocity in crosswind

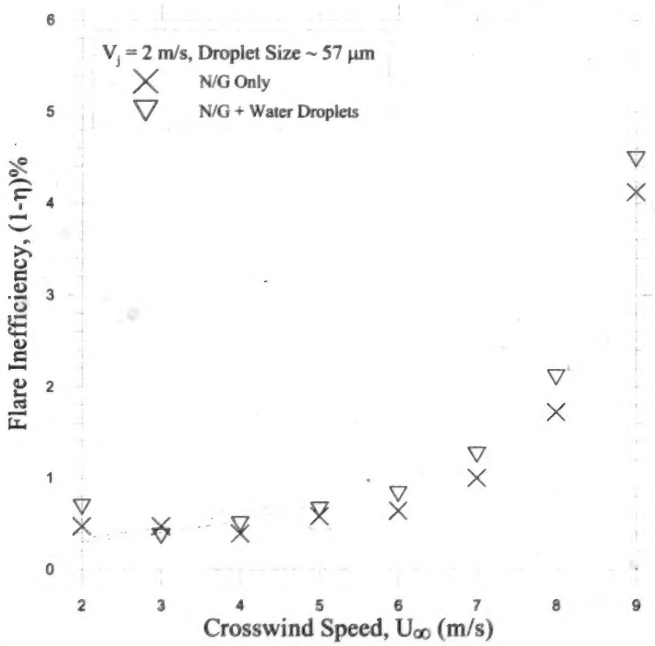

Figure 4.19: Effects of distilled water droplets on the inefficiency of the flare with high flare gas exit velocity in crosswind

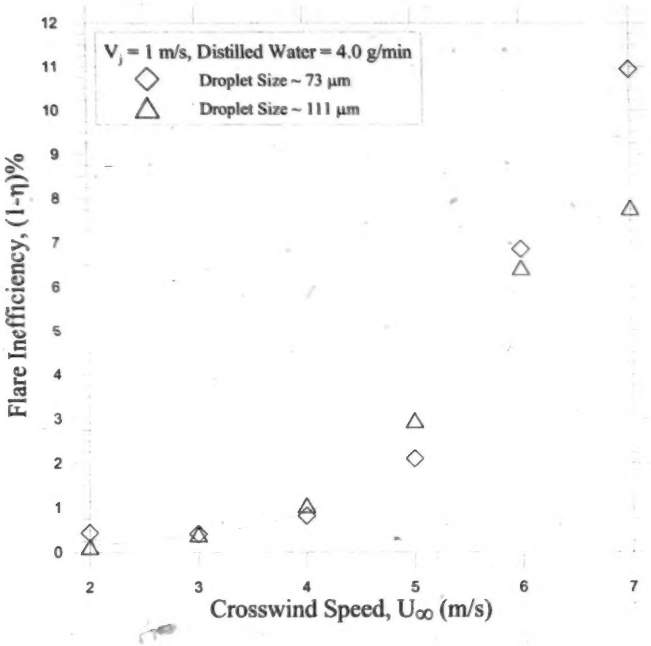

Figure 4.20: Effects of water droplet size on the flare inefficiency in crosswind

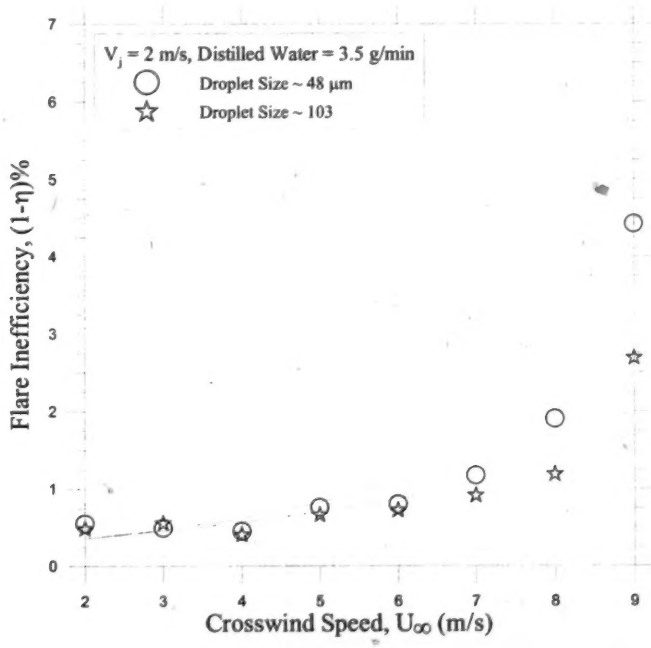

Figure 4.21: Inefficiency analysis of the flares with higher jet exit velocity having two different sizes of water droplets in the flare stream

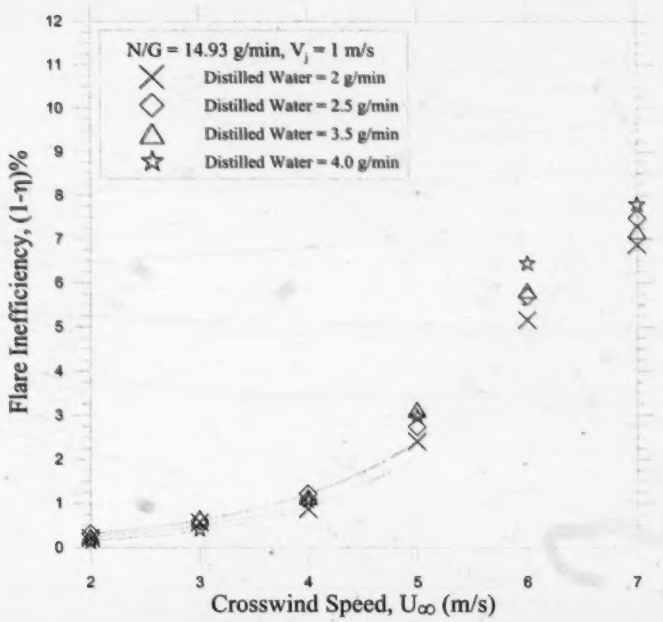
N/G = 14.93 g/min, V_j = 1 m/s
Distilled Water = 2 g/min
Distilled Water = 2.5 g/min
Distilled Water = 3.5 g/min
Distilled Water = 4.0 g/min
Flare Inefficiency, (1-η)%
Crosswind Speed, U_∞ (m/s)

Figure 4.22: Inefficiency of the flares having low jet exit velocity with varying flow rates of distilled water using 18 kHz droplet generator

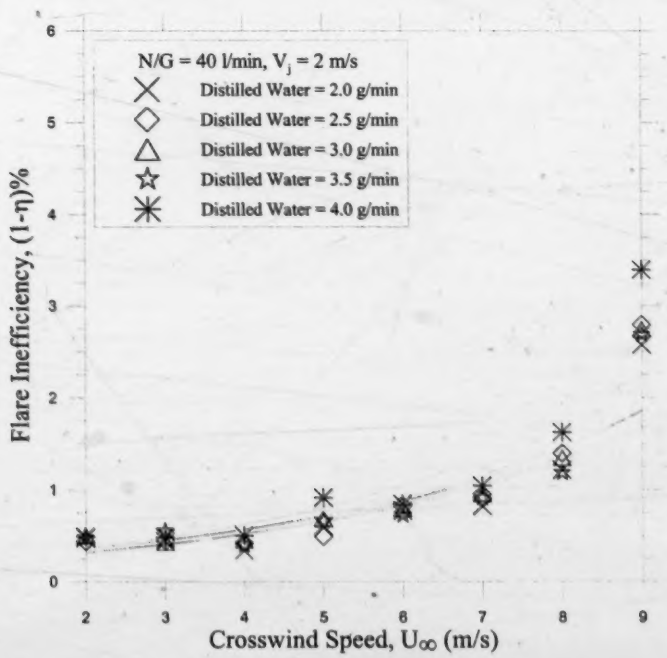
N/G = 40 l/min, V_j = 2 m/s
Distilled Water = 2.0 g/min
Distilled Water = 2.5 g/min
Distilled Water = 3.0 g/min
Distilled Water = 3.5 g/min
Distilled Water = 4.0 g/min
Flare Inefficiency, (1-η)%
Crosswind Speed, U_∞ (m/s)

Figure 4.23: Inefficiency of the flares having high jet exit velocity with varying flow rates of distilled water using 48 kHz droplets generator

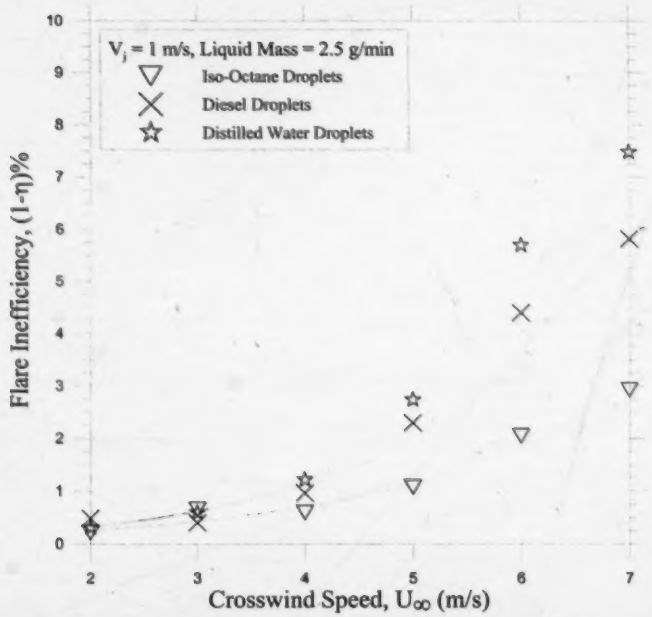

Figure 4.24: Effects of iso-octane, diesel, and distilled water droplets on the inefficiency of the flares of low jet exit velocities in crosswinds

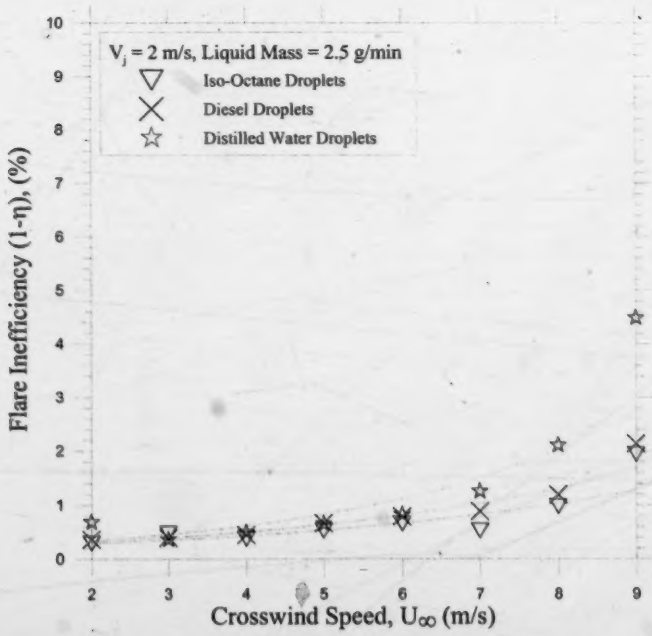
V_j = 2 m/s, Liquid Mass = 2.5 g/min
Iso-Octane Droplets
Diesel Droplets
Distilled Water Droplets
Flare Inefficiency (1-η), (%)
Crosswind Speed, U_∞ (m/s)

Figure 4.25: Effects of iso-octane, diesel, and distilled water droplets on the inefficiency of the flares of high jet exit velocities in crosswinds

References:

1. Kostiuk, L.W. (2000), *"Interim Report November 1996-June 2000"*, University of Alberta Flare Research Poject.

2. Johnson, M.R., and Kostiuk, L.W. (2000)," *Efficiency of Low Momentum Jet Diffusion Flames in Crosswind"*, Combustion and Flare, 123: 189-200.

Chapter 5

RESULTS AND DISCUSSION ON THE EFFECTS OF TURBULENT CROSSWINDS AND STACK DIMENSION ON THE FLARES

The effects of turbulent crosswind and the flare stack wall thickness on the inefficiency of natural gas flares are discussed in this chapter. The wind tunnel facility is designed to generate crosswinds of low turbulence intensity in the test section. To study scaled down modeled flares under turbulent crosswind conditions modifications were required in the wind tunnel to produce turbulent crosswinds in the test section. Turbulence-generating grids were placed at various locations upstream the flare stack to generate turbulence of various intensities at the tip of the flare stack.

The flare stack used for previous studies in this thesis was a 24.7 mm quartz stack with 1.3 mm wall thickness. Steel stacks with various wall thicknesses were used to study the influence of varying stack dimensions on the combustion efficiency of the scaled down modeled flares. The inside diameter of all the stacks were kept unchanged, only the outside diameters were varied.

5.1 Effects of Turbulent Crosswind on the Flare Inefficiency

Tests were conducted on natural gas flares to evaluate the effects of turbulent crosswinds on the combustion efficiency of the flares, when two different turbulence-generating grids were placed at different locations upstream the flare stack in test section of the wind

tunnel. The sketches of these grids are shown in Figures 3.7 and 3.8. Natural gas flow rates were 14.93 g/min and 29.86 g/min during the tests and the crosswind speed was fixed at 4 m/s. Figure 5.1, shows the inefficiency of flares as a function of turbulence intensity, when a grid of 50.8 mm square hole was used to generate turbulence in the crosswind. Natural gas flow rate was 14.93 g/min with the jet exit velocity of 1 m/s. The inefficiency of the flare at 4 m/s crosswind with low turbulence intensity in the wind (*i.e.* without grid in the wind tunnel) was 0.75%.

The results showed that the flare inefficiency increased up to 14%, when turbulence of various intensities was generated in the crosswind. In a turbulent flow, eddies of various length scales are formed that are responsible for the transfer of kinetic energy of the flow. The energy is dissipated from large to small eddies and this process continues till the total energy is dissipated by viscous effects of the fluid. Figure 5.2, shows eddies of various sizes generated in a turbulent flow. The largest length scale in a turbulent flow is known as macroscale, where the smallest length scale that can be found in the flow is named as Kolmogorove length scale. Studies on turbulent flows showed that the flow becomes homogenous and isotropic at a distance between 10M to 40M. There were no instabilities in the flow as the open areas in both grids were more than 60% (*i.e.* $\frac{d}{M} \sim 0.2$). d and M are shown in Figures 3.7 and 3.8, for both grids used in this study. At 20% turbulence intensity in the crosswind, turbulence length scale of eddies were 3.77cm. These large eddies lowered the oxidation rate of the flare gas by stripping off the fuel from the flame. The flare flickered at a wider range from its central axis. The incomplete combustion of the flare gas due to higher turbulence intensity in crosswind resulted in a higher

inefficient flare. The products of combustion had higher concentrations of unburned hydrocarbons (HC) and CO, when investigated under these conditions.

Eddies of various sizes are generally produced, when the air passes through a hole of a grid. Small eddies produced by the edges and corners of a hole live a short life and die very soon after their generation. However, large eddies remain in the flow for a longer time and are helpful in dissipating the energy. It is difficult to conclude whether the turbulent length scales have any profound effect on the flare inefficiency. With the decrease in turbulence intensity in the crosswind, the inefficiency of the flares was also decreased. At a grid distance of 256.5 cm from flare stack, turbulence intensity was 2.5%. Eddies that would reach the flare stack would not have much of the energy left to strip off a considerable amount of fuel from the flare stream that could result in a comparatively higher inefficient flare.

Figure 5.3, shows the inefficiency of flares as a function of turbulence intensity, when the flow rate of the flare gas was higher (29.86 g/min). The jet exit velocity was 2 m/s and the flares were tested under varying turbulence intensities ranging from 2.5% to 20% at 4 m/s crosswind speed. It was observed that the flare inefficiency increased up to 12.5% with an increase in turbulence in the crosswind. However, when flare inefficiencies of both low and high flare gas flow rates were compared, it was observed that the change in flare gas exit velocities had the same affect on inefficiencies of the flares, when the crosswind had turbulence intensities of 2.5% to 10%.

Figure 5.4, demonstrates the curves of flares having two different jet exit velocities and flare gas flow rates. The concentrations of CO_2, CO, and HC were higher in the products of combustion for flares having a high gas flow rate than flares with lower gas flow rates. Since the increase in flow rate of the gas increased carbon content in the fuel. The oxidation rate of the fuel was also higher and the products of combustion contained higher concentrations of CO_2 and resulted in less inefficient flares irrespective of the presence of higher concentrations of HC and CO. The study showed that the addition of turbulence into the crosswind had a profound effect on inefficiency of the flares having low and high jet exit velocities. At 20% turbulent intensity, the effect of the flare gas flow rate was observed and the inefficiency decreased with an increase in gas flow rate.

A series of test were conducted on flares that were subject to turbulence of various intensities in a crosswind when a grid of 25.4 mm square holes was used to generate the turbulence. The crosswind speed during the tests was 4 m/s with the jet exit velocities of 1 m/s and 2 m/s. The flow rates of the flare gas were 14.93 g/min and 29.86 g/min. The grid was placed at three different locations upstream the flare stack to generate the turbulence intensities of 8.6%, 5%, and 2.5% in the crosswind. The location of the flare stack in the test section and the flare ignition system limited the possibility to move the grid further towards the flare stack to generate turbulence intensity higher than 8.6%. Figure 5.5, represents the flare inefficiency, as a function of turbulence intensity, when the jet exit velocity and flare gas flow rate were low. The observed flare inefficiency increased up to 5% as the induced turbulence intensity in the crosswind was increased up to 8.6%. The length scale of eddies produced by this grid were smaller than eddies

generated by the other grid (*i.e.* 50.8 mm square hole grid) having the same turbulence intensities in the crosswind. When inefficiencies of the flares were compared at the respective turbulence intensities generated by both grids in the crosswind, it was observed that flare inefficiencies were lower, when the 50.8mm square holes grid was used. Since eddies generated by the grid with smaller square holes were comparatively smaller in size but had higher energy, when reaching the tip of the flare. These small scale eddies affected oxidation of the fuel and resulted in higher inefficiency flares. The concentrations of HC and CO were high with comparatively low concentrations of CO_2 in the combustion products from these flares.

Figure 5.6, shows the effects of turbulence intensities on flare inefficiency, when the flares had higher gas flow rate and jet exit velocity. The grid with 25.4 mm square holes was used for turbulence generation. The flares were tested under 4 m/s crosswind with turbulence intensities of 2.5% to 8.6%. The results showed that flare inefficiency increased as turbulence intensity was increased in the crosswind. When, these results were compared with the results from flares having a lower gas flow rate, as shown in Figure 5.7, it was observed that the higher flow rate of the flare gas lowered the inefficiency, when subjected to the same turbulent conditions in the crosswind. It is important to note that the scale of turbulence affected the inefficiency of the scaled down modeled flares, it is difficult to relate these results directly to atmospheric turbulence and a full size flare stack. The results in Figures 5.5 and 5.6, show that turbulence intensity has a significant effect on flare inefficiency, as it increased drastically with an increase in turbulence intensity. However, with the same turbulence intensity in the crosswind

generated by two different grids, the differences in the flare inefficiencies were less than 1%. Therefore, the length scales of turbulence in the range tested were considered to have no profound effect on flare inefficiency.

5.2 Effects of the Flare Stack Wall Thickness on the Inefficiency of the Flares

To understand the effects of the flare stack dimensions on the inefficiency of natural gas flares, steel stacks of various wall thicknesses were used. Eight stacks were used with wall thickness of 0.65 mm to 13 mm, as shown in Table 3.2. The inside diameter of all steel stacks used for this study were kept the same (*i.e.* 22.1 mm). The steel stack with 24.7 mm out side diameter and wall thickness of 1.3 mm is considered the standard flare stack for this study. Results of the tests conducted on flares using this flare stack are used as a reference when comparing the results of the tests conducted using the other stacks with various wall thicknesses. The flares were tested under the crosswind speeds from 2 m/s to 7 m/s. A series of tests were conducted on natural gas flares at two different flow rates (*i.e.* 14.93 g/min and 29.86 g/min) with jet exit velocities of 1 m/s and 2 m/s respectively. Figure 5.8, shows flare inefficiency as a function of crosswind speed, when the flow rate of the flare gas and jet exit velocity were low. Two steel stacks of different wall thickness were used. The wall thickness of one stack was half of the wall thickness of the other. The crosswind speed showed significant effect on the flare inefficiencies, as the inefficiencies increased with an increase in crosswind speed. The results showed no significant change in inefficiency of the flares and it was observed that flare inefficiencies were almost the same under the varying crosswind conditions, when the

wall thickness was reduced to half of the standard wall thickness of the flare stack (*i.e.* 1.3 mm).

Figure 5.9, shows the results of the tests conducted on natural gas flares using the same two flare stacks, when subjected to crosswind speeds of 2m/s to 7 m/s. Flare inefficiencies are shown as a function of crosswind speed. Natural gas flow rate was 29.86 g/min during the tests and the jet exit velocity was 2 m/s. The effects of high flow rate and jet exit velocity was observed, as the flare inefficiencies were low at the respective crosswind speeds. No notable change was observed on inefficiency at crosswind speeds of 2 m/s to 4 m/s. A slight change in the inefficiency was observed at 5 m/s to 7 m/s, as inefficiencies of the flares using the standard steel stack were lower than the one with reduced wall thickness. Since the difference in inefficiency at each of these three crosswind speeds were very low (<0.3%), a decrease in the wall thickness of the flare stack was considered to have no significant effect on the flare inefficiency under the investigated crosswind speeds.

The reduction in the wall thickness did not show an observable affect on the flare inefficiency. Therefore, steel stacks with wall thickness greater than the standard flare stack were selected and tests were conducted on natural gas flares using those flare stacks. Figure 5.10, demonstrates results of the tests conducted on natural gas flares using two stack with different wall thickness (*i.e.* 1.3 mm and 3.3 mm). The flow rate of natural gas was 14.93 g/min and the jet exit velocity was 1 m/s during the tests. Inefficiencies of the flares are presented as a function of crosswind speed. Results showed that

inefficiency increased with an increase in wall thickness of the flare stack from 1.3 mm to 3.3 mm. At low wind speeds (*i.e.* from 2 m/s to 4 m/s) the effect of wall thickness was not significant, as the difference in inefficiencies was observed to be very low (<0.2%). The prominent effects of wall thickness on flare inefficiencies were observed at higher crosswind speeds (*i.e.* 5 m/s to 6 m/s). At the crosswind speed of 7 m/s, no profound effect of increased wall thickness on the flare inefficiency was observed, as the inefficiencies were same. In light of the results, it was concluded that the inefficiency of the flare with low flow rate of the flare gas and low jet exit velocity increased with the increase in wall thickness of flare stack.

A series of tests were conducted on natural gas flares with higher flare gas flow rate and jet exit velocity to study the effects of the increasing wall thickness on the inefficiency of these flares. Natural gas was flowing at the rate of 29.86 g/min and 2 m/s exit velocity. Figure 5.11, shows results of tests conducted with these high flow rate and jet exit velocity using stacks with wall thickness of 1.3 mm and 3.3 mm respectively. It was observed that the effects of the increased wall thickness were same at low crosswind speeds (*i.e.* 2 m/s to 4 m/s). The inefficiencies were higher at 5 m/s and 6 m/s, when the stack with higher wall thickness was used. At 7 m/s, the difference in the wall thickness of the flare stack had the same effect on the flare inefficiency. Since measured inefficiencies were low (<1.5%), the effects of increased wall thickness were not clearly observed. Though the differences in the flare inefficiencies were observed at each individual crosswind speeds, no trend was evident.

A series of test were conducted on natural gas flares using various flare stacks with wall thickness ranging from 1.3 mm to 13 mm. The flare inefficiencies were measured under the crosswind speed varying from 2 m/s to 7 m/s. Flare gas flow rates were 14.93 g/min and 29.86 g/min and the jet exit velocities were 1 m/s and 2 m/s. Results of these tests showed that inefficiency increased with the increase in wall thickness (*i.e.* from 1.3 mm to 13 mm) at each individual crosswind speed. However, Figures 5.12 and 5.13, show flare inefficiencies as a function of flare stack wall thickness when the flares were tested under 4 m/s and 5 m/s crosswind speeds. Natural gas flow rate was 14.93 g/min with jet exit velocity of 1 m/s. The data in Figure 5.12, show a gradual increase in inefficiency with an increase in wall thickness up to 6.45 mm then a slight decrease in flare inefficiency with further increase in the flare stack wall thickness. The reason for this variation in inefficiency was not known and require further investigation. Similarly, data in Figure 5.13, show a gradual rise in inefficiency as wall thickness is increased to 4.85 mm and then dropped down with further increase in the wall thickness. The reasons for this drop were not investigated. The inefficiency raised up to 6.5% when the flare stack wall thickness was 13 mm.

The inefficiency of high jet exit velocity flares are shown as a function of flare stack wall thickness in Figures 5.14 and 5.15. The natural gas flow rate was 29.86 g/min during the tests. The results showed that the flare inefficiency increased with the increase in the wall thickness of the flare gas at crosswind speeds of 2 m/s to 7 m/s. However, results of the tests conducted on the flares at 5 m/s and 6 m/s are shown in the figures. The results in Figure 5.14, show a gradual increase in flare inefficiency when wall thickness of the flare

was increased up to 8 mm. The inefficiency dropped down, when the wall thickness was 9.6 mm. A similar drop in inefficiency was observed in Figure 5.15, at 8 mm and 9.6 mm flare stack wall thickness. While, the inefficiency increased with the increase in the wall thickness up to 6.5 mm. The reasons of the fluctuation in inefficiencies were not known.

Summary:

Scaled down modeled flares were studied, when subjected to turbulent crosswind conditions. It was observed that flare inefficiency increased with an increase in turbulence intensity in the crosswind. The reason for this result is believed to be strictly due to the fluid mechanics of dispersion of the fuel stream after leaving the flare stack but before reaching the flame. When the crosswind pushes the flame over to the leeward side of the stack, it exposes a section of the fuel stream to the air. If the air is more turbulent it is proposed that it is more effective in mixing and dispersing the fuel into atmosphere and thereby avoiding being burned. The higher the level of turbulence, a greater portion of the fuel is dispersed and the flare is less efficient. It was also observed that the turbulent length scale had no profound effect on flare inefficiency.

Wall thickness of a modeled flare stack was varied to understand its effects on flare inefficiency. The inside diameter of the flare stack was kept constant and outside diameter was varied. A decrease in wall thickness did not show an observable effect on flare inefficiency. However, increase in wall thickness showed a profound effect on the flare inefficiency as it increased with an increase in wall thickness of the flare stack.

Flare inefficiency increased with increase in wall thickness up to 4.85 mm and dropped down with further increase in wall thickness of the flare stack in case of flares with low flare gas flow rate. Similarly, inefficiency of flares with high gas flow rates increased with wall thickness up to 6.45mm and dropped down with further increase in wall thickness of the flare stack. The reason of this local maximum in flare inefficiency is not known and requires further investigation.

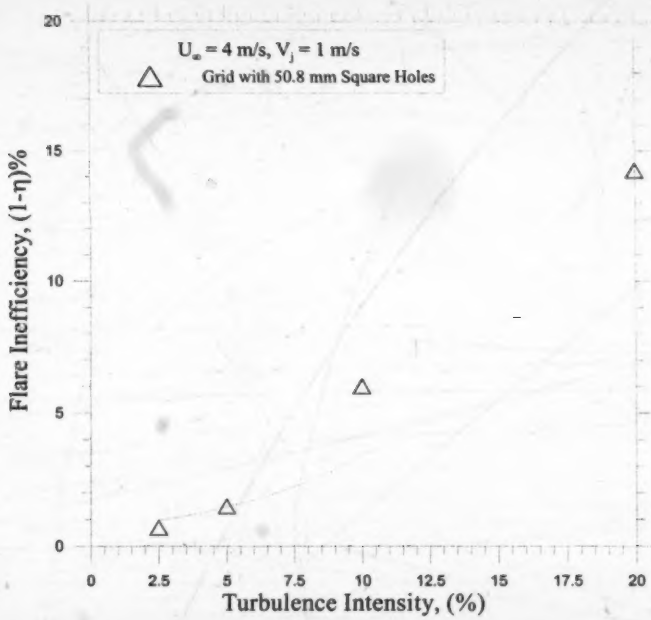

Figure 5.1: Inefficiency of the flares having low flare gas flow rate subjected to varying turbulence intensities generated by the grid with 50.8 mm square holes

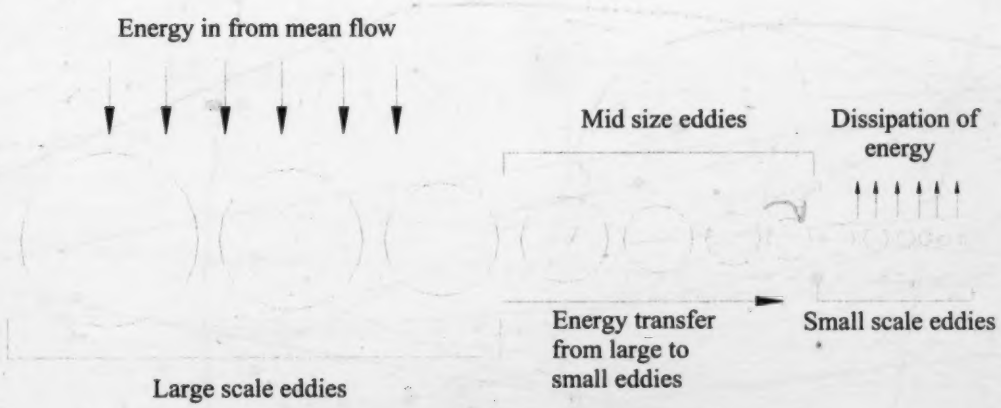
Energy in from mean flow
Mid size eddies
Dissipation of energy
Energy transfer from large to small eddies
Small scale eddies
Large scale eddies

Figure 5.2: Eddies generated in turbulent flow

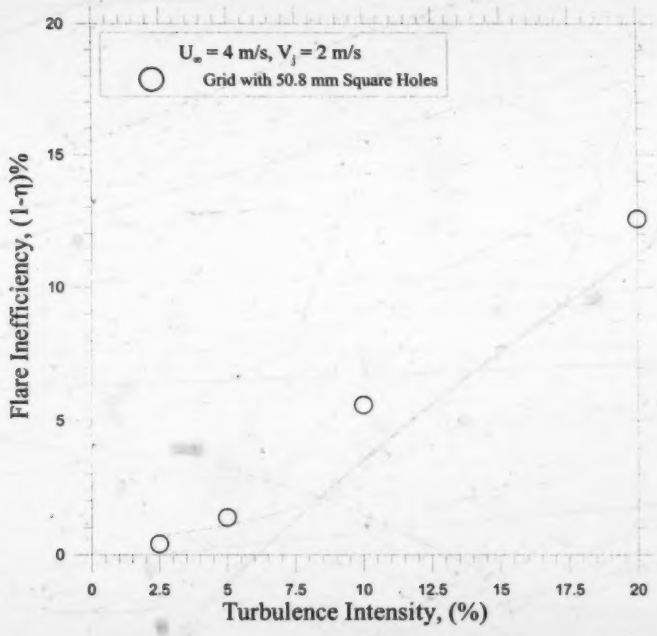

Figure 5.3: Inefficiency of the flares having high flare gas flow rate subjected to varying turbulence intensities generated by the grid with 50.8 mm square holes

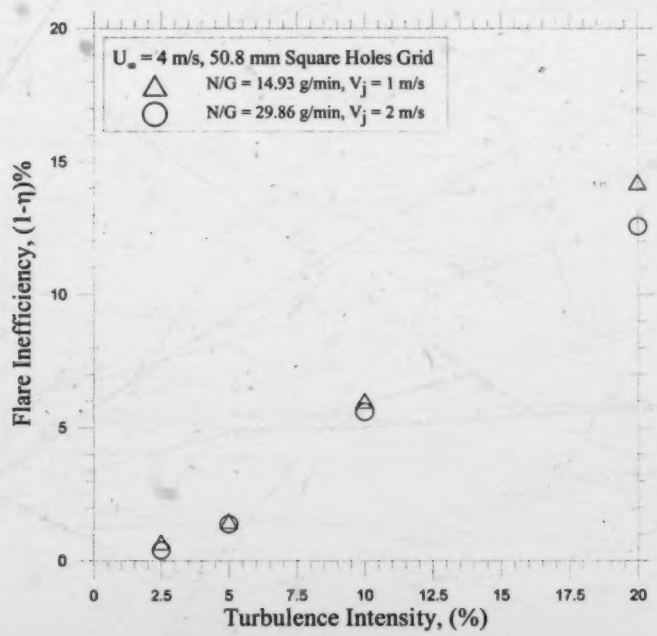

Figure 5.4: Comparison of the inefficiencies of the flares with high and low flow rates of the flare gas under the same turbulent crosswind conditions

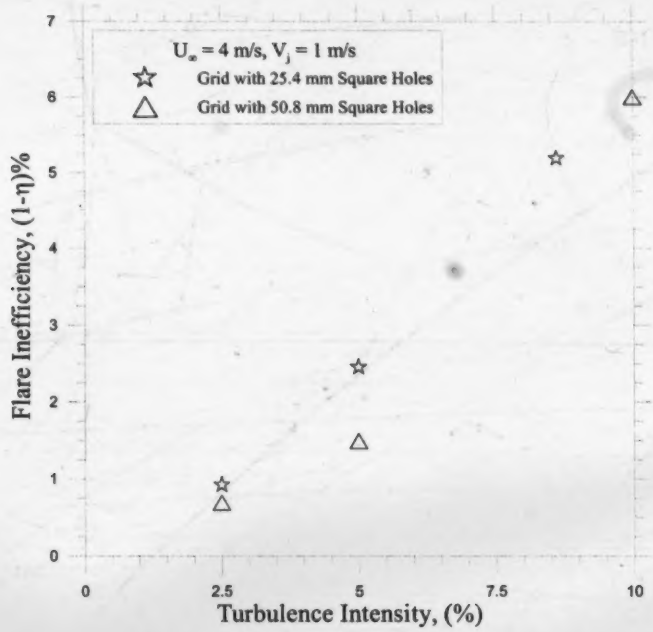

Figure 5.5: Inefficiency of the flares having low flare gas flow rate subjected to varying turbulence intensities generated by the grid with 25.4 mm square holes

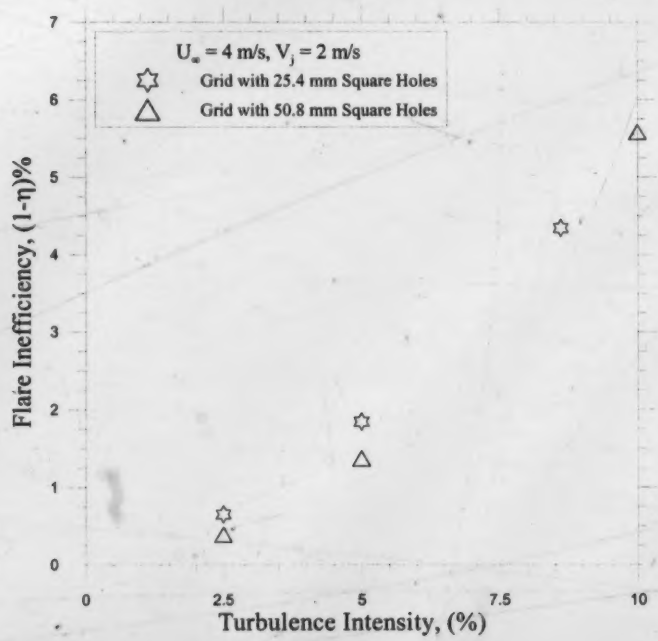

Figure 5.6: Inefficiency of the flares having high flare gas flow rate subjected to varying turbulence intensities generated by the grid with 25.4 mm square holes

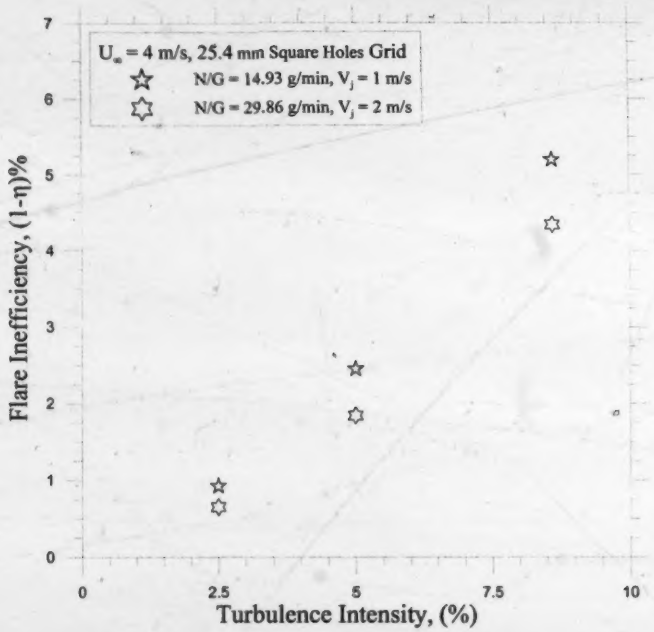

Figure 5.7: Inefficiency comparison of the flares with two different flare gas flow rates subjected to the same turbulent crosswind conditions

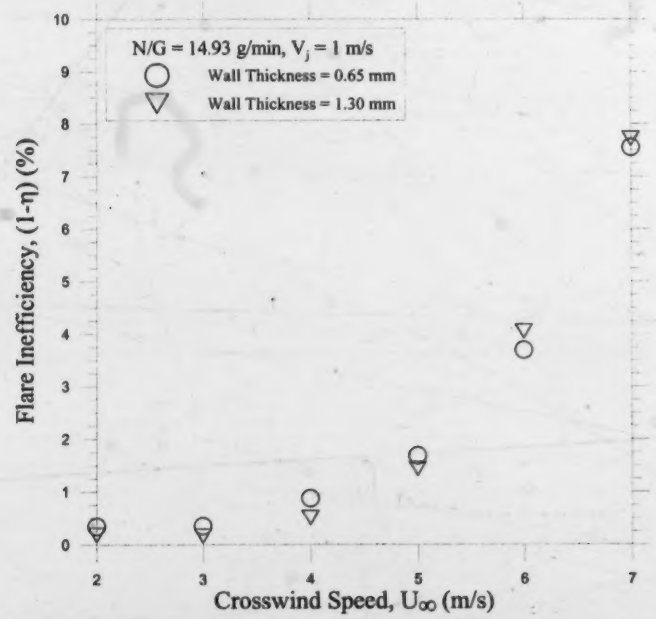

Figure 5.8: Effects of decreased wall thickness on the inefficiency of the flares having low flare gas flow rates and jet exit velocity in crosswind

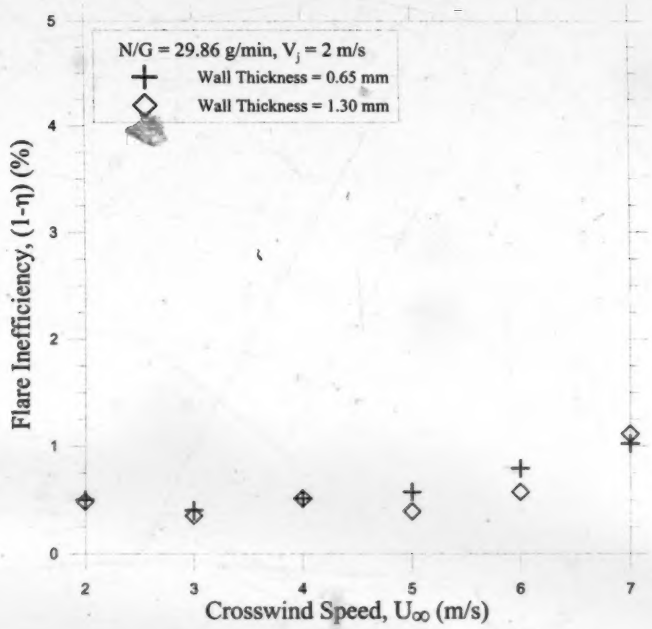

Figure 5.9: Effects of decreased wall thickness on the inefficiency of the flares having high flare gas flow rates and jet exit velocity in crosswind

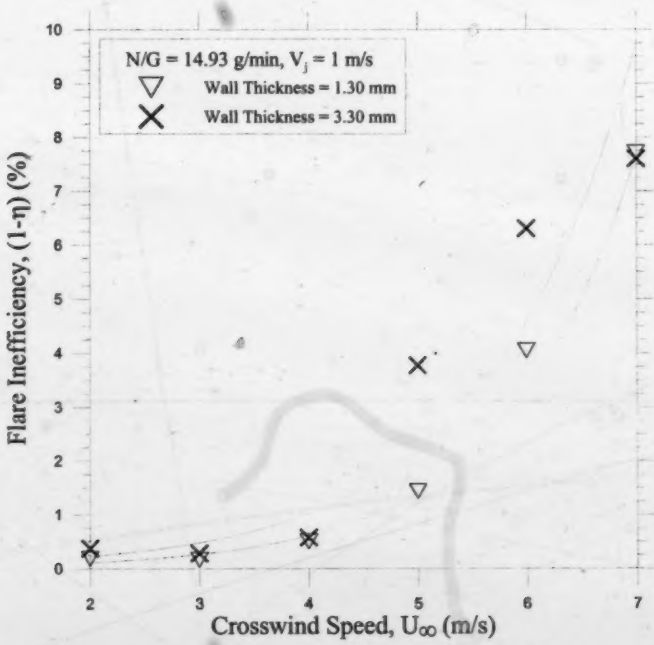

Figure 5.10: Effects of increased wall thickness on the inefficiency of the flares having low flare gas flow rates and jet exit velocity in crosswind

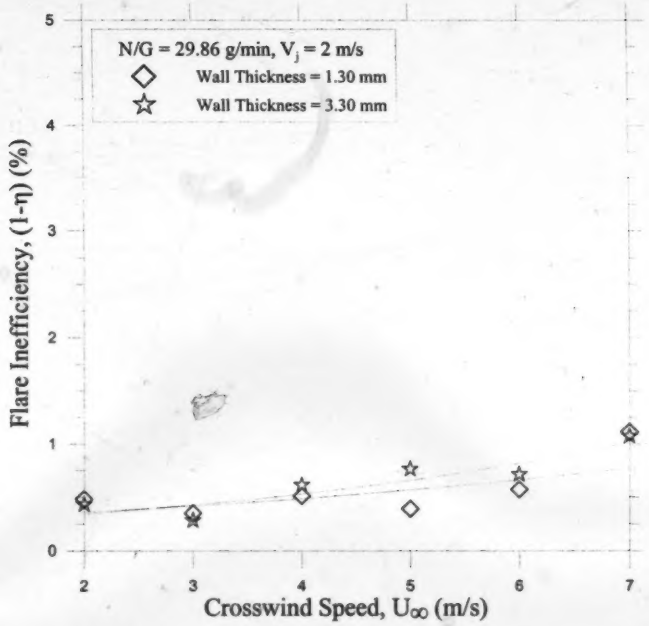

Figure 5.11: Effects of increased wall thickness on the inefficiency of the flares having high flare gas flow rates and jet exit velocity in crosswind

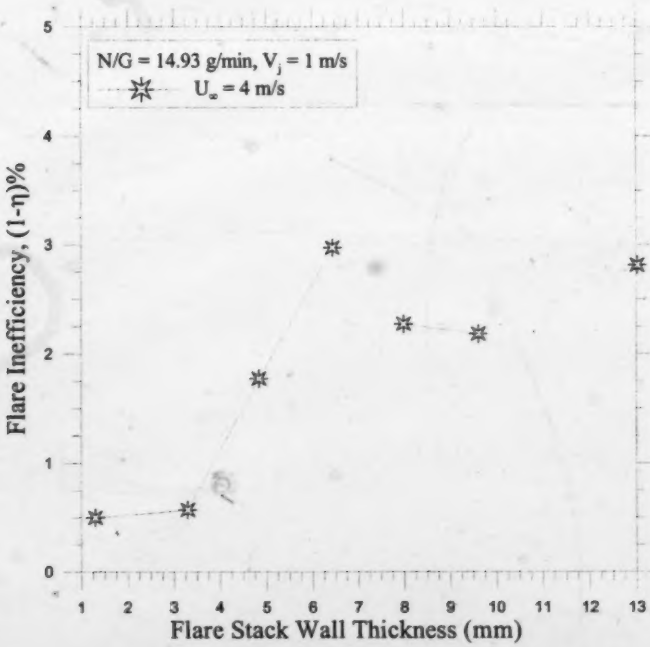

Figure 5.12: Effects of varying wall thickness on the inefficiency of low jet exit velocity flare at 4 m/s

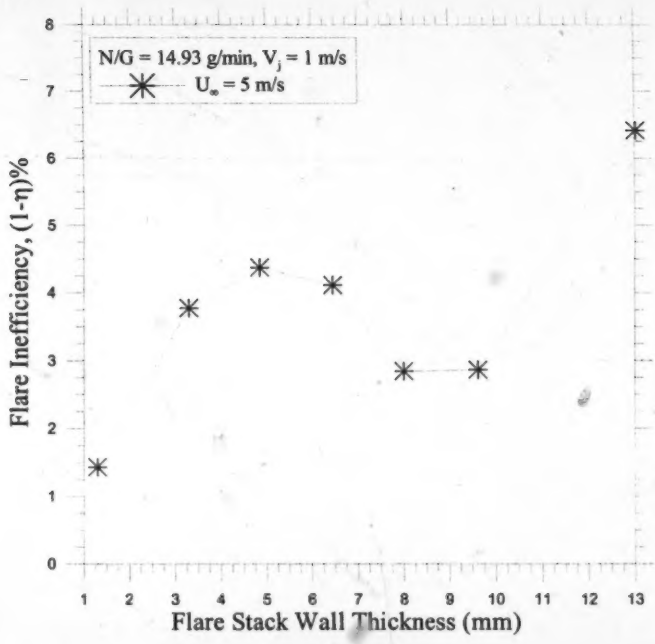

Figure 5.13: Effects of varying wall thickness on the inefficiency of low jet exit velocity flare at 5 m/s

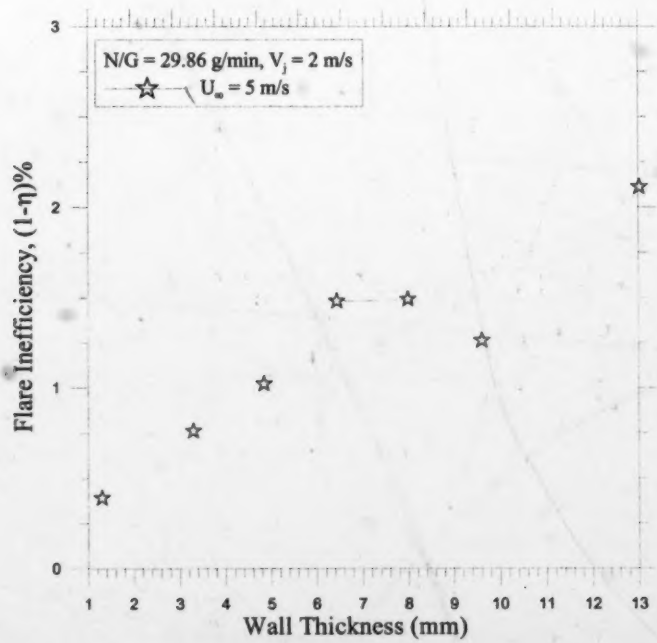

Figure 5.14: Effects of varying wall thickness on the inefficiency of high jet exit velocity flare at 5 m/s

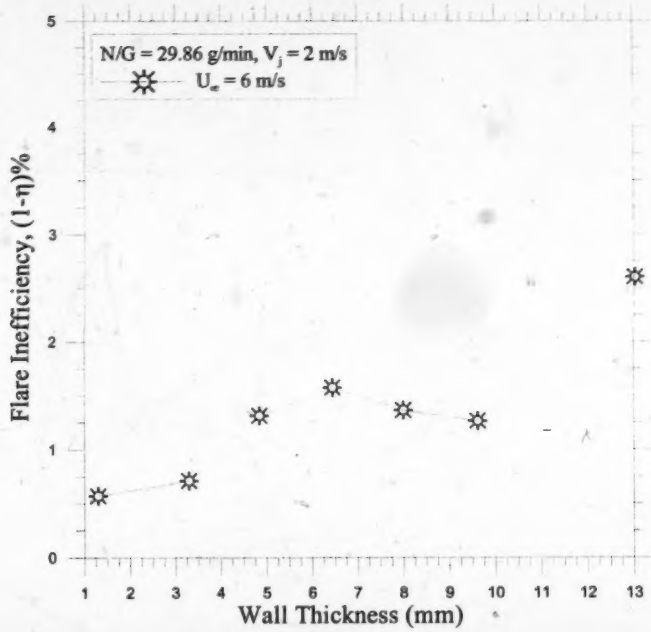

Figure 5.15: Effects of varying wall thickness on the inefficiency of high jet exit velocity flare at 6 m/s

Chapter 6

CONCLUSIONS

6.1 Effects of the Liquid Droplets on the Flare Inefficiency

This dissertation is the experimental study on measuring inefficiency of the scaled down modeled flares with and without liquid droplets in their flare streams. Sales grade natural gas was used as a flare gas and tests have been conducted in closed-loop wind tunnel facility of the Flare Research Project at University of Alberta. For this thesis research, two different natural gas flow rates were selected with jet exit velocities of 1 m/s and 2 m/s. The flares have been tested in varying crosswind speeds ranging from 2 m/s to 9 m/s. A 24.7 mm quartz stack was used with the ratio of its inside to outside diameter (d_i/d_o) equal to 0.9, in order to keep it geometrically similar with an actual flare stack. Droplets of three different liquids (*i.e.* iso-octane, diesel, and distilled water) were added to the gaseous flare stream in various proportions and droplet sizes to understand their effects on flare inefficiency. Two different ultrasonic droplet generators were used for generation and inclusion of droplets into the gaseous flare stream.

The flares were highly susceptible to crosswind speeds as the inefficiency of the flares with and without droplets increased with an increase in crosswind speed. The flare gas flow rate also showed a profound effect on flare inefficiency and it was observed that flares with a higher momentum flux ratio (R) were less inefficient than flare with a lower momentum flux ratio. The inefficiency of flares with a higher jet exit velocity were less

than 1% up to the crosswind speed of 7 m/s. Further increases in wind speed up to 9 m/s, raised the inefficiency up to 4%. The inefficiency of flares at 3 m/s were lower than inefficiency of flares at 2 m/s crosswind speed. The reason of this change was unknown.

Addition of iso-octane and diesel droplets into a gaseous fuel stream had a notable effect on flare inefficiency. At the same flare gas flow rate and jet exit velocity, the inefficiency of flares with droplets of iso-octane and diesel were lower than flares with gaseous fuel only, when tested under the same crosswind conditions. However, flares with distilled water droplets in their fuel streams had higher inefficiencies than flares with no droplets. The flare gas flow rate and jet exit velocity also showed their effects on flares with liquid droplets. It was observed that the inefficiency of flares with higher flare gas flow rates and jet exit velocity were less inefficient than for flares having lower flare gas flow rates irrespective of the type of liquid droplet they had in their flare stream.

Droplets of iso-octane, diesel, and distilled water were divided into two major categories, which were small and large droplets. When both sizes of droplets of each individual liquid were added to the gaseous fuel, their effects were almost the same under the investigated crosswind conditions.

Iso-octane, diesel, and distilled water were added to the gaseous flare stream with various flow rates to understand their effects on flare inefficiency. The results showed that flow rates of these liquids had only a modest effect on flare inefficiency. Flares with high and low flow rates had slightly different inefficiencies under the same crosswind conditions.

The comparative study of the effects of these three different liquids showed that inefficiency of flares with iso-octane droplets were lower than flares with diesel droplets in their flare stream at the same crosswind conditions. Flares with distilled water droplets had higher inefficiencies than flares having droplets of iso-octane or diesel in the flare stream under the investigated crosswind speed, irrespective of the flare gas flow rate and jet exit velocity.

When droplets of a non-combustible liquid (*e.g.* distilled water) are added to the flare stream, they extract energy from the flare to vaporize. The energy density of flares decreases that results in low combustion rate of the flare stream. The flare inefficiency increases due to the droplets that become inert vapors.

The droplets of a combustible liquid (*e.g.* liquid hydrocarbon) do extract energy from the flares for their vaporization, when added to the flare stream. These droplets have high chemical energy and increase the energy density of the flare stream. The combustion of flare stream is enhanced and results in a decrease in the flare inefficiency.

6.2 Effects of Turbulent Crosswinds on the Flare Inefficiency

The closed-loop wind tunnel facility is designed to generate crosswinds of very low turbulence intensity in the test section. The study of scaled down modeled flares in turbulent crosswinds required a few modifications in the wind tunnel. Two different grids with 25.4 mm and 50.8 mm square holes were made and introduced into the wind tunnel

to generate high intensity turbulence in the crosswind. The grid with 25.4 mm square hole was located at three different positions upstream the flare stack so as to generate turbulence intensity of 8.6%, 5%, and 2.5% at the tip of the flare stack. Similarly, the grid with 50.8 mm square holes was located at four positions to produce 20%, 10%, 5%, and 2.5% turbulence intensities at the tip of the flare stack. The flares were tested at a crosswind speed of 4 m/s. Inefficiencies of the flares having both high and low flare gas flow rates increased with an increase in the turbulence intensity in the crosswind. The flare inefficiency increased drastically with an increase in turbulence intensity in the crosswind using both types of grids. However, results showed that the differences in flare inefficiencies were less than 1% with the same turbulence intensities in the crosswind generated by different grids. Therefore, the turbulent length scale has no profound effect on flare inefficiency.

The fuel stream is exposed to the air when the crosswind pushes the flare over to the leeward side of the stack. Turbulent air becomes more effective in mixing with and dispersing the fuel into atmosphere rather than burning. The higher the level of turbulence, a greater portion of the fuel is dispersed and the flare less efficient.

6.3 Effects of Flare Stack Wall Thickness on the Inefficiency of the Flare

The experimental work on measuring the effects of flare stack wall thickness on flare inefficiency was also conducted in the closed-loop wind tunnel facility. The plate for holding the modeled flare stack in upright position in the wind tunnel was designed for a

specific size of the flare stack. Stainless steel modeled flare stacks of various wall thicknesses were made in such a way that only one supporting plate could be used to hold all the investigated steel stack. The flare inefficiencies were measured under the crosswind speeds of 2 m/s to 7 m/s with two different sales grade natural gas flow rates. At low and high flare gas flow rate, results showed no significant change in flare inefficiency when the flare stack wall thickness was reduced to half of the wall thickness of a standard modeled flare stack (1.3 mm) under the same crosswind conditions. At low flow rate of the gas, flare inefficiency increased with an increase in the wall thickness up to 4.85mm and dropped down with further increase in wall thickness. Similarly, at high gas flow rate, flare inefficiency increased with an increase in the wall thickness up to 6.45 mm and dropped down with further increase in the wall thickness. The reason of this local maximum in flare inefficiency is not known and requires further investigation.

APPENDIX A

UNIVERSITY OF ALBERTA FLARE RESEARCH PROJECT

This study has been carried out using the University of Alberta Flare Research Facility in the Department of Mechanical Engineering. The facility is comprised of a combustion wind tunnel built by the Combustion & Environment Group. This Group is also responsible for the operation & maintenance of the flare research facility.

A.1 Combustion Wind Tunnel

The combustion wind tunnel is shown schematically in Figure A.1. It is built on two floors with the test section and measuring equipment on the first floor. The main fan/motor, mixing section and exhaust dampers are on the second floor (Kostiuk, 2000). The closed-loop profile of wind tunnel provides the ease of collecting and analysing the product of combustion after burning a flare gas using a model flare stack. The approximate internal air volume of the wind tunnel is 350 m^3. For producing the crosswind in the tunnel, a 3 m diameter fan driven by a 150 kW DC motor is used, which can either be controlled either by a computer or operated manually. The fan is capable of producing stable crosswinds between 1 m/s to 35 m/s (3.6 kph to 126 kph) in the test section of the wind tunnel. Arrays of turning vanes are employed at each of the four corners of the tunnel to avoid formation of recirculation zones or secondary flows at these corners and to maintain the integrity of the mean flow. Two dampers are provided for sucking fresh air into the tunnel and purging the product of combustion after an

experiment is completed. Both sets of dampers are located in such a way that as there is a little chance of mixing of the fresh air with the product of combustion. A series of three fine mesh screens and a 6.3:1 area ratio convergent nozzle produces a near uniform plug flow in the test section that follows contraction section and a low turbulence (~0.4%) is also generated in the test section by this contraction section (Johnson *et. al.*, 2001). Detail of the measuring turbulent flow has been published in the use of a closed-loop wind tunnel for measuring the combustion efficiency of the flames in a crossflow (Johnson *et. al.*, 1999).

The test section of the wind tunnel is approximately 11.8 m long, 2.4 m wide and 1.2 m high. The purpose of locating the flare stack well downstream in the test section is to provide enough space for any grids or array of obstacles to be placed upstream the flare stack to introduce turbulence in the flow if necessary (Kostiuk, 2000).

A.1.1 Auxiliary Equipment in the Tunnel

All the gases emitted from the flare are advected downstream and mix with the tunnel air with the help of 6 mixing fans. Each of these 0.6 m diameter fans is powered by a 0.56 KW motor. Mixing of the products of combustion with the tunnel air is necessary for two reasons. First, to minimise the impact of using a closed-loop wind tunnel so that the combustion products could not return to the flare in any coherent form and affect the combustion process. Second, to calculate the combustion efficiency, it is necessary to measure the total accumulation rates of various chemical species in the tunnel. The size,

number, and orientation of the fans were decided by a trail and error process to achieve uniformity in tunnel gas composition at the sampling point (see Figure A.1).

The mean velocity in the tunnel is measured using a Pitot-static tube located in the test section at the same downstream location as the flare stack. A series of three pressure transducers with different ranges are used to measure the mean dynamic pressure from the Pitot-static tube over all potential speeds. The gas temperature in the tunnel is measured with a semi-conductor (AD590) transducer. A mercury barometer is used to record the room pressure outside the tunnel. Both pressure and temperature of the gases with in the tunnel are needed to estimate the gas density in order to convert Pito-static pressure measurement in to wind velocity.

The ignition system used for flares is a retractable hydrogen jet diffusion flame shown schematically in Figure A.2. A manual high-voltage spark system, based on an automotive ignition system, is used to light the hydrogen fuel jet issuing from 6 mm diameter pipe. This pipe can be raised vertically to approximately the same height as the flare stack so that the ignitor flame passes directly over the flare exit. Once the hydrogen flame is correctly placed, the flow of flare gas is easily ignited. After the flare is ignited the flow of hydrogen is turned off and the pipe is lowered back to the floor level so it does not affect the flow around the flare stack.

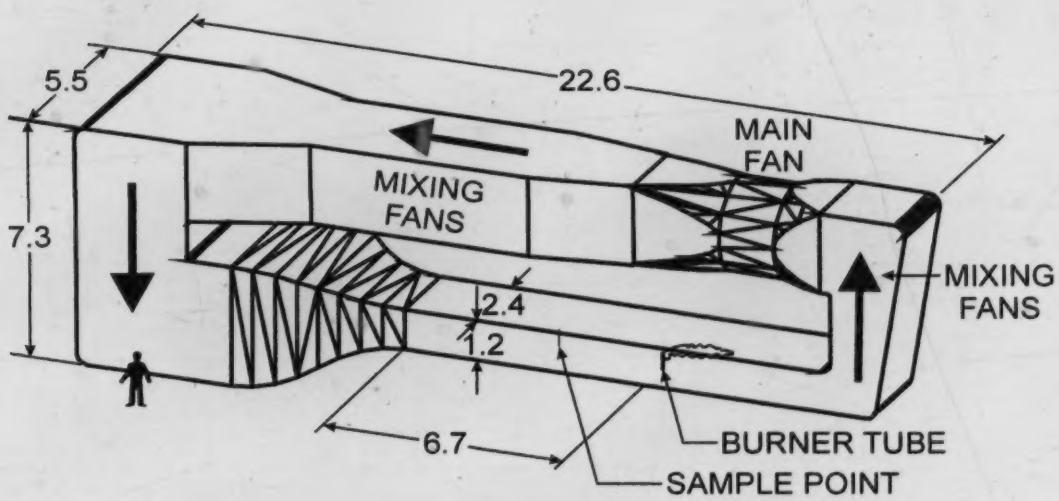

Figure A.1: Schematic of a closed-loop combustion wind tunnel (All dimensions are in meters)

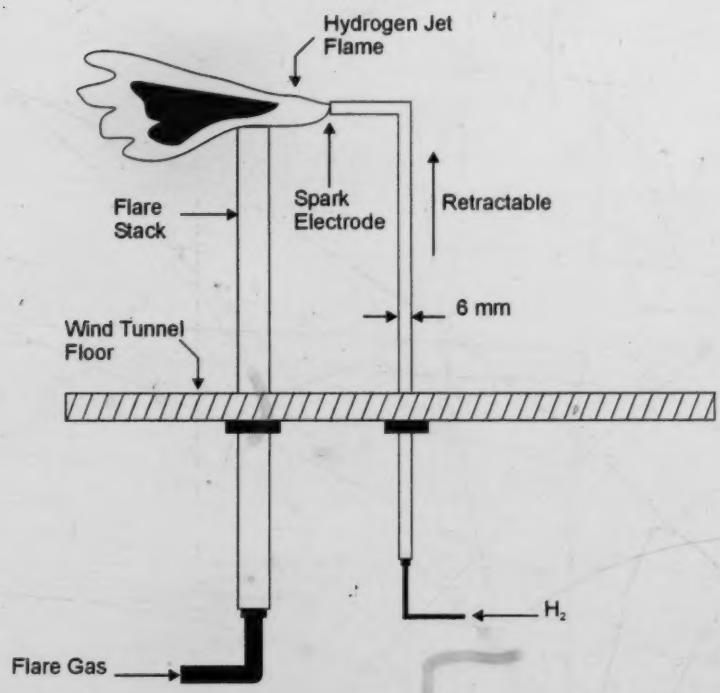

Figure A.2: Flare ignition system

References:

1. Kostiuk, L. W. 2000, *"Interim Report November 1996-June 2000"*, University of Alberta Flare Research Project.
2. Johnson, M. R., Kostiuk, L. W., Majeski, A. J., Poudenx, M. R., and Wilson, D. J. 1999, *"An Investigation of Parameters that Affect Conversion Efficiency of Wake-Stabilized Diffusion Flames"*, Proceedings of the Combustion Institute, Vol. 28, 2001.
3. Johnson, M. R., Bourguignon, E., and Kostiuk, L. W. 2001, *"The Use of a Closed-Loop Wind Tunnel for Measuring the Combustion Efficiency of Flames in a Crossflow"*, Combustion and Flame 119:319-334 (1999).

APPENDIX A.2

FLARE GAS SUPPLY SYSTEM

The flare gas used for this study was sales grade natural gas. The energy density of this fuel gas is 37.52 MJ/m^3, which represents the higher heating value of the fuel at 1 atmosphere pressure and 15^0C. The schematic of the fuel supply system is shown in Figure A.3. Natural gas is supplied from a tank (under high pressure, located under the wind tunnel). The pressure of the gas is reduced by two regulators to a pressure that is usable by the mass flow controllers. The mass flow controllers are controlled by a computer interface that is used to set the flare gas to a model flare stack. Each mass flow controller is calibrated to an uncertainty in mass flow of approximately $\pm$ 1% of full scale. With the reduction in the pressure of the gas from the tank to the mass flow controllers, its temperature also decreases. Therefore, the flare gases are piped by Teflon tubing from the regulators to metal coils of tubing placed in a constant temperature water bath. The gas then flows to the mass flow controllers through another set of Teflon tubing with constant temperature. The constant temperature is necessary because the mass flow controllers are based on measuring the temperature rise of the metered gas, when a small but fixed amount of energy is added to the stream. This type of meter requires that the specific heat capacity of the gas being metered remain constant. Without a water bath, the gas temperature and its specific heat capacity at the meter becomes dependent on cylinder pressure and the gas flow rate.

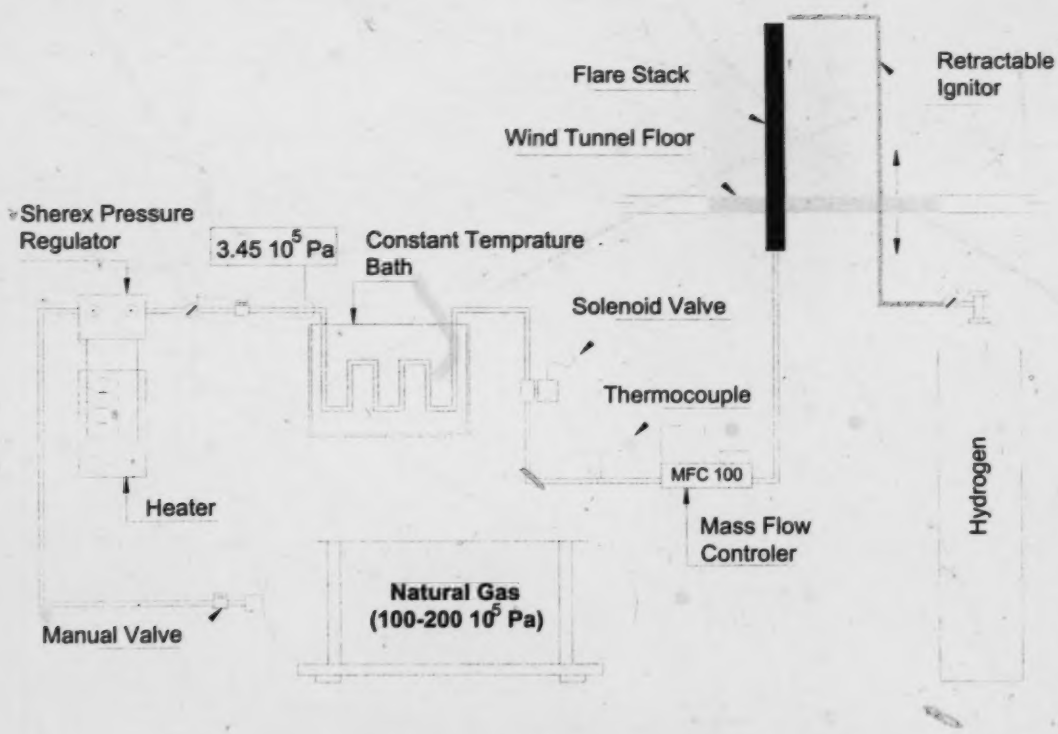

Figure A.3: Schematic of natural gas supply system

APPENDIX A.3

MODELED FLARE STACK

Typical flare stacks used for solution gas flaring at the battery sites in Alberta are constructed from nominal 10 cm, schedule-40 pipe. The flare used in this study was a scale model quartz flare stack. The outer diameter (d_o) and the inner diameter (d_i) of the full-scale flare are 114.3 mm and 102.3 mm respectively. In order to maintain geometric similarity for scale-down flares the ratio d_i/d_o (0.9) has been constant in all precision work. Only one flare stack was scale modelled, other stacks were used to look at the effects of wall thickness on the efficiency of a flare. As discussed in Chapter 3, other diameter ratios were constructed.

The height of a typical solution gas flares (H_s) used in the field are approximately 10 m. As the experiments are conducted on scale-down flares in the wind tunnel, the equivalent length of stack exposed to the wind in the tunnel represents the top portion of a full size flare. The maximum height to which a stack may be raised in the tunnel is approximately ¾ of the tunnel height. This stack height is acceptable in high wind conditions when the flame is bent over in the horizontal direction.

APPENDIX A.4

GAS ANALYZERS

For measuring combustion efficiency of the flare, it is necessary to measure concentrations of the major carbon containing species within the products of combustion. These species are considered to be unburned hydrocarbons (HC), carbon dioxide (CO_2), and carbon monoxide (CO) in this study. Oxygen (O_2) was also measured to monitor the quality of the air in the wind tunnel. For measuring the concentrations of the above mentioned gases, the analyzers used were manufactured by Rosemount Instruments and are a part of their NGA2000 series analyzers. The concentration of (HC) was measured using flame ionization detector, (FID). The concentrations of (CO_2) and (CO) were measured using a non-dispersive infrared technique and oxygen (O_2) was measured with a paramagnetic device. The gas sampled from the tunnel was extracted by a 6 mm tube located upstream the flare stack. A schematic of gas sampling system is shown in Figure A.4.

Appendix A.4.1 Flame Ionization Detector, (FID)

A flame ionization detector (FID) is used to measure hydrocarbon concentrations in air or exhaust gases from the flare. The principle of FID is based on the phenomenon that a pure hydrogen flame produces very little ionization, but if hydrocarbon molecules are introduced, this flame produces a large amount of ionization. The ionization is

proportional to the number of carbon atoms present in the hydrocarbon molecules. The basis of flame ionization technology is shown in Figure A.5.

Hydrogen is mixed with the sample and burned at a small jet. Surrounding the flame is a cylindrical electrode and relatively high voltage is applied between the jet and the electrode to collect the ions that are produced in the flame. The resulting current is amplified by a high impedance amplifier and the output fed to a data acquisition system. The gases normally used are hydrogen for combustion, helium as a carrier gas and oxygen or air as the combustion agent. The detectors used in this study for measuring concentrations of unburned hydrocarbons have full scale ranges of 4, 10, 40, 100, 250, 1000, 2500, 10000 ppm with an uncertainty of $\pm$ 1% of their full-scale reading.

Appendix A.4.2 Non-Dispersive Inrfared Analyzer (NDIR)

Non-dispersive infrared analyzers have been used to measure variety of gases including CO_2, CO, NO, and HC. For this study, NDIR has been used specifically for measuring CO_2 and CO concentrations in the products of combustion from the flare. The theory upon which NDIR works is differential absorption of energy from an infrared radiation source between two optical cells. One of which is a reference cell, filled with an inert gas like nitrogen. The other cell is the sample cell through which the gas of interest is allowed to pass. When infrared radiation are directed upon these cells, it passes through the reference cell without any change in its energy. On the other hand, when it passes through the sample cell, some of its energy is absorbed by the component of interest in the sample. The amount of energy absorbed from the infrared radiation is proportional to

the concentration of component of interest. The infrared radiation is interrupted by a chopper at a frequency of 5 Hz. A schematic of an NDIR, is shown in Figure A.6.

The detector is generally filled with the same gas being analyzed. The infrared radiation is therefore absorbed at the same wavelengths in the detector as that in the sample cell, making the detector specific for the analyzed component. The detector converts the difference in energy between sample cell and reference cell to a capacitance change.

Although, NDIR may be set at various ranges for measuring the concentrations of CO_2 and CO. For this study, the available full-scale ranges for CO_2 measurements are 1000, 2500, 5000, 10000 ppm with an uncertainty of $\pm$ 1% of its full-scale reading. While the ranges for CO are 100, 200, 500, 1000, 2000 ppm with an uncertainty of $\pm$ 1% of its full-scale reading.

Appendix A.4.3 Paramagnetic Detector

When oxygen is placed in a magnetic field, it becomes magnetic. That is why it is said to be strongly paramagnetic. The magnetic susceptibility of the oxygen in gases is sensed in the detector or a magnetic assembly, as shown in Figure A.7. A dumbbell shaped hollow glass test body, filled with nitrogen is suspended in platinum/nickel alloy ribbon in non-uniform magnetic field.

The spheres of test body are subjected to displacement forces because of a "magnetic buoyancy" effect, resulting in a displacement torque proportional to the magnetic

susceptibility of the gas surrounding the test body. Measurement is accomplished by a null-balance system, whereas, the displacement torque is opposed by an equal restorative torque. The restoring current is automatically maintained to the correct level by an electro-optical feedback system. A beam of light from the light source (LED) is reflected off the square mirror attached to the test body onto a photocell. The current required to keep the test body to the null position is a linear function of the total magnetic susceptibility of the sample gas.

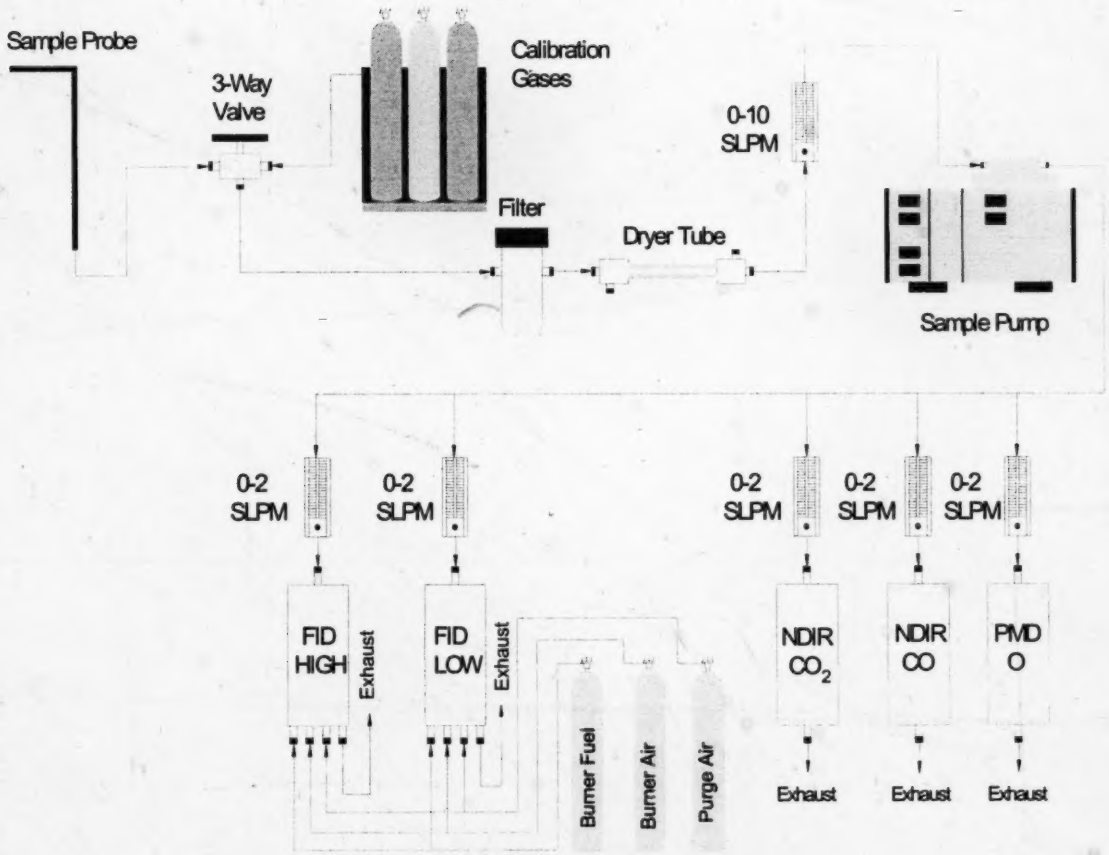

Figure A.4: Schematic of gas sampling system

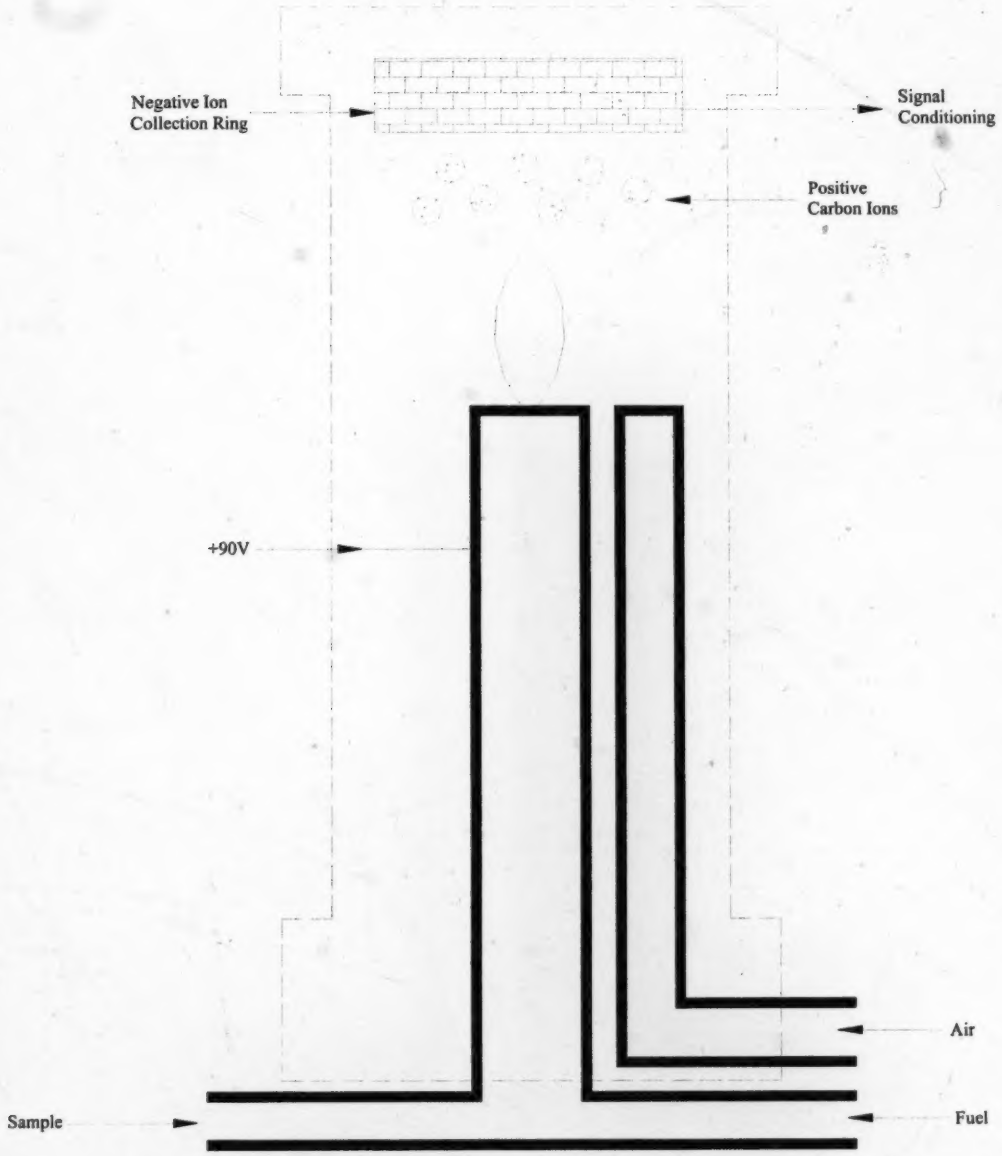

Figure A.5: The Flame Ionization Technology

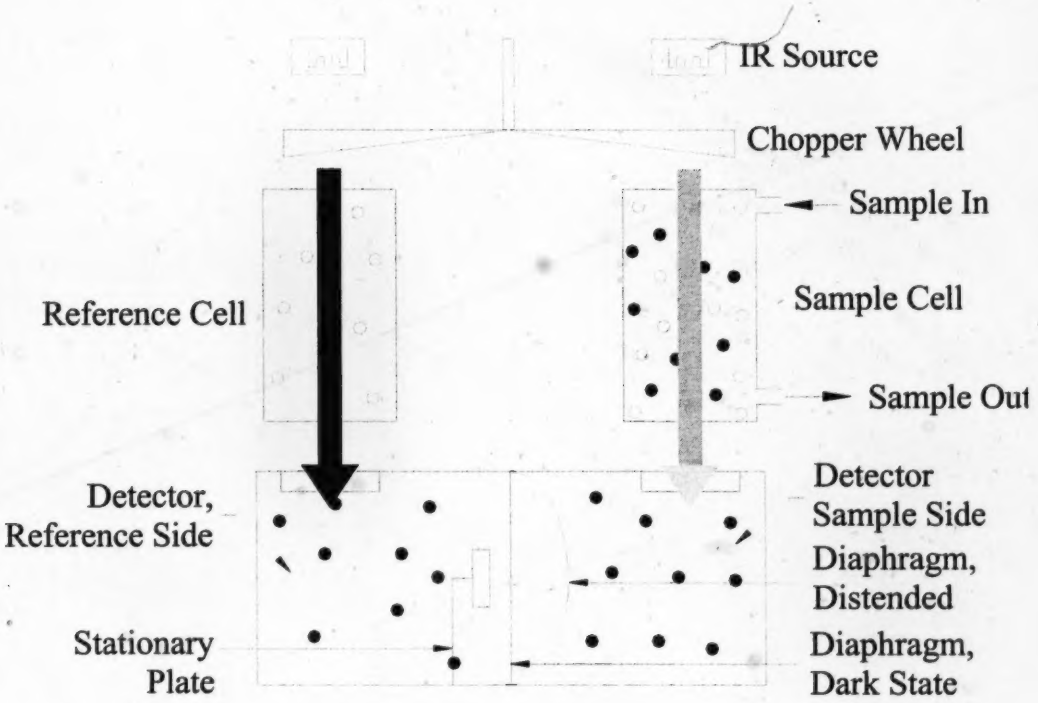

Figure A.6: Non-dispersive Infrared Analyzer

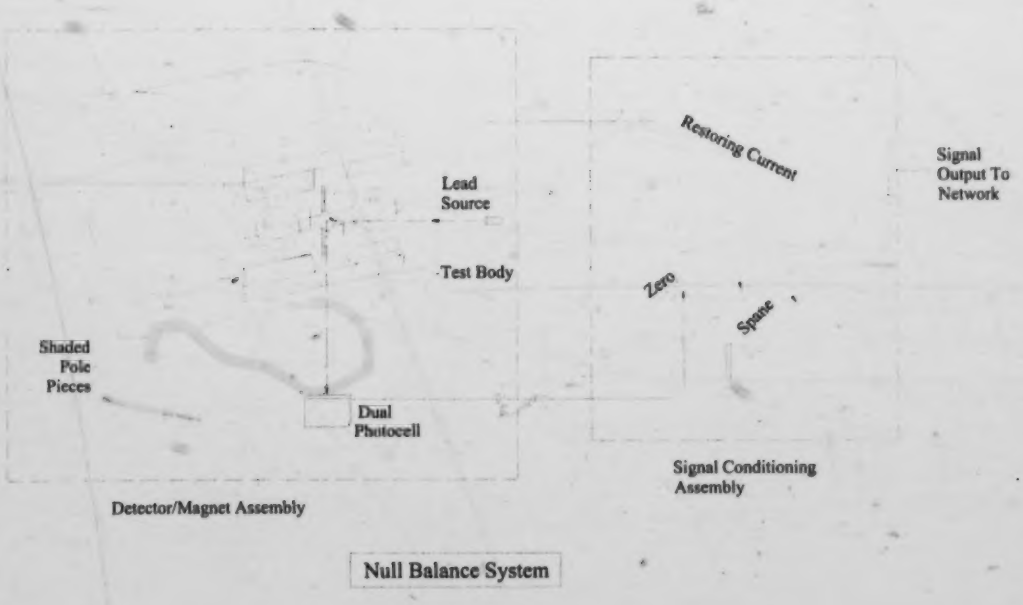

Figure A.7: Paramagnetic Detector Technology

Reference:

1. NGA2000, June 1997, "*Non-Dispersive Infrared Analyzer Module*", Rosemount Analytical Inc., California, U.S.A.
2. NGA2000, April 1995, "*Paramagnetic Detector Analyzer Module*", Rosemount Analytical Inc., California, U.S.A.
3. NGA2000, April 1995, "*Flame Ionization Detector Analyzer Module*", Rosemount Analytical Inc., California, U.S.A.

APPENDIX B

METHODOLOGY FOR MEASURING CARBON CONVERSION EFFICIENCY

The closed-loop wind tunnel acts as a reaction vessel in which the flare is burned and the product gases are collected, contained, and analyzed. In practice, there are several complexities that must be carefully considered to ensure the accuracy of the methodology. The analysis presented here was developed by L.W Kostiuk, Gorge Skinner and M.R Johnson.

Theoretically, one could simply burn a flare for a fixed period of time at a specified flow rate and measure the concentration of CO_2 in the tunnel at the end of this time. The efficiency could then be calculated knowing volume of the tunnel and composition of the flare gas. But there are several uncertainties associated with this approach, which may have a significant affect on the accuracy of calculated efficiency. The uncertainties include accurately measuring flow rate of the gas, volume of the tunnel, and absolute concentration of CO_2 (Kostiuk, 2000). Ideally, the wind tunnel would be sealed so that all the products of combustion would be captured within the tunnel for analysis. However, in practice, the tunnel leaks. Ambient air enters the tunnel, diluting the products of combustion, and the gases from tunnel leak out. Another complication that needs to be considered is the re-circulation of combustion products. This recirculation exposes part of unburned hydrocarbons in the tunnel to the flame, where they could be oxidized (Johnson *et.al.*, 2001). The effects of tunnel leakage, reburning, ignition transients and temperature

changes during the experiments need to be accounted for mass balance. The closed-loop wind tunnel is modelled as constant pressure enclosure in Figure B, that exchanges gases with the surroundings where:

Q_{in} is the volume flow rate of ambient air into the tunnel,

Q_{out} is the volume flow rate of tunnel gases flowing out of the tunnel,

$Q_{combust}$ is the volume flow rate of tunnel air involved in combustion.

P, T, Y and ρ are pressure, temperature, mole fraction, and density, respectively.

The choice of selecting a control volume within the tunnel that includes ambient air but excludes the flame is convenient to perform mass balance on the wind tunnel. It means that there is no chemical reaction within the control volume and hence mass is only transported in and out of the control volume. Therefore the expression of the conservation of mass for the accumulation of species i in the wind tunnel is given by:

$$\underbrace{V\frac{d}{dt}[\rho_i Y_i]}_{\text{Accumulation}} = \underbrace{\rho_i Y_{i,\infty} Q_{in}}_{\substack{\text{Transported in with infiltration of ambient air}}} - \underbrace{\rho_i Y_i Q_{out}}_{\substack{\text{Transported out with exfiltration of tunnel air}}} + \underbrace{\rho_i Q_{i,emitted}}_{\substack{\text{Emitted into the control volume by combustion of flare gases}}} + \underbrace{\rho_i Q_{i,inert}}_{\substack{\text{Flow into tunnel as part of flare gas}}} \pm \underbrace{\eta \rho_i Y_{HC} Q_{combust}}_{\substack{\text{Net flow in or out due to combustion, where fuel mass originates from the air side}}} \quad \text{(B.1)}$$

Tunnel and ambient conditions are specified with and without the subscript ∞. Where, subscript i represent properties relating to a particular chemical species. In Equation B.1, V is the tunnel volume and Y_{HC} is the mole fraction of hydrocarbons in the tunnel air. $Q_{i,emitted}$ is the volume flow rate of the species i emitted into the tunnel by flaring process.

Q_{inert} is the volume flow rate of the flare gases flowing into the wind tunnel unaffected by combustion (*e.g.* CO_2). It is assumed that the hydrocarbons entering with the ambient air burn with the same efficiency as hydrocarbons supplied via fuel stream in order to model the last term of the equation. As long as Y_{HC} remains small, the mass fluxes associated with this term will be extremely small, so the importance of this assumption is almost negligible. The sign of the last term is negative if i is a reactant and positive if i is a product (Johnson *et. al.*, 2001).

The volume flow rates of the gases infiltrating and exfiltrating the wind tunnel are given as:

$$\underbrace{Q_{out}}_{\text{Exfiltration}} = \left[\underbrace{Q_{in}}_{\text{Infiltration}} + \underbrace{\gamma' Q'_{fuel}}_{\substack{\text{Molar imbalance between the fuel and products of gaseous fuel}}} + \underbrace{Q_{inert}}_{\substack{\text{Inert flow in flare stream}}} \right] \underbrace{\frac{T}{T_\infty}}_{\substack{\text{Heating of the wind tunnel gases}}} \tag{B.2}$$

where γ' is coefficient that account for the number of moles of combustion products introduced into the tunnel relative to the number of moles of gaseous fuels.

The total flow rate issued by the flare, when the flare gas stream is assumed to be comprised of gaseous phase, is given as:

$$Q_{flare} = Q'_{fuel} + Q_{inert} \tag{B.3}$$

where Q'_{fuel} is the volume flow rate of gaseous fuel and Q_{inert} is the volume flow rate of inert gases.

Substituting Equation B.2, into Equation B.1, gives the mass balance for a particular species in the wind tunnel, which is:

$$V\frac{d}{dt}[\rho_i Y_i] = \rho_i Y_{i,\infty} Q_{in} - \rho_i Y_i \left[Q_{in} + \gamma' Q'_{fuel} + Q_{inert}\right]\frac{T}{T_\infty} + \rho_i Q_{i,emitted} + \rho_i Q_{i,inert} \pm \eta \rho_i Y_{HC} Q_{combust} \quad \text{(B.4)}$$

Equation B.4, is valid during the experiment at all times. The quantities like Q_{in} and $Q_{combust}$ are very difficult to measure. In order to simplify Equation B.4, a time t_0, is chosen, when the accumulated concentration of species used in calculation of efficiency are very small or approaching zero in the wind tunnel. Applying this condition on the above equation, the last term becomes negligible since, Y_{HC} is small. Similarly, $T \rightarrow T_\infty, Y_i \rightarrow Y_{i,\infty}, \rho_i \rightarrow \rho_{i,\infty}$. Thus Equation B.4 becomes:

$$V\frac{d}{dt}[\rho_i Y_i]\Big|_{t\rightarrow t_0} = \rho_{i,\infty} Y_{i,\infty}\left[\gamma' Q'_{fuel} + Q_{inert}\right] + \rho_{i,\infty} Q_{i,emitted} + \rho_{i,\infty}\, Q_{i,inert} \quad \text{(B.5)}$$

Assuming ideal gas behaviour, Equation B.5, becomes:

$$VT_\infty \frac{d}{dt}\left[\frac{Y_i}{T}\right]\Big|_{t\rightarrow t_0} = Y_{i,\infty}\left[\gamma' Q'_{fuel} + Q_{inert}\right] + \rho_{i,\infty} Q_{i,emitted} + \rho_{i,\infty}\, Q_{i,inert} \quad \text{(B.6)}$$

Equation B.6, is the final expression for the mass balance of species *i* that can then be exploited experimentally to determine combustion efficiency.

Equation B.6, implies when the flare steam is considered to be gaseous phase only that converts into gaseous products with a little or no soot in the products of combustion.

Equation B.6, gives conservation of mass for any accumulated species within the wind tunnel, for example substituting CO_2, CO, and HC with *i*, simultaneously.

When the flare produces little or not soot, the overall combustion equation for general hydrocarbon (C_xH_y) can be written as:

$$C_xH_y + aO_2 \rightarrow b\alpha CO_2 + b(1-\alpha)\,CO + dC_mH_n + eH_2O \qquad \text{(B.7)}$$

Where C_xH_y = general hydrocarbon fuel

a,b,d,e = unknown stoichiometric coefficients

α = molar fraction between fully oxidized carbon (CO_2) and partial oxidized carbon (CO)

C_mH_n = general hydrocarbon in the product of combustion

The stoichiometric coefficients in Equation B.7, can be solved in terms of variables, when Equation B.6, is written separately for CO_2, CO and HC that result in three different forms of equations:

$$\frac{VT_\infty}{Q_{flare}}\frac{d}{dt}\left[\frac{Y_{CO_2}}{T}\right]\Bigg|_{t\to t_0} = Y_{CO_2,\infty}\left(\gamma Y_{C_xH_y} + Y_{inert}\right) + \eta x Y_{C_xH_y} + Y_{CO_2,flare} \tag{B.8}$$

$$\frac{VT_\infty}{Q_{flare}}\frac{d}{dt}\left[\frac{Y_{CO}}{T}\right]\Bigg|_{t\to t_0} = Y_{CO,\infty}\left(\gamma Y_{C_xH_y} + Y_{inert}\right) + \frac{(1-\alpha)}{\alpha}\eta x Y_{C_xH_y} \tag{B.9}$$

$$\frac{VT_\infty}{Q_{flare}}\frac{d}{dt}\left[\frac{Y_{HC}}{T}\right]\Bigg|_{t\to t_0} = Y_{HC,\infty}\left(\gamma Y_{C_xH_y} + Y_{inert}\right) + x\left[1-\frac{\eta}{\alpha}\right]Y_{C_xH_y} \tag{B.10}$$

There are three unknowns in the above equations: efficiency η, molar split between CO_2 and CO, α, and volume of the wind tunnel, V. The remaining quantities in these equations can be measured experimentally. Due to the coupling between the unknowns (α, η and V), it is not possible to obtain an explicit expression for efficiency. Hence it is determined using an iterative technique.

Figure B.2, shows time trace of the measured concentrations of CO_2, CO and HC as they accumulate in the wind tunnel during a typical experiment. Before igniting the flare, the species exist at their ambient background concentrations and can be neglected in the terms involving ambient concentrations in Equations B.8-B.10. With the passage of time, the concentrations of all the three species increases in a steady and linear fashion. It is further assumed that the mass fluxes produced other than those produced by flaring (*i.e.* species produce by reburning of hydrocarbons) are small and hence neglected. As can be

seen from Figure B.2, the measured concentrations of CO and HC at the end of the experiment are of the order of tens of ppm, this is the reason why reburning term is neglected.

Figure B.3, shows the time trace of the measured concentrations of CO_2, CO and HC, divided by absolute temperature within the wind tunnel during the experiment. The slope of each curve in this figure is a direct measure of differential term in Equations B.8-B.10. The data from this typical experiment allows assessment of magnitude of each term in Equations B.8-B.10, and further more it can be shown that the initial background concentrations of the species, if neglected, would not influence the accuracy of calculations. When these equations are solve explicitly for efficiency, η, the following equation is obtained:

$$A = \frac{d}{dt}\left[\frac{Y_{HC}}{T}\right]_{t \to t_0}$$

$$\eta = \frac{\frac{B}{A+C} - \frac{Y_{CO_2,flare}}{xY_{C_xH_y}}}{1 + \frac{B}{A+C}} \qquad \text{where} \qquad B = \frac{d}{dt}\left[\frac{Y_{CO_2}}{T}\right]_{t \to t_0} \tag{B.11}$$

$$C = \frac{d}{dt}\left[\frac{Y_{CO}}{T}\right]_{t \to t_0}$$

Equation B.11, is the final version of the efficiency equation and is much more simpler than the previous equations. Closer look on this equation reveals that it reduces to slopes of the species, whose concentrations have been measured in the wind tunnel during the experiment. If the flare stream has no CO_2, then Equation B.11, can be written as:

$$\eta = \frac{B}{A+B+C} \tag{B.12}$$

This measurement of combustion efficiency of the flare under certain set conditions takes about 15 minutes which includes 8-10 minutes of burning time and the remaining for purging the wind tunnel.

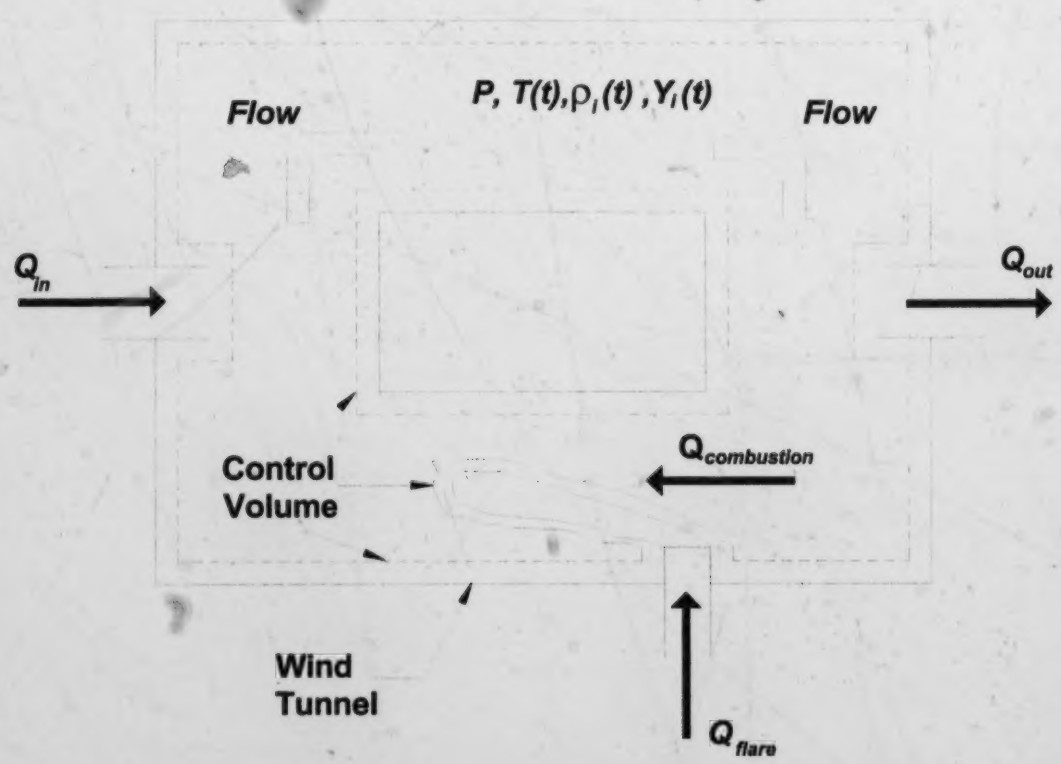

Figure B.1: A model for wind tunnel as constant pressure enclosure (Johnson *et.al.*, 2001)

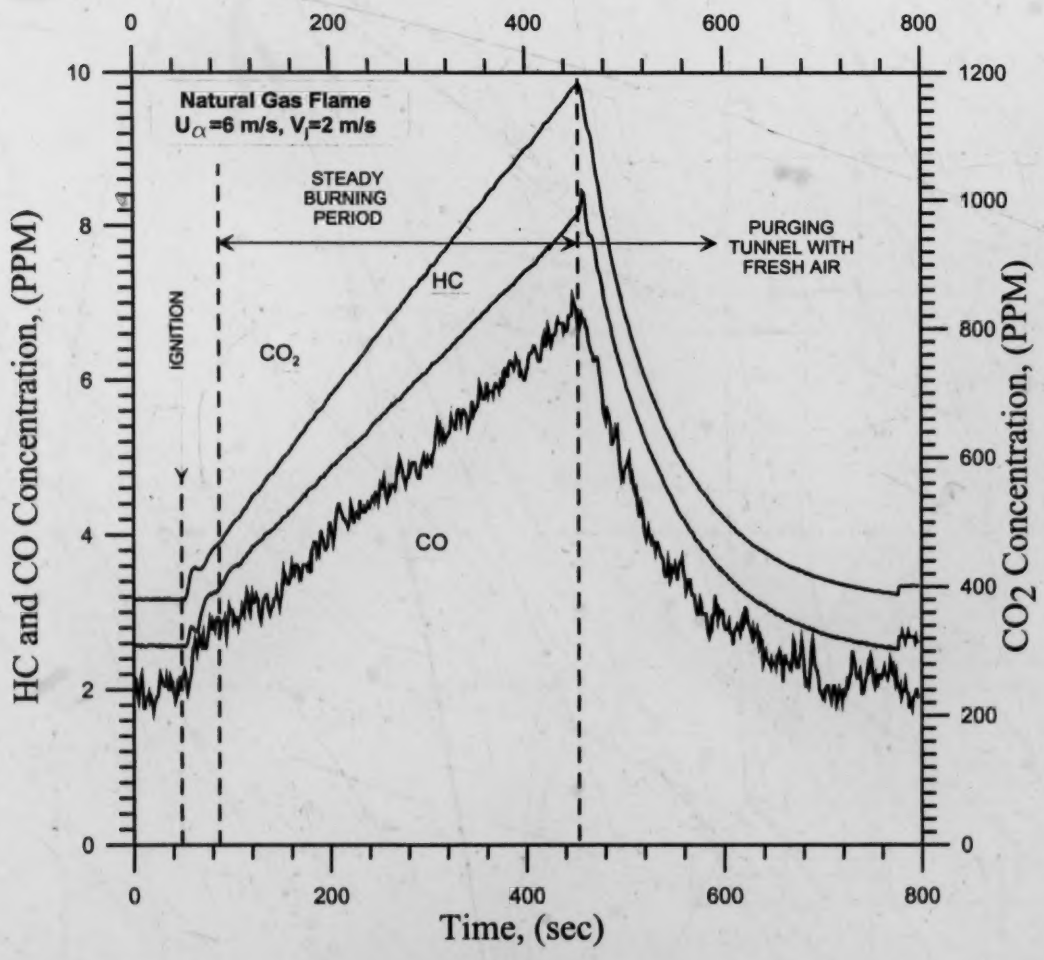

Figure B.2: Time trace of concentrations of CO_2, HC and CO during an experiment in the closed-loop wind tunnel

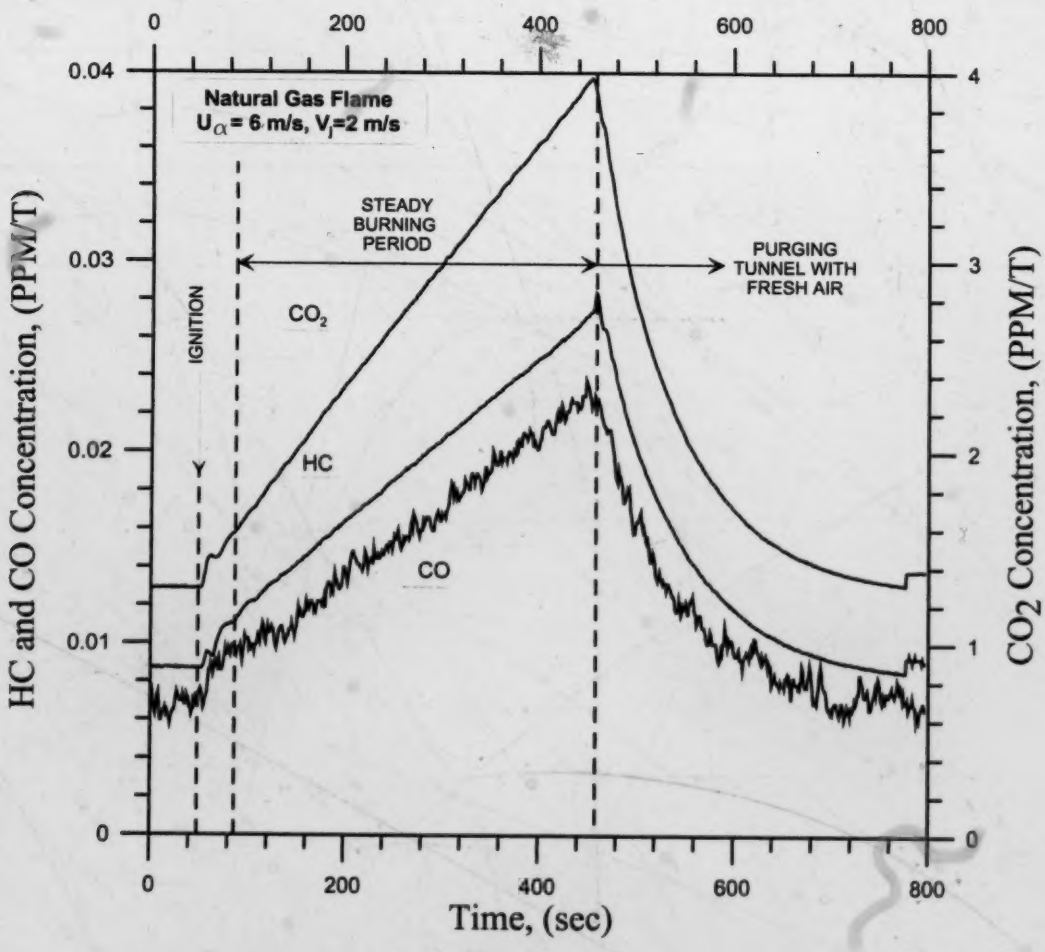

Figure B.3: Ratio of concentrations of major carbon containing species divided by temperature during an experiment in tunnel

References:

1. Kostiuk, L. W. 2000, "*Interim Report November 1996-June 2000*", University of Alberta Flare Research Project.
2. Johnson, M. R., and Kostiuk, L. W., and Bourguignon, E. 2001, "*The Use of a Closed-Loop Wind Tunnel for Measuring the Combustion Efficiency of Flames in a Crossflow*", Combustion and Flame 119:319-334 (1999).

APPENDIX C

ULTRASONIC DROPLETS GENERATOR

For this study, an ultrasonic atomizing nozzle (droplets generator) provided by Sono-Tec Corporation has been used to generate liquid droplets. The droplets are then introduced into the flare stream. Ultrasonic droplets generator is a device, which vibrates at the frequency beyond that of the human hearings (*i.e.* in excess of 20 kHz). Ultrasonic atomization is totally a surface phenomenon. A thin film of liquid is brought in contact with a smooth surface, which is then set into vibrating motion in such a way that the direction of vibration is perpendicular to the surface of the liquid. The liquid film absorbs some of the vibrational energy resulting in unstable capillary waves that form a rectangular grid on the surface of the liquid. This grid has regular crest and troughs extended in both directions. When, the amplitude of vibration is increased, the amplitude of the waves also increase until a critical amplitude is reached at which the height of capillary waves exceed the value required to maintain their stability. As a result, the waves collapse and forms small drops of various sizes. The amount of the liquid atomized depends upon the rate at which liquid is introduced onto the surface. Therefore, this device gives a large variability with respect to flow rates.

One of its major advantages over other atomization devices is its low velocity character of the spray. It produces a spray at 0.18 to 0.37 meter per second as compared to 10.67 to 21.34 meter per second for standard pressure atomizing nozzle and this reduction in spray

velocity results in approximately 10,000 times reduction in kinetic energy (Nozzle System).

Ultrasonic droplets generator is shown schematically in Figure C. A high frequency electrical energy is provided by a power generator, which is converted into mechanical energy at the same frequency by disc shaped ceramic piezoelectric transducers. The two titanium cylinders surrounding these transducers amplify the vibrations produced by these transducers. The resulting vibrations are then directed onto atomizing surface for droplet generation. A large diameter feed tube that runs through the length of the droplets generator is used to deliver the liquid to the atomizing surface. The advantage of using a large diameter feed tube is to prevent it from clogging. Titanium is selected for this purpose because of its corrosion resistance, high strength, and good acoustical characteristics (Nozzle System).

The high frequency electrical energy is provided by an Ultrasonic Generator, which operates over a frequency range of 20-120 kHz. It keeps the power to the nozzle constant and if the system is malfunctioned then produces an alarm. The detail specifications of Ultrasonic Generator can be read from operating instructions for ultrasonic atomizing nozzle systems.

Ultrasonic droplets generator can produce spray in any orientation but it is kept in upright position for this study with the help of a custom capsule. This capsule also serves the

purpose of providing a passage for flare gas so as to carry maximum numbers of liquid droplets up to the top of the flare stack.

Ultrasonic droplets generator is a passive device that atomizes whatever is delivered to the atomizing surface. Which means that a proper liquid delivery system is a dominant factor to make the nozzle work properly. For this study, pressurized canister type liquid delivery system has been chosen for the supply of liquid to the droplets generator. The principle of operation of this system is that the liquid is kept under high pressure in a vessel by nitrogen gas, which enables the liquid to flow into the nozzle. The flow rate of the liquid to the nozzle is controlled by two rotameters provided with the system.

To prevent the droplets generator from overheating, the liquid is supplied before energizing it. If the droplets generator is kept ON without any liquid flowing through it, its internal temperature may rise, which may cause thermal instabilities, when the flow of liquid is resumed. This may destabilized the spray process. The droplets generator is usually turned off, 5-10 seconds after the liquid delivery has ceased. Due to its vibrating actions along the central axis, the liquid within the generator may be pumped out of the exit orifice even though the liquid delivery is OFF, produces a very small spray, which may be objectionable, when precise short sizes are required (Nozzle System).

The power to energize the droplets generator and initiate ultrasonic atomization process is an important factor and best results can be achieved within a narrow input power range. The power required depends upon, type of nozzle, liquid characteristics, and flow rate.

Different nozzles have different geometry and shapes, therefore, the power required for the generating droplets of the same liquid will be different. Similarly, if the liquid is pure and less viscous, the power required for atomization will be low. On the other hand, if the liquid to be atomized is more viscous or liquids with high solid content, the power required is higher. Similarly, for lower flow rates of the liquid, the nozzle requires minimum power and vice versa. At the same time, exit diameter of orifice and atomizing surface area determines the upper flow rate limit for a particular ultrasonic droplets generator. The turn-down ratio of the flow rate for a given nozzle is in the range of 5:1. Ultrasonic droplets generator do not rely on the pressure, so they may have various turn-down ratios. But practically, the lower limit of the flow rate does exist. If the flow of liquid to the nozzle is very low, it will move with slower velocity resulting in distorted spray pattern. This phenomenon can be avoided in some cases like chemical reaction chambers, where stable spray patterns are unimportant. Therefore the selection of turn-down ratio for a particular flow rate depends upon application (Nozzle System).

The size of the droplet produced as a result of atomization of a liquid by ultrasonic droplets generator depends upon the frequency at which the nozzle operates, surface tension, and the density of the liquid. But frequency is the dominant factor. There are various parameters, which can be used to characterize particular drop distribution. For example number median diameter, number mean diameter, weight mean diameter and Sauter mean diameter. The first one defines 50% point on the drop size (*i.e.* one-half of the drops have diameter larger than this value and the other half has diameter less than this value). The number mean diameter is obtained by adding the diameters of the drops

in a sample and then divide this sum by the total number of drops in the sample. The weight mean diameter is obtained by adding the volume of each drop in a spray sample, then taking the cube root of this sum and then divide it by total number of drops in the sample. The Sauter mean diameter is specifically used in combustion applications, it measures the effective ratio of the drop volume to the surface area (Nozzle System).

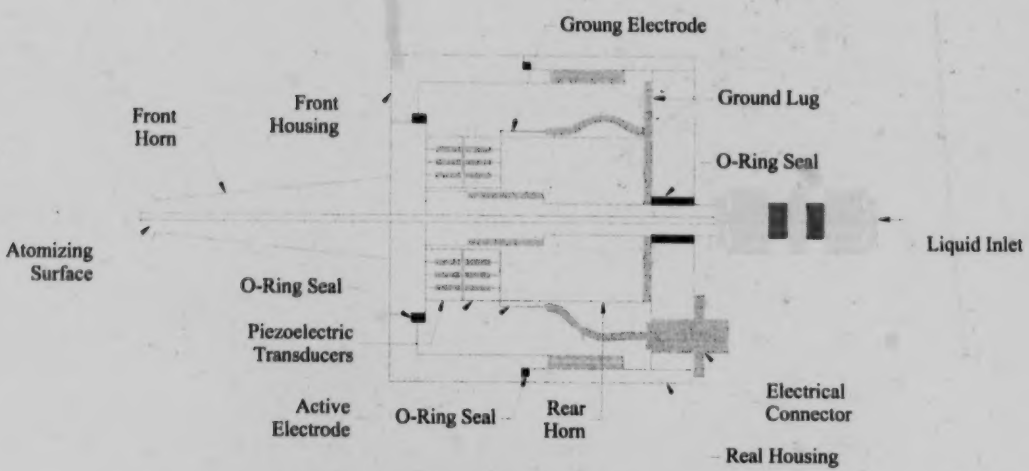

Figure C: Ultrasonic atomizing droplets generator

References:

1. Ultrasonic Atomizing Nozzle System, *"Operating Instructions"*, Sono-Tek Corporation, USA.

APPENDIX D

DROPLET SIZE MEASUREMENT

Droplet size data can be collected through many methods using various instruments. Since, performance of a droplet generator requires repeatable test results it is necessary to adopt a testing procedure that takes into account all variables in the sampling technique best suited for both method and instrumentation.

A simple technique for particle size analysis is to spray water into a pan of oil and then count and size each individual droplet using a microscope. By spraying water onto liquid sensitive paper or a dye onto stationary card, the size of an individual particle can be measured. But the disadvantage of techniques is that the larger droplets can break-up while impacting the surface. Similarly, the smaller droplet may be deflected away from the surface due to spray velocity.

Optical methods for particle size analysis have been used for several years. For measuring the size of an individual particle, an average size, or the size distribution, the light is scattered in a certain angle in space. Modern electronic and computer technology made it possible to analyze particle size distributions quicker and more reproducible. Figure D.1, shows the physical principle of a diffraction pattern analyzer, which was first described by Fraunhofer. When, stationary or moving particles suspended in a gas or liquid, are introduced in to a laser beam, diffraction pattern with very bright center and a series of concentric dark and bright rings are obtained in the focal plane of the lens. The

detector collects various light intensities produced by different size particles, which are then converted into particle size distribution by a microcomputer (Micheal and Leschonski, 1985). The same physical principle has been used in the modern laser diffraction equipment with the development of laser that provides a source of monochromatic light and powerful microcomputers for the calculation of particle size distribution from the light intensity distribution detected by the detector (Puckhaber and Röthele, 1999).

Laser diffraction technology is applicable for powders, suspensions, emulsions, granulates and sprays. The main advantage of this technique is its simplicity, speed, and reproducibility over a large range of droplet sizes, which makes it ideal for both quality control and research and development (Röthele and Lake, 1992).

The same technique has been adopted for droplet size distribution in this thesis research. A droplet size analyzer manufactured by Sympatec Corporation (Helos BFS), was used to characterize the probability size distribution of the droplets that exit the flare stack. This instrument is capable of measuring the droplet size up to 875 μm. The instrument consists of a light source, usually a laser that generates a monochromatic coherent parallel beam. The beam is expanded by a beam processing unit. This expanded beam then passes through a measuring zone, where the particles to be analyzed are dispersed. Sales grade natural gas and dry air have been used to carry the droplets through the measuring zone of the instrument. These moving droplets generate the diffraction patterns in the focal plane of the lens after introduced into a laser beam. The laser from the lens is focussed on

a special multi-element detector (Witt and Röthele, 1994). The light intensity distribution across the detector appears as concentric light and dark rings, getting weaker with the increasing distance from the center. Since, the diffraction angle is inversely proportional to the size of the droplet that produces it small droplets show large diffraction angle directing the light to the outer edge of the detector. Similarly, the light will be directed towards the center by large droplets showing small diffraction angle (Röthele and Lake, 1992).

The movement of these particles spreads out the phase relationships of different particles and allows superimposition of intensities instead of amplitudes of the light waves of different particles. An angular intensity distribution is generated as a result of the interaction between droplets and incident wave-field in terms of absorption, refraction, deflection, and diffraction. The angular intensity distribution is converted into spatial intensity distribution by Fourier optics (usually a lens). A multi-element photo-detector measures this intensity and converts it into a set of photocurrents. An input data in terms of intensity vector is obtained through computer software. The geometric parameters of the detection unit and the wavelength convert the intensity vector into the droplet size information in terms of output data (Witt and Röthele, 1994).

Figure D.2, shows the particle size analysis of a test performed on iso-octane droplet. Dry compressed air was used as a carrier gas with jet exit velocity of 1 m/sec and 18 kHz ultrasonic droplets generator was used to generate the droplets. Mass flow rate of octane was 7 g/min and the power to the droplets generator was 5.5 W. The figure shows

cumulative distribution, Q3(x), density distribution, q3(x), and particle size, x. The measuring range varied from 0 to 875μm. Each individual point of the distribution represents the amount of the particles smaller than or equal to the corresponding size on x-axis. For this particular test, 50% of the droplets generated had the size equal to 48μm.

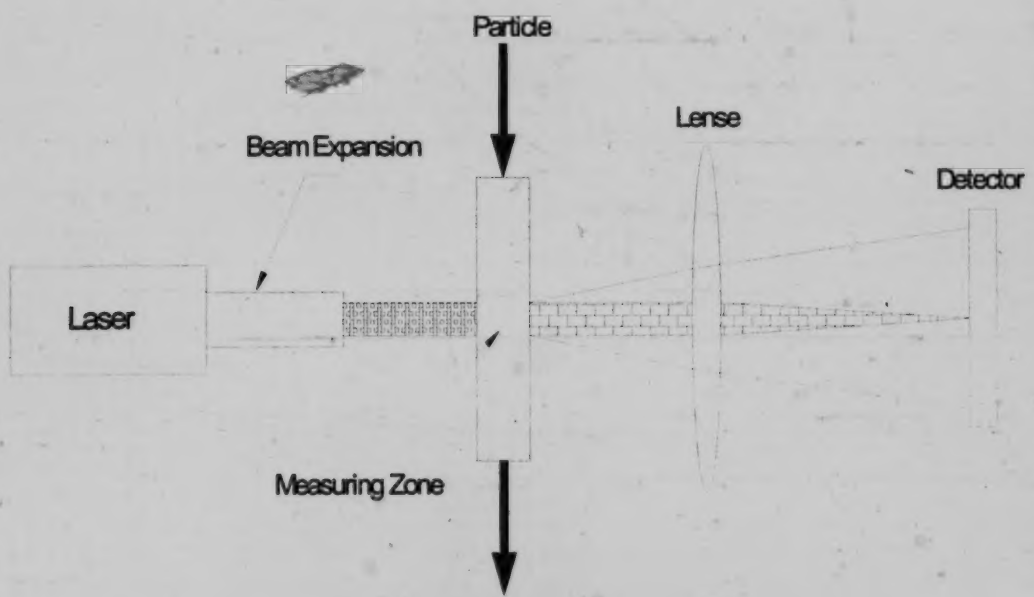

Figure D.1: Optical setup for the measurement of diffraction patterns (Puckhaber and Röthele, 1999)

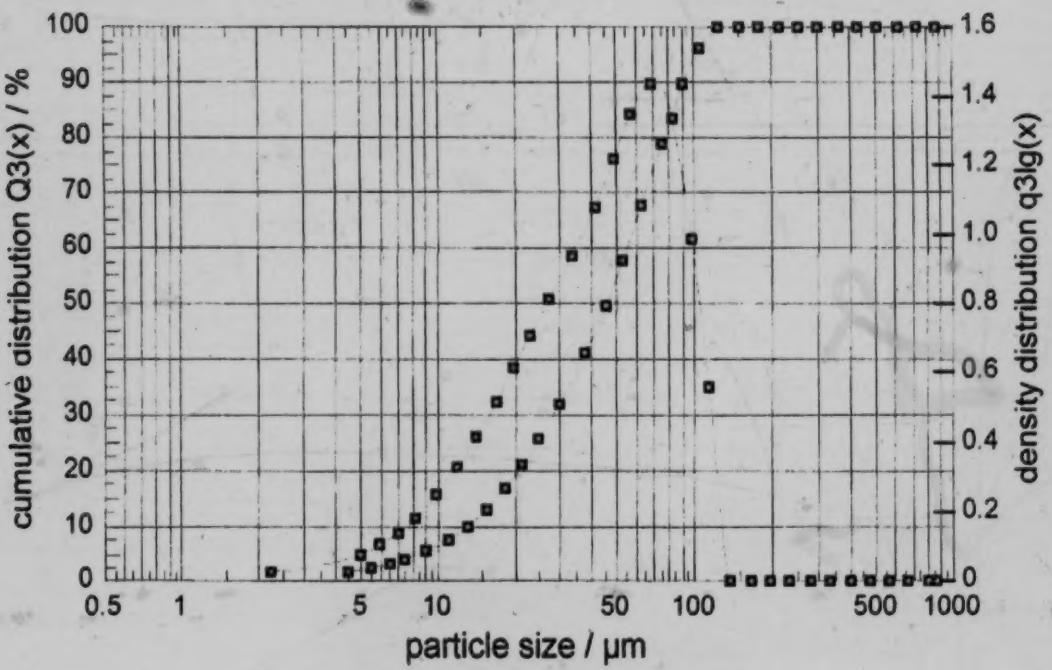

Figure D.2: Particle size analysis

References:

1. Röthele, S., Lake, A. P. 1992," *Laser Diffraction Technology Focussing on the Future",* A Company Profile of Sympatec Gmbh, Volume 4, Number 1, March 1992.
2. Puckhaber, M., Röthele, S. 1999, " *Laser Diffraction Millennium-Link for Particle Size Analysis",* Vol. 11, No. 1, January/March 1999.
3. Michael Heuer, Kurt Leschonski," *Results Obtained with a New Instrument for the Measurement of Particle Size Distributions from Diffraction Patterns",* Part: Chapter 2 (1985).
4. Witt, W.,Röthele, S. 1994, "*Laser Diffraction*", Sympatec GmbH, System-Partikel-Technik, 1994, Germany